Jacklyn Dias Reis   **Design and Optimization Next Generation Passive All-Optical Networks**

Jacklyn Dias Reis

Design and Optimization Next Generation Passive All-Optical Networks

o júri / the jury

presidente / president   **Doutor Vasile Staicu**
Professor Catedrático da Universidade de Aveiro

vogais / examiners committee   **Doutor António Luís Jesus Teixeira**
Professor Associado da Universidade de Aveiro (orientador)

Doutor Josep Joan Prat Goma
Professor Catedrático da Universitat Politècnica de Catalunya

Doutor Daniel Diogo Ferrão da Trindade Fonseca
Diretor do grupo de Engenharia Ótica da Nokia Siemens Networks

Doutor José Rodrigues Ferreira da Rocha
Professor Catedrático da Universidade de Aveiro

**agradecimentos /
acknowledgments**

Resumo

Este trabalho investiga novas metodologias para as redes óticas de acesso de próxima geração (NG-OAN). O trabalho está dividido em quatro tópicos de investigação: projeto da rede, modelos numéricos para efeitos não lineares da fibra ótica, impacto dos efeitos não lineares da fibra ótica e otimização da rede.

A rede ótica de acesso investigada nesse trabalho está projetado para suprir os requisitos de densidade de utilizadores e cobertura, isto é, suportar muitos utilizadores ($\sim$1000) com altas velocidades de conexão dedicada ($\sim$1 Gb/s) ocupando uma faixa estreita do espectro ($\sim$25 nm) e comprimentos de fibra ótica até 100 km. Os cenários são baseados em redes óticas passivas com multiplexagem por divisão no comprimento de onda de alta densidade (UDWDM-PON) utilizando transmissores/receptores coerentes nos terminais da rede. A rede é avaliada para vários ritmos de transmissão usando formatos de modulação avançados, requisitos de largura de banda por utilizador e partilha de banda com tecnologias tradicionais de redes óticas passivas (PON).

Modelos numéricos baseados em funções de transferência das séries de Volterra (VSTF) são demonstrados tanto para a análise dos efeitos não lineares da fibra ótica quanto para avaliação do desempenho total da rede. São apresentadas as faixas de potência e distância de transmissão nas quais as séries de Volterra apresentam resultados semelhantes ao modelo referência Split-Step Fourier (SSF) (validado experimentalmente) para o desempenho total da rede. Além disso, um algoritmo, que evita componentes espectrais com intensidade nulo, é proposto para realizar cálculos rápidos das séries. O modelo VSTF é estendido para identificar unicamente os efeitos não lineares da fibra ótica mais relevantes no cenário investigado: Self-Phase Modulation (SPM), Cross-Phase Modulation (XPM) e Four-Wave Mixing (FWM).

Simulações numéricas são apresentadas para identificar o impacto isolado de cada efeito não linear da fibra ótica, SPM, XPM e FWM, no desempenho da rede com detecção coerente UDWDM-PON, transportando canais com modulação digital em fase (M-ária PSK) ou modulação digital em amplitude (M-ária QAM). A análise numérica é estendida para diferentes comprimentos de fibra ótica mono modo (SSMF), potência por canal e ritmo de transmissão por canal. Por conseguinte, expressões analíticas são extrapoladas para determinar a evolução do SPM, XPM e FWM em função da potência e distância de transmissão em cenários NG-OAN.

O desempenho da rede é otimizada através da minimização parcial da interferência FWM (via espaçamento desigual dos canais), que nesse caso, é o efeito não linear da fibra ótica mais relevante. Direções para melhorias adicionas no desempenho da rede são apresentados para cenários em que o XPM é relevante, isto é, redes transportando formatos de modulação QAM. A solução, nesse caso, é baseada na utilização de técnicas de processamento digital do sinal.

Abstract

This work investigates novel methodologies and models for Next-Generation Optical Access Networks (NG-OAN). The work is divided into four main topics of research: network design, numerical models for fiber nonlinear effects, impact of fiber nonlinear effects and network optimization.

The used case optical access network is designed to cope with high user density over extended reach, i.e. support large number of users (∼1000) with high speed dedicated connections (∼1 Gb/s) in a narrow bandwidth (∼25 nm) distributed up to 100 km. The scenarios rely on Ultra-Dense Wavelength-Division Multiplexing Passive Optical Networks (UDWDM-PON) employing coherent transceivers in the network terminals. The network is evaluated for various transmission rates using advanced modulation formats, transmitters and receivers specifications, user bandwidth requirements and coexistence with legacy Passive Optical Network (PON) technologies.

Numerical models based on Volterra Series Transfer Function (VSTF) are demonstrated for both the analysis of fiber nonlinear effects and evaluation of the overall network performance. It is presented the power and transmission ranges that Volterra series provides accurate results, compared to the reference model Split-Step Fourier (SSF) (experimentally validated), for the overall network performance. Moreover, an algorithm is proposed to provide fast numerical calculations of the series by avoiding zero intensity signal frequency components. The VSTF model is extended to identify the sole effect of the most relevant fiber nonlinearities in UDWDM-PON network scenarios: Self-Phase Modulation (SPM), Cross-Phase Modulation (XPM) and Four-Wave Mixing (FWM).

Numerical simulations are performed to identify the impact of each nonlinear effect, SPM, XPM and FWM, on the performance of coherent UDWDM-PON transporting either M-ary PSK (Phase-Shift Keying) or M-ary QAM (Quadrature Amplitude Modulation) modulated channels. The analysis is extended to different lengths of Standard Single-Mode Fibers (SSMF), power per channel and bit rate per channel. From that, analytic expressions are extrapolated to find the evolution of SPM, XPM and FWM with power and transmission distance for NG-AON scenarios.

The performance of the network is optimized by mitigating some of the FWM crosstalk (unequally spaced channels), which in this case is the most relevant fiber nonlinear effect. The directions for further performance improvements are pointed out for scenarios in which XPM is enhanced, i.e. networks transporting QAM signaling. The solution in this case is based on digital signal processing techniques.

"Don't get set into one form, adapt it and build your own, and let it grow, be like water. Empty your mind, be formless, shapeless — like water. Now you put water in a cup, it becomes the cup; You put water into a bottle it becomes the bottle; You put it in a teapot it becomes the teapot. Now water can flow or it can crash. Be water, my friend."

— Bruce Lee: A Warrior's Journey (2000)

To my parents,
To Darlene.

Contents

Main contributions

[J1] J. D. Reis, D. M. Neves, and A. L. Teixeira. Analysis of Nonlinearities on Coherent Ultra-Dense WDM-PONs Using Volterra Series. *Journal of Lightwave Technology*, 30(2):234–241, 2012.

[J2] J. D. Reis, D. M. Neves, and A. L. Teixeira. Weighting nonlinearities on future high aggregate data rate PONs. *Optics Express*, 19(27):26557–26567, December 2011.

[J3] J. D. Reis and A. L. Teixeira. Unveiling nonlinear effects in dense coherent optical WDM systems with Volterra series. *Optics Express*, 18(8):8660–8670, April 2010.

[J4] J. D. Reis and A. L. Teixeira. Cross-phase modulation impact on coherent optical 16 QAM-WDM transmission systems. *Microwave and Optical Technology Letters*, 53(3):633–636, March 2011.

[J5] J. D. Reis, B. Neto, P. S. André, and A. L. Teixeira. WDM ring performance improvement by means of four-wave mixing crosstalk minimization algorithm. *Microwave and Optical Technology Letters*, 51(8):1949–1952, August 2009.

[J6] F. P. Guiomar, J. D. Reis, A. Carena, G. Bosco, A. L. Teixeira, and A. N. Pinto. Experimental demonstration of a frequency-domain Volterra series nonlinear equalizer in polarization-multiplexed transmission. *Optics Express*, Accepted, January 2013.

[J7] F. P. Guiomar, J. D. Reis, A. L. Teixeira, and A. N. Pinto. Mitigation of intra-channel nonlinearities using a frequency-domain Volterra series equalizer. *Optics Express*, 20(2):1360–1369, January 2012.

[J8] F. P. Guiomar, J. D. Reis, A. L. Teixeira, and Armando N. Pinto. Digital Postcompensation Using Volterra Series Transfer Function. *IEEE Photonics Technology Letters*, 23(19):1412–1414, October 2011.

[J9] M. V. Drummond, J. D. Reis, R. N. Nogueira, P. P. Monteiro, A. L. Teixeira, S. Shinada, N. Wada, and H. Ito. Error-free wavelength conversion at 160 Gbit/s in PPLN waveguide at room temperature. *Electronics Letters*, 45(22):1135–1137, 2009.

[C1] J. D. Reis, A. Shahpari, R. Ferreira, F. P. Guiomar, D. M. Neves, A. N. Pinto, and A. L. Teixeira. Analysis of Transmission Impairments on Terabit Aggregate PONs. In *Optical Fiber Communication Conference*, page OM2A5, Anaheim, USA, 2013. Optical Society of America, IEEE.

[C2] J. D. Reis and A. L. Teixeira. Architectural Optimization of Coherent Ultra-Dense WDM based Optical Access Networks. In *Optical Fiber Communication Conference*, page OTuB7, Los Angeles, USA, 2011. Optical Society of America, IEEE.

[C3] J. D. Reis, M. V. Drummond, A. L. Teixeira, R. N. Nogueira, P. P. Monteiro, S. Shinada, N. Wada, and G. T. Beleffi. Experimental Demonstration of a Nonlinear Effects Crosstalk Minimization Algorithm. In *Optical Fiber Communication Conference*, page JThA32, San Diego, USA, 2010. Optical Society of America, IEEE.

[C4] J. D. Reis, L. N. Costa, and A. L. Teixeira. Nonlinear Effects Prediction in Ultra-Dense WDM Systems Using Volterra Series. In *Optical Fiber Communication Conference*, page JWA9, San Diego, USA, 2010. Optical Society of America, IEEE.

[C5] J. D. Reis, B. Neto, P. S. André, and A. L. Teixeira. WDM Ring Performance Improvement by Means of a Nonlinear Effects Crosstalk Minimization Algorithm. In *Optical Fiber Communication Conference*, page JThA77, San Diego, USA, 2009. Optical Society of America, IEEE.

[C6] A. L. Teixeira, A. Shahpari, J. D. Reis, and M. Lima. Spectral Management in Flexible Multiwavelength PONs. In *Optical Fiber Communication Conference*, page JW2A09, Anaheim, USA, 2013. Optical Society of America, IEEE.

[C7] J. D. Reis, D. M. Neves, and A. L. Teixeira. Weighting nonlinearities on future high aggregate data rate PONs. In *European Conference and Exposition on Optical Communications*, volume 35, page We.10.P1.109, Geneva, Switzerland, 2011. Optical Society of America, IEEE.

[C8] J. D. Reis, D. M. Neves, and A. L. Teixeira. Density and Guard Band in Migration Scenarios to Coherent Ultra-Dense WDM. In *2011 IEEE Global Telecommunications Conference*, pages 1–5, Houston, TX, USA, December 2011. IEEE.

[C9] A. L. Teixeira and J. D. Reis. Optical transmission modeling by means of Volterra series (Invited). In *SPIE Photonics West*, page 8647-15, San Francisco, USA, 2013. SPIE.

[C10] J. D. Reis, D. M. Neves, and A. L. Teixeira. Physical Impairments on High Aggregate Data Rate Passive Coherent Optical Networks. In *2011 SBMO/IEEE MTT-S International Conference on Microwave and Optoelectronics*, pages 366–370, Natal, RN, Brazil, 2011. IEEE.

[C11] J. D. Reis, P. M. A. Monteiro, and A. L. Teixeira. Fiber nonlinear impact on hybrid ultra-dense WDM based optical networks. In *2010 12th International Conference on Transparent Optical Networks*, page Th.A.1.5, Munich, Germany, June 2010. IEEE.

[C12] J. D. Reis, B. Neto, P. S. André, and A. L. Teixeira. Optimization of Passive Optical Networks by means of fiber nonlinearities interference reduction. In *2009 11th International Conference on Transparent Optical Networks*, page Tu.C5.4, Azores, Portugal, 2009. IEEE.

[C13] J. D. Reis and A. L. Teixeira. Reduction of Inter-Channel FWM Crosstalk on Coherent QPSK Ultra-Dense WDM Transmission. In *Latin America Optics and Photonics Conference*, volume 35, page TuB4, Recife, Brazil, 2010. Optical Society of America.

[C14] J. D. Reis and A. L. Teixeira. Impact of Nonlinear Effects Distortion on Hybrid Ultra- Dense WDM based Networks. In *Access Networks and In-house Communications*, number 5, page ATuB5, Karlsruhe, Germany, 2010. Optical Society of America.

[C15] J. D. Reis, D. M. Neves, and A. L. Teixeira. Transmission aspects on broadband coherent optical access networks. In *2011 IEEE Third Latin-American Conference on Communications*, pages 1–6, Belem, Brazil, October 2011. IEEE.

[C16] P. M. Coelho, J. D. Reis, B. Neto, P. S. André, and A. L. Teixeira. Monitoring of Fiber Nonlinearities in WDM Based Passive Optical Networks. In *2009 10th International Conference on Telecommunications*, pages 277–281, Zagreb, Croatia, 2009. IEEE.

[C17] F. P. Guiomar, J. D. Reis, A. Carena, G. Bosco, A. L. Teixeira, and A. N. Pinto. Experimental Demonstration of a Frequency-Domain Volterra Series Nonlinear Equalizer in Polarization-Multiplexed Transmission. In *European Conference and Exposition on Optical Communications*, number 1, page Th1D1, Amsterdam, Netherlands, 2012. Optical Society of America, IEEE.

[C18] F. P. Guiomar, J. D. Reis, A. L. Teixeira, and A. N. Pinto. Mitigation of Intra-Channel Nonlinearities Using a Frequency-Domain Volterra Series Equalizer. In *European Conference and Exposition on Optical Communications*, number 1, page Tu6B1, Geneva, Switzerland, 2011. Optical Society of America, IEEE.

[C19] M. V. Drummond, J. D. Reis, R. N. Nogueira, P. P. Monteiro, A. L. Teixeira, S. Shinada, N. Wada, and H. Ito. 160 Gb/s Wavelength Conversion in a PPLN Waveguide at Room Temperature. In *Nonlinear Photonics*, page NMB3, Karlsruhe, Germany, 2010. Optical Society of America.

[C20] M. V. Drummond, J. D. Reis, R. N. Nogueira, P. P. Monteiro, A. L. Teixeira, S. Shinada, N. Wada, and H. Ito. Wavelength conversion of a 160 Gb/s RZ OTDM signal in a PPLN waveguide at room temperature. In *2009 International Conference on Photonics in Switching*, pages 5–6, Piza, Italy, 2009. IEEE.

[P1] C. Rodrigues, P. Mão-Cheia, F. P. Guiomar, A. N. Pinto, J. D. Reis, and A. T. Teixeira. Método de Equalização Não-Linear do Canal Óptico no Domínio da Frequência. 105765, June, 2011.

List of Acronyms

viii

x

List of Figures

List of Tables

Chapter 1

Introduction

Why do people need Telecommunications nowadays?

Video streaming, online gaming, cloud computing and Internet Protocol Television (IPTV) in full high definition (1080i/p) and ultra high definition (4k / 8k) are just a few examples of high-demanding bandwidth applications that access networks have to cope with. Solid foundations in Fiber-to-the-Home (FTTH) projects have to be built for even faster Internet connections. How much data information can be transported by the current optical fiber infrastructure is one of questions that this Ph.D. work tries to answer it.

1.1   Passive Optical Networks

The needs for broadband connections have been driving several research groups and the telecom industry to put a lot of effort towards the development of new technologies. Greater attention has been given to the deployments and development of cost-effective, reliable and easy to upgrade architectures for access networks based on point-to-multipoint Passive Optical Network (PON) [1, 2]. Gigabit-capable Passive Optical Networks (GPON) [3] standardized by the International Telecommunication Union - Telecommunication Standardization Sector (ITU-T) and Ethernet Passive Optical Networks (EPON) [4] standardized by the Institute of Electrical and Electronics Engineers (IEEE) have been deployed around the world. By 2006, 80 % of the worldwide FTTH deployments were based on EPON whereas the remaining 20 % were represented by GPON. The majority of the EPON subscribers has been concentrated in Asia (mostly China, South Korea and Japan) whereas GPON technology has been adopted in North America (e.g. USA) and in some countries in Europe (e.g. France) [5]. It is

expected however that the number of GPON subscribers worldwide increases due to the fact that BRIC (Brazil, Russia, India and China) and some European countries have been investing mostly on GPON deployments to enhance their broadband capabilities (according to *Infonetics Research*[1]).

In both technologies, several users share the same fiber infrastructure via Time-Division Multiplexing (TDM) techniques. GPON delivers asymmetric 1.25 Gb/s for upstream and 2.5 Gb/s for downstream directions whereas EPON provides symmetric 1 Gb/s for upstream and downstream. In addition, upgraded versions of these technologies, one referred as 10-Gigabit-capable Passive Optical Network (XG-PON) [6], will be deployed in the following years in order to extend reach and capacity. 10 Gb/s Ethernet Passive Optical Networks (10G-EPON) [7] has already been deployed since 2009.

Although GPON and EPON are cost effective technologies in terms of deployment and maintenance, they both lack on exploiting the full potential of the fiber capacity since the users share the same channel wavelength. One way to efficiently use the populated wavelength spectrum is by using Wavelength-Division Multiplexing (WDM), as shown in Fig. 1.1, to enable point-to-point physical connections between Optical Network Unit (ONU)s and Optical Line Termination (OLT) in the Central Office (CO). As a result, Wavelength-Division Multiplexing Passive Optical Network (WDM-PON) can support higher number of users and higher bit rates per user compared to exclusively TDM based PONs if the interference among WDM channels is addressed by any optical or electrical multiplexing. Therefore, several wavelengths can be closely packed to provide dedicated physical connections. Both capacity and reach can be further improved by the use of mixed architectures based on Dense Wavelength-Division Multiplexing (DWDM) rings and TDM trees. For instance, the authors in [8] presented a double-fiber WDM ring architecture with 32 channels reaching up to 100 km with 1:32 TDM trees. Remotely pumped nodes, which may increase the cost of the network, in the WDM ring are used to provide broadband connections up to 1000 users.

Some WDM-PON trends require replacing the existing power splitter with an Arrayed Waveguide Grating (AWG) router (see the filtered scenario in Fig. 1.1). On the other hand, this upgrade is not particularly desirable, as it requires work on the outside plant and disrupts existing customers. A centralized split PON (star topology as in the fully transparent scenario

---

[1]*Infonetics Research*: *GPON Equipment in Brazil, Russia, India and China (BRIC) Market Share and Forecast* http: // www.infonetics.com /cgp / lp.asp?id=552 (last access, October 2012.)
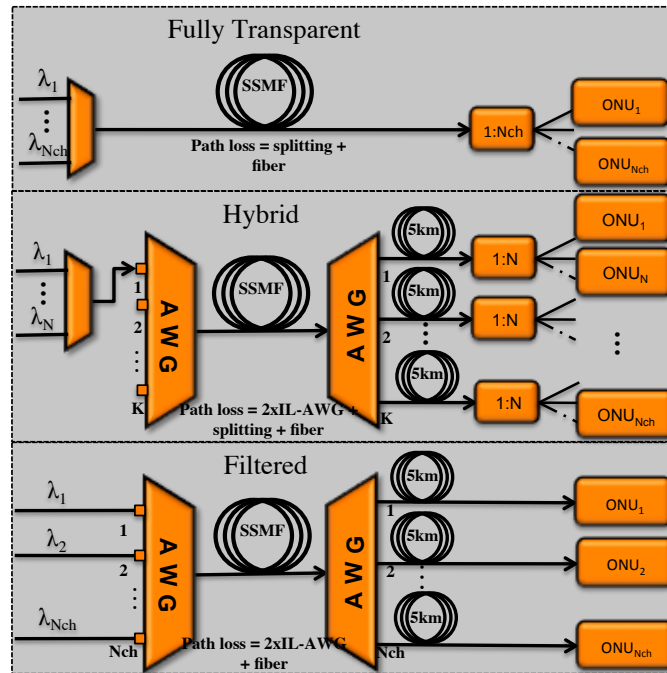
Figure 1.1: Different architectures for PONs. (Top) Fully transparent; (Middle) Hybrid; (Bottom) Filtered

in Fig. 1.1) can relatively easily be upgraded to such a kind of WDM-PON. For distributed split PONs (tree and branch), it is impractical to take this upgrade path. This limitation can be overcome if each ONU selects any of the wavelengths without optical filtering in the Optical Distribution Network (ODN), i.e. "tunable" ONUs.

In order to overcome the aforementioned limitations, coherent communications may play an important role for Next-Generation Optical Access Network (NG-OAN) [9]. For instance, using the ONUs as digital coherent receivers, the local oscillator selects each wavelength and the information is recovered digitally [10].

1.2 Coherent Communications

The first important aspect of coherent WDM-PON is that the information conveyed in both directions among ONUs and OLT is modulation transparent in the optical counter-part of the transceivers if the electrical signals are encoded and decoded digitally. Since Digital Signal Processing (DSP) at ONU/OLT is easily adapted, any advanced modulation format, such as Phase-Shift Keying (PSK) [11], quadrature amplitude modulation Quadrature Amplitude

Modulation (QAM) [12] or even Orthogonal Frequency-Division Multiplexing (OFDM) [13], can be employed throughout the network keeping almost the same optical components in the transmitters (laser and IQ modulators) and receivers (local oscillator, optical hybrid, balanced detectors etc). In addition, the ONU requires only one tunable local oscillator used for both upstream and downstream transmissions since *heterodyne* detection can be used in the downstream direction whereas the original wavelength is reserved for the upstream direction [10]. Secondly, the spectral efficiency is enhanced by the combination of low channel spacing (or wavelength separation below 25 GHz), high-order modulation formats (M-ary Phase-Shift Keying (MPSK) or M-ary Quadrature Amplitude Modulation (MQAM)) and high channel count (higher than 32). This architecture, sometimes referred as Ultra-Dense Wavelength-Division Multiplexing (UDWDM) based PON, has the potential to theoretically exploit nearly the ultimate capacity of the optical fiber, i.e. 9 bit/s/Hz per polarization over 500 km of fiber [14]. As an example, transporting 1000 channels / wavelengths / users spaced by only 3.125 GHz, employing 256-ary Quadrature Amplitude Modulation (256QAM) at 3 Gbaud (quasi Nyquist-WDM), the aggregate data rate reaches 24 Tb/s over 3.125 THz ($\sim$ 24 nm) resulting nearly 8 bit/s/Hz per polarization over 100 km of fiber assuming a split ratio of 1:1000. If dense multiplex/demultiplex [C2] or blocking filter [15] exist in the network (as shown in Fig. 1.1), it is possible to reuse devices by multiplexing ultra-dense channels over DWDM filters, which alleviates the required split ratio. Current research works demonstrated DWDM using Orthogonal Frequency-Division Multiple Access (OFDMA) based PON with 1.92 Tb/s aggregate over 100 km with split ratio of 1:64 [16]. Another example is found in [17] where self-coherent reflective PON has been demonstrated to provide up to 42 dB power budget in the ODN.

1.3   Design Aspects

UDWDM technology relies on employing high-order modulation formats along with coherent detection to provide key network functionalities such as (1) high wavelength selectivity to alleviate the need for costly and technology challenging ultra-dense filter technology; (2) better receiver sensitivity to enable a system with higher split ratios and extended reach (power budget); (3) bit rate upgradeability by electrically increasing the modulation order keeping the optical counter part unchanged; (4) digital signal processing to implement equalizers for

transceiver imperfections and transmission impairments.

Excluding the performance limitations imposed by the transmission over the optical fiber, the network performance is limited by the optical and electrical components used both in the OLT and ONUs. Regarding electronics, most of the research works carried out for optical transport networks have been addressing sampling rates, required bandwidth and bit resolutions of Analog to Digital Converter (ADC) and Digital to Analog Converter (DAC) in the transmitters and receivers to operate at target users' data rate [18, 19, 20]. In the optical counterpart, the goal is how to compensate for the phase and/or amplitude optical noise induced by Erbium-Doped Fiber Amplifier (EDFA), lasers' phase noise, modulators, filters, IQ imbalance etc [21, 22].

1.4 Transmission Aspects

As far as transmission impairment is concerned, fiber nonlinearities have become a great concern as the channel density and power launched into the fiber increases pushing the system towards nonlinear Shannon's limit of the optical fiber [23, 14]. Interference among ultra-dense channels [J1] and with already deployed legacy technologies such as G/EPON [C8] and video overlay [24] may impair the system's performance. For that reason, prior knowledge about transmission aspects such as intra-channel and inter-channel nonlinearities and their dependence on link length, power and modulation is mandatory for the system to convey information in a reliable way. This can be addressed by recurring to mathematical models capable of analyzing and simulating accurately the system's performance and different contributions of the most relevant physical impairments. On that regard, by using a Volterra series approach, one is able to estimate the Signal-to-Noise Ratio (SNR) of the received constellation with respect to different nonlinearities effect and further equalize those unwanted effects.

Volterra series have gained a lot of attention from the optical communication community over the past years on research topics such as: modeling the nonlinear propagation over the optical fiber [25]; post-processing nonlinear equalizer on coherent optical transmission systems [26], [J8]; analysis of fiber nonlinearities on direct detection systems [27] and coherent optical systems [J3, J1].

1.5 Motivation and Outline

This Ph.D. thesis aims at investigating coherent optical solutions for Next-Generation Optical Access Networks. As such, the work was carried out targeting the following objectives:

1. Identify physical and technical challenges on future high aggregate data rate Passive Optical Networks;

2. Test different receiver and transmitter designs as to fulfill bandwidth upgradability and user density requirements on Terabit aggregate PONs;

3. Develop strategies for assessing the overall system's performance of different Next-Generation Optical Access Network architectures;

4. Evaluate the most relevant sources of transmission impairments such as cross effect among different technologies in the same PON structure and the dependence of fiber nonlinearities on feeder power, transmission distance and advanced modulation formats;

5. Propose transmission impairment compensation schemes, either via all-optical processing or digital signal processing techniques to boost transmission capabilities as to comply with network coverage and capacity.

In order to fulfill the aforementioned objectives, the thesis is divided into 6 Chapters briefly described as follows:

Chapter 1 reviews the state of the art on coherent optical solutions for NG-OAN and discusses the organization of the thesis structures as well as its main scientific contributions;

Chapter 2 addresses the network subsystems in the OLT, ODN and ONUs in terms of architecture, user density, bandwidth, coexistence with legacy technologies and transceivers performance;

Chapter 3 describes the mathematical model based on Volterra series for the evaluation of the overall system's performance and different contributions of fiber nonlinearities. It is also presented the numerical validation against Split-Step Fourier simulations for different modulation formats and transmission distances;

Chapter 4 presents the impact of fiber nonlinearities such as self-phase modulation, cross-phase modulation and four-wave mixing on the system's performance. The impact on the

performance versus launch power is evaluated numerically, based on the Volterra model presented in Chapter 3, when network transports different modulation formats and transmission distances;

Chapter 5 discusses performance optimization schemes to mitigate some of the fiber nonlinearities. The main contribution arises from the well-known unequally channel spacing scheme to partially eliminate four-wave mixing crosstalk without imposing a bandwidth penalty. The proposed algorithm is experimentally and numerically investigated.

Chapter 6 concludes the work and give some directions for future projects exploiting the concepts addressed by the this thesis.

As detailed in the following section, most of the concepts discussed in this thesis were either published or submitted to prestigious scientific journals of the present research areas [J1]–[J9], and also presented in international conferences [C1]–[C20]. This thesis was therefore written as a comprehensive complement to the published papers, which contain most of the information. Consequently, Chapters 2 to 5 begin with an introduction followed by the description of the methods, scenarios, results and discussions.

It is important to point out that all the numerical simulations were carried out in a simulation platform implemented by the author in Matlab$^{®}$ programming language. This simulation platform, which includes all network elements such as transmitter, receivers and optical channel, has been experimentally validated for an heterogeneous network scenario comprised by a coherent UDWDM comb (16×1.25 Gb/s coherent Quadrature Phase-Shift Keying (QPSK)) in the presence of 10 Gb/s–NRZ signaling with variable guard bands and optical powers. The transmission over the optical channel was numerically modeled using both Split-Step Fourier (SSF) and Volterra Series Transfer Function (VSTF). SSF simulations were accelerated (up to 10× faster than Central Processing Unit (CPU) based simulations) by using Graphics Processing Unit (GPU) parallel computing so that the simulation time was fairly reduced for UDWDM network scenarios.VSTF was numerically implemented for both transmission propagation as well as for the analysis of nonlinearities in UDWDM network scenarios.

1.6   Main Contributions

This Ph.D. work has contributed beyond the state of the art on several research topics including the design and optimization schemes to extend the transmission capabilities of Next-Generation Passive Optical Networks. Most part of the work is published in top international conferences (20 papers) and prestigious journals (9 papers) on optical communications and related topics with accumulated impact factor of 21 (Journal Citation Reports 2011).

- The first part of the work, covering objectives 1, 2 and 3, contributed to the design and performance aspects for high data rate aggregate PONs. The work was described in 1 journal paper [J2] and 7 conference papers [C7], [C2], [C8], [C10], [C4], [C16], [C6]. We determined how the user density (channel spacing and number of channels) and guard band to legacy technologies in the wavelength spectrum impact on the performance. In addition, bandwidth, reach and capacity were considered in the transmitters and receivers designs to fulfill the requirements of network performance;

- Secondly, objective 4, a special attention was given to the identification of the most relevant transmission impairments on such a network. The work contributed to 3 journals [J1], [J3], [J4] and 5 conference papers [C1], [C9], [C11], [C14], [C15]. We described how Volterra series efficiently solves the signals' linear and nonlinear interaction over the optical fiber. Therefore, it allows to estimate independently the performance contributions of self-phase modulation, cross-phase modulation and four-wave mixing in a coherent ultra-dense WDM-PON which is limited mostly by inter-channel nonlinearities. The validity ranges, in terms of power and transmission distance, were established based on caparison to Split-Step Fourier simulations for different modulation formats.

- The later part of the work, objective 5, addressed the optimization of the network performance with respect to users' bandwidth upgradability. The contributions were reported in 5 journal papers [J5], [J1], [J6], [J7], [J8] and 6 conference papers [C5], [C3], [C13], [C12], [C17], [C18] and one patent [P1]. Channel frequency allocation schemes, based on Genetic Algorithm or randomly optimized coefficients, were proposed to compensate in part for the inter-channel four-wave mixing without penalize the total bandwidth. The optimized frequency coefficients updates the frequency of transmitters and receivers

lasers for coherent systems. The proposed algorithms were experimentally and numerically demonstrated. In addition, digital signal processing techniques, based on Volterra back propagation to eliminate some deterministic nonlinearities, have been developed to further improve the system's performance when impaired by self-phase and possibly cross-phase modulation.

It is important to point out that the experimental validation of the optimization algorithm [C3, C5] was partially carried out at the National Institute of Information and Communications Technology (NiCT, Photonic Network Research Institute) in Tokyo, Japan (2009). In addition, this Ph.D. work has collaborated with other works on all-optical wavelength conversion during the 3-month stay at NiCT [J9, C20, C19].The experimental investigation presented in [C17, J6] were obtained in cooperation with Politecnico di Torino (POLITO) in Turin, Italy, during a two-week stay in the summer of 2011.

Chapter 2

Architectural and Design Optimization

The increased demand for broadband in optical access networks has pushed engineers and scientists around the world to develop new solutions to better exploit the capabilities of Passive Optical Network (PON). The problem to be solved is

how to maximize the number of users, the users' data rate and reach at minimal cost, complexity and bandwidth?

On that sense, coherent communication either based on Orthogonal Frequency-Division Multiplexing (OFDM) [13] or Wavelength-Division Multiplexing (WDM) [28] is a notorious technological advance for enabling Next-Generation Optical Access Network (NG-OAN). As discussed in Chapter 1, employing coherent transceivers in both Optical Line Termination (OLT) and Optical Network Unit (ONU) provides key network functionalities such as wide-range tunable ONUs, improved receiver sensitivity, data rate upgradeability and physical impairment compensation. The first two functionalities are related to the presence of a light source in the ONU that is used for both channel selection and detection without the need for optical amplification and filtering. Digital Signal Processing (DSP) techniques can be applied to any digital modulation formats for the equalization of both transmission impairments and transceivers imperfections. Particularly, the spectral efficiency is enhanced by the combination of reduced channel spacing, higher order modulation formats such as M-ary Phase-Shift Keying (MPSK) and M-ary Quadrature Amplitude Modulation (MQAM) and high number of wavelength channels. These characteristics are the foundations of coherent Ultra-Dense Wavelength-Division Multiplexing Passive Optical Network (UDWDM-PON) [29], which has the potential to explore more efficiently the available optical fiber capacity, predicted as 9

bits/s/Hz per polarization over 500 km [14].

This Chapter, based on Journal [J2] and Conference papers [C4],[C6], [C7], [C8] and [C10], investigates key parameters to better exploit the transmission capabilities of optical access networks employing coherent transceivers. Firstly, WDM based PONs architectures and their dependence on spectral efficiency and link budged are outlined in Section 2.1. The experimental validation of the simulation platform is presented in Section 2.2 considering an heterogeneous network. The transmitter design in the OLT is addressed in Section 2.3. Some transmission aspects in the Optical Distribution Network (ODN) such as the cross effect with other PON technologies are discussed in Section 2.4. Finally, Section 2.3 describes some parameters of the receiver in the ONU to cope with the upgradeability of users' data rate.

2.1   PON Architectures

Some designs of Wavelength-Division Multiplexing Passive Optical Network (WDM-PON) may require replacing the existing power splitter with an Arrayed Waveguide Grating (AWG) router if the ONUs do not have the ability to receiver information in other wavelengths. On the other hand, this limitation can be solved if each ONU selects any of the wavelengths ("tunable" ONU) without the need of optical filtering. As a result, it is relevant that future network architectures employ tunable ONUs so that some already deployed devices, i.e. splitters and/or AWGs can be reused.

In order to overcome the aforementioned limitations, coherent communications may play an important role for NG-OAN. For instance, using the ONUs as digital coherent receivers, the local oscillator selects any of the transmitted wavelengths to down-convert to the electrical and the information is recovered digitally [10].

The coherent UDWDM-PON scenario investigated in this work has a total of N_{ch}=64 Quadrature Phase-Shift Keying (QPSK) modulated channels at 1 Gb/s. This scenario, depicted in Fig. 2.3, may be implemented in 3 different architectures:

(i) *fully transparent*: all coherent channels spaced by 3.125 GHz are transmitted through 25 km of fiber to the ONUs only recurring to a 1:64 splitter. The optical spectrum before fiber is shown in Fig. 2.1(b);

(ii) *hybrid*: K sub-groups of N channels (spaced at 3.125 GHz) multiplexed via $K \times BW$ AWG (e.g. 4×100 GHz), are transmitted over 20 km of fiber. Then, the information is

routed to ONUs via $K \times BW$ AWG, followed by 5 km and 1:N passive splitter. The optical spectrum for K=2 is depicted in Fig. 2.1(c). We considered that the AWGs have 4 dB of intrinsic loss and minimal bandwidth of 6.25 GHz due to the limited band in the simulation setup (400 GHz divided for 64 channels).

(iii) *filtered*: N_{ch}=64 channels multiplexed via 64 × 6.25 GHz AWG, are transmitted through 20 km of fiber followed by 64 × 6.25 GHz AWG. The information reaches the ONUs 5 km away without a power splitter. The related optical spectrum is shown in Fig. 2.1(d).

Fig. 2.2 shows the spectral efficiency and total link loss as a function of the number of AWG ports (K) for all architectures. On top of the figure, it is shown the related splitting factor for each value of K. Here, we define the spectral efficiency as the aggregated bit rate divided by the total occupied bandwidth and the total link loss as the overall attenuation accounting for
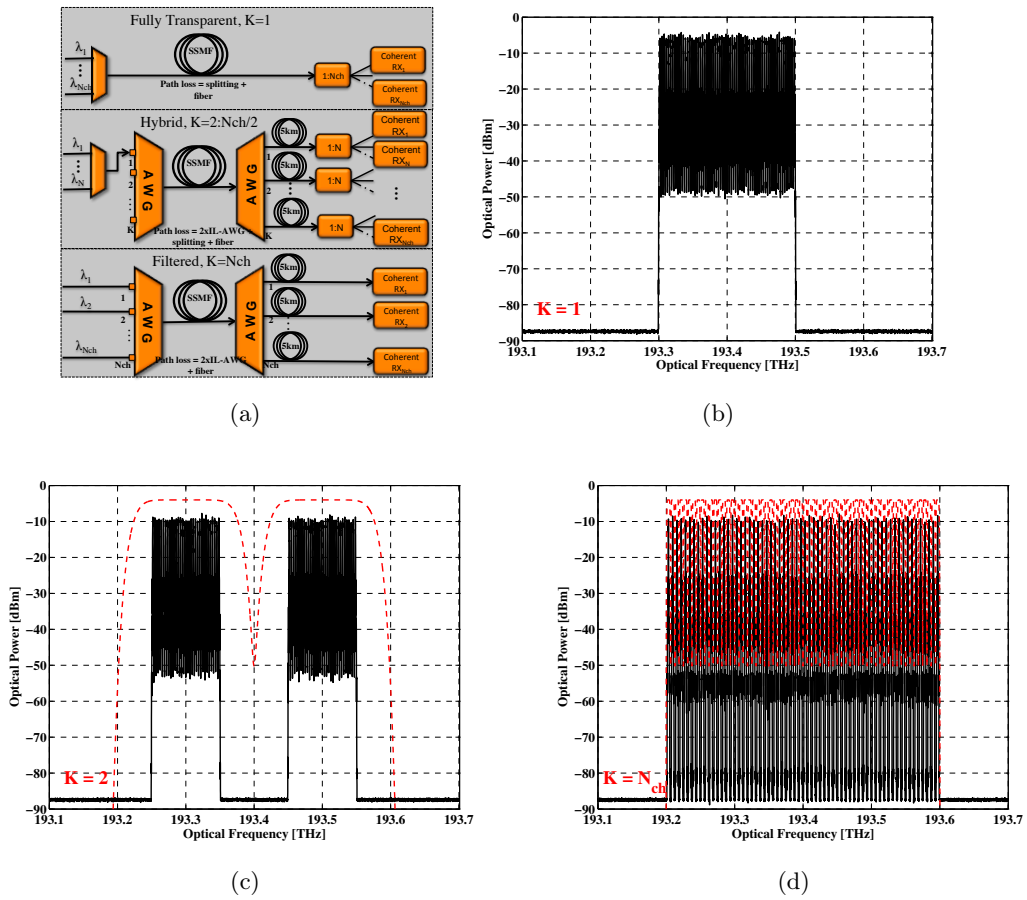
Figure 2.1: (a) Different architectures for UDWDM based PONs. Optical spectra before fiber for (b) *Fully transparent*, (c) *Hybrid* and (d) *Filtered*.
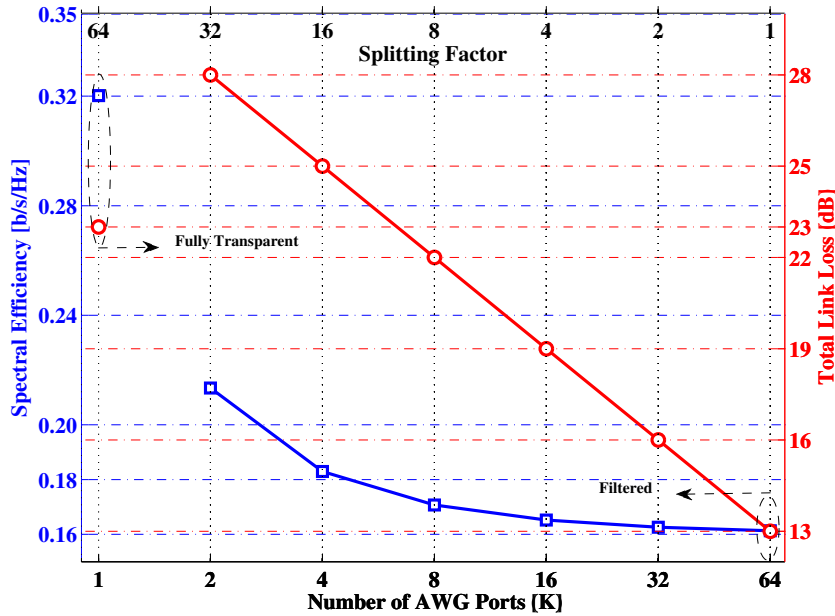
Figure 2.2: Spectral efficiency (blue line + squares) and point-to-point link loss (red line + circles) as a function of number of AWG ports. Related splitting ratios shown on top.

AWGs, fibers and splitter. The *fully transparent* (reference) architecture positioned at K=1 (1:64) has the highest spectral efficiency among all the compared. The spectral efficiency is reduced by 50 % for K>4 (1:16) *hybrid* and *filtered* architectures. The *fully transparent* system has 23 dB (1:64 splitter plus 5 dB for fiber) of link loss and the *filtered* architecture (K=64) has the lowest link loss (13 dB) accounted for the intrinsic loss of 2 AWGs plus fiber.

Scenarios with higher splitting factors, in which several ultra-dense channels are closely packed, provide higher spectral efficiency and flexibility since coherent channels can be traded by higher speed technologies (e.g. 100GbE) in broader AWG ports. Furthermore, these architectures may reuse the already installed PON infrastructures such as 1:16 splitters. Scenarios with lower splitting factors (<1:16) provide extended reach thanks to the lower link loss. Since the number of channels per AWG band is reduced, the transmission is not strongly impaired by nonlinear crosstalk as it is discussed in Chapter 4. On the other hand, these architectures lack on spectral efficiency and flexibility since narrower AWG band limits the use of alternative broadband technologies. For instance, it is technological challenging to allocate 40G–Intensity Modulation Direct Detection (IMDD) channels on 50 GHz or 25 GHz–AWG.

Another possibility for the *fully transparent* architecture is when the UDWDM-PON co-
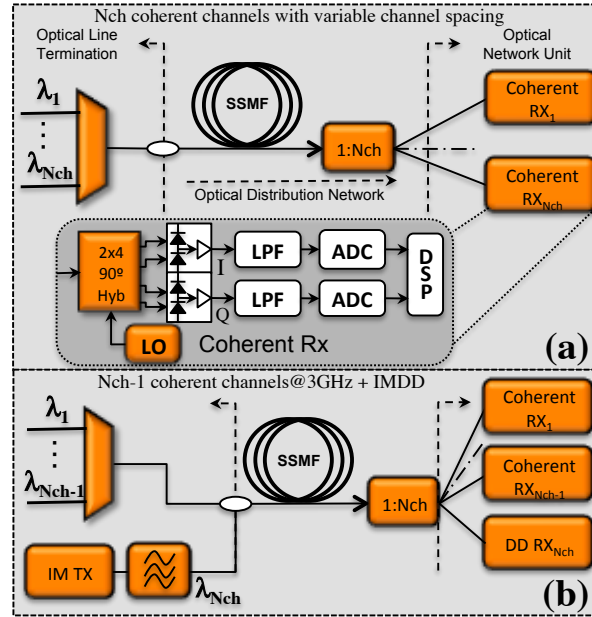
Figure 2.3: System scenarios for the *Fully Transparent* architecture: (a) *Homogeneous* network. (b) *Heterogeneous* network.

exists with legacy technologies as the Gigabit-capable Passive Optical Networks (GPON) or with upcoming deployments as the 10-Gigabit-capable Passive Optical Network (XG-PON). Since both GPON and XG-PON are based on IMDD systems, the *fully transparent* architecture is further subdivided into *Homogeneous* scenario, transporting only coherent channels and *Heterogeneous* scenario, transporting coherent and IMDD channels as depicted in Fig. 2.3. These scenarios will be detailed in section 2.4 to study the cross effect on different technologies sharing the same fiber plant.

2.1.1   Simulation Parameters and Methodologies

The following results address some relevant parameters to test the capabilities of coherent UDWDM-PON, both in its homogeneous (coherent channels only) or in its heterogeneous (coherent channels coexisting with IMDD channels) versions. Therefore, it is described below some parameters and methodologies used in the simulated results.

In the transmitter side, each wavelength channel shown in Fig. 2.3 is comprised by a laser light source followed by an optical modulator which is fed by radio frequency electrical signals. The laser light source has zero phase and intensity noise. The effect of laser phase noise is

addressed in sub-section 2.5.2 when digital modulation formats are studied for different laser linewidths. For coherent channels, the modulator is an optical IQ modulator fed by in-phase and quadrature Non-Return to Zero (NRZ) electrical signals. The transfer function of the modulator is implemented according to equation (2.16) in [30]. The NRZ electrical signals are independent and shaped by a 5th order Bessel filter with bandwidth approximately twice the bit rate. The intensity modulated channels have similar structure, but the IQ modulator is replaced by a Mach-Zehnder Modulator (MZM) fed by only one NRZ electrical signal. The MZM transfer function is defined in equation (2.13) in [30].

Following the transmitter, there is an optical filter to simulate the presence of AWGs multiplexers in the case of WDM scenarios. The filter transfer function follows a 2nd order super-Gaussian curve in which the bandwidth is tuned to 80 % of the channel spacing. As an example, the bandwidth is about 2.5 GHz for 3.125 GHz of channel spacing. This rule does not apply to the intensity modulated channels where the filter bandwidth is tuned to about 4 times the bit rate.

After multiplexing all the channels, the resulting optical signal is transmitted over the fiber, Standard Single-Mode Fiber (SSMF): reference frequency 193.4 THz ($\sim$ 1550 nm), fiber attenuation $\alpha = 0.20 \ dB/km$, chromatic dispersion $D = 16.5 \ ps/(nm.km)$, chromatic dispersion slope $S = 0.07 \ ps^2/nm.km$ and nonlinear parameter $\gamma = 1.35 \ (W \cdot km)^{-1}$. The optical propagation is simulated by the Split-Step Fourier (SSF) method implemented according to [31, 32]. Volterra Series Transfer Function (VSTF) method, detailed in Chapter 3, is also used for simulating the optical propagation and modeling fiber nonlinearities. In both cases, linear effects (attenuation and Chromatic Dispersion (CD)) and fiber nonlinearities (Self-Phase Modulation (SPM), Cross-Phase Modulation (XPM) and Four-Wave Mixing (FWM)) are taken into account. Higher order nonlinearities such as Self-Steepening (SS), Stimulated Raman Scattering (SRS) and Stimulated Brillouin Scattering (SBS) are not considered in the simulations.

After propagation, the optical signal reaches the receiver side via splitters, AWG + splitters or AWG, as illustrated in Fig. 2.1(a).

In the receiver side, the coherent channels are detected by a conventional coherent receiver shown in the inset of Fig. 2.3(a). The received optical signal is mixed along with the 0 dBm local oscillator (linewidth = 0 Hz) through $2 \times 4 - 90^o$ optical hybrid. The local oscillator is tuned to the channel under test. Both in-phase and quadrature components of the resulting

optical signal is optical-to-electrical down-converted using two pairs of balanced photo detectors (responsivity $R \approx 1$). Thermal noise of the receiver circuitry (front-end impedance of 50 Ω) and photocurrent shot noises are considered in the coherent receiver. The electrical signal is then filtered using a 5th order low-pass Bessel filter with 3 dB bandwidth around 0.7 $\times$ symbol rate. The analog signal is further down sampled at symbol rate (one sample per symbol) and converted to the digital domain using an Analog to Digital Converter (ADC) with 8 bits resolution to minimize any quantization errors as discussed in sub-section 2.5.1. Thus, the recovered symbols are normalized to 1 (average constellation energy) and the phase synchronization is performed as detailed in section 3.4. The last step is to estimate the performance of the recovered complex symbols as the root mean squared Error Vector Magnitude (EVM) for N symbols, defined as

$$EVM_{rms} = \sqrt{\frac{\sum_{i=1}^{N} |s_i - s_i'|^2}{\sum_{i=1}^{N} |s_i|^2}} \tag{2.1}$$

where $s_i' = a_i' + j * b_i'$ and $s_i = a_i + j * b_i$ are the received symbols and ideal transmitted symbols, respectively. EVM can be expressed in either in percentage, $EVM(\%) = EVM_{rms} \cdot 100$, or in dB, $EVM(dB) = 10 \cdot \log_{10}(EVM_{rms}^2)$. Throughout this work, it is included in the figure results a dash line around EVM=32.4 % ($\sim$-9.8 dB), which theoretically corresponds to a system Bit Error Ratio (BER)=10^{-3} using QPSK [33]. This BER value is the reference threshold for a typical limit of 7 % overhead Forward Error Correction (FEC). For more information on the relations of EVM, BER and Signal-to-Noise Ratio (SNR) for both MPSK and MQAM formats, refer to Appendix A.

The intensity modulated channel is firstly filtered by a pass-band optical filter, with the same characteristics as the one in the transmitter side. Then, the resulting signal is directly detected ($|\cdot|^2$) via a photo receiver (responsivity $R \approx 1$) followed by a low-pass filter (5th order Bessel) with bandwidth around 0.7 $\times$ bit rate. After the decision logic, the performance is estimated using the Q factor defined as:

$$Q_{dB}^2 = 20 \cdot \log_{10} \left(\frac{\mu_1 - \mu_0}{\sigma_1 + \sigma_0} \right) \tag{2.2}$$

where μ_i and σ_i are the mean and standard deviation values for mark ($i = 1$) and space ($i = 0$), respectively.

2.2   Experimental Validation of the Simulation Model

This section addresses the experimental demonstration of the *fully transparent heterogeneous* network comprised by 16×1.25 Gb/s–coherent QPSK channels plus 10 Gb/s–IMDD channel transmitted over 20 km of SSMF. The main goal of this section is to experimentally validate the simulation model employed throughout this work using the lab infrastructure shown in Fig. 2.4.
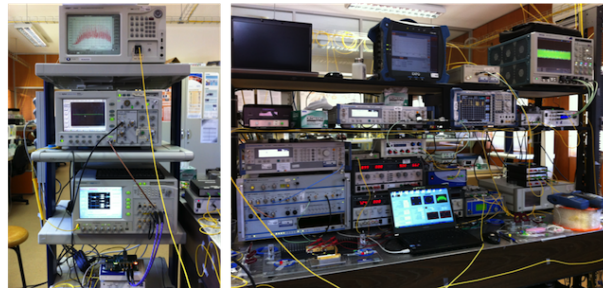
Figure 2.4: Picture of the instrumentation used in the experiments.

The experimental setup is depicted in Fig. 2.5. An External Cavity Laser (ECL) source with ∼100 kHz–linewidth is modulated using IQ Modulator (IQM) fed with two 625 Mb/s NRZ electrical signals. Each electrical signal carries 2^9 Pseudo Random Binary Sequence (PRBS). The resulting optical 1.25 Gb/s–QPSK is injected to a MZM driven by two 3.125 GHz radio frequency signals with phase relation between them around $3\pi/2$. The QPSK channels, equally spaced by 3.125 GHz, are filtered by a Wave Shaper (WS) (Finisar 4000S) tuned to 50 GHz of bandwidth. The optical power is set to around -3 dBm per channel using an Erbium-Doped Fiber Amplifier (EDFA).

The Ultra-Dense Wavelength-Division Multiplexing (UDWDM) comb is multiplexed with a 10 Gb/s–NRZ channel via a 100 GHz–WDM filter. The 10G–NRZ, whose extinction ratio is limited to 10 dB and optical power adjusted using an EDFA, is based on an Electro-absorption Modulator integrated Laser (EML) fed with 2^{23} PRBS. This channel has different guard bands to the center QPSK channel (channel under test) as depicted in the measured optical spectra using a Optical Spectrum Analyzer (OSA) (Apex) shown in Fig. 2.5(b): 100 GHz (0.8 nm), 150 GHz (1.2 nm) and 200 GHz (1.6 nm).

The total optical signal (UDWDM comb plus 10G–NRZ) is transmitted over 20 km of SSMF.

(a)

(b)
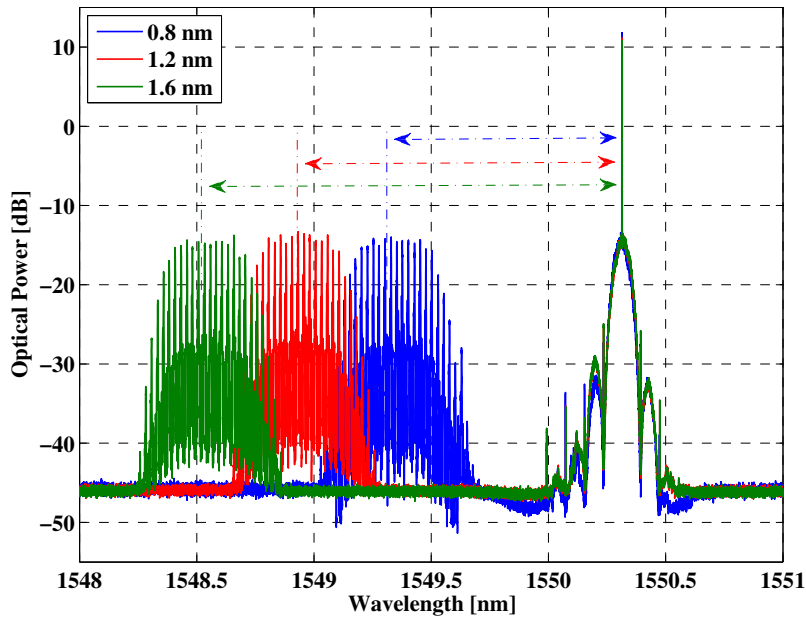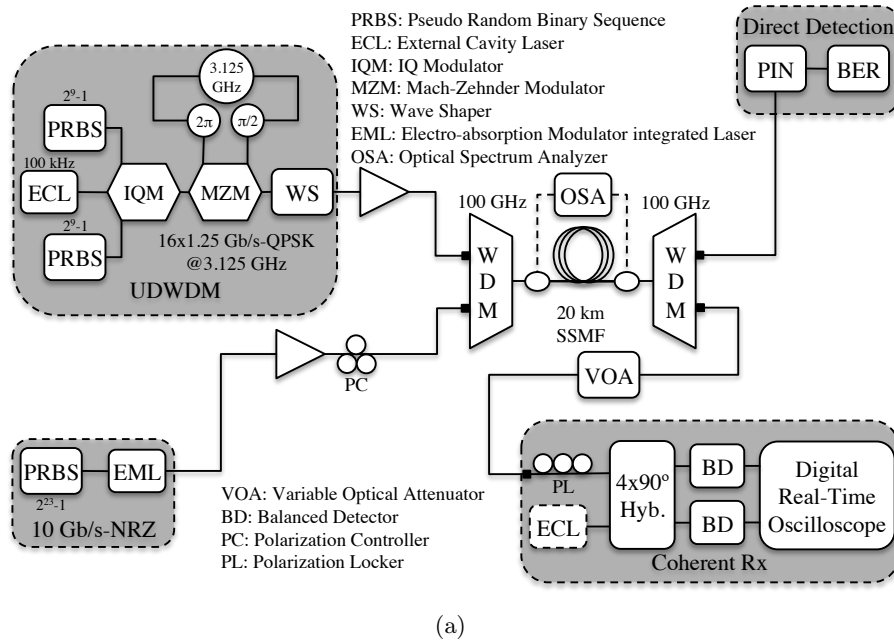
Figure 2.5: (a) Experimental setup: 16×1.25 Gb/s–QPSK + 10 Gb/s–NRZ. (b) Measured Optical Spectra for different guard bands between coherent QPSK and 10G–NRZ.

After transmission, the total signal is demultiplexed using a similar WDM filter as in the transmitter side. The 10G–NRZ reaches a direct detection receiver whereas the UDWDM comb transporting all the QPSK channels reach the coherent receiver depicted in Fig. 2.5(a).

Although the 10G–NRZ channel performance is not reported in this work, the simulations carried out in sub-section 2.4.1 indicate that the effect of UDWDM comb on 10G–NRZ is minimal for guard bands higher than 100 GHz. Thus, the experimental validation is focused on the performance of the QPSK channels. The received QPSK signals are mixed with the local oscillator tuned to the center channel under test using a $2 \times 4 - 90^o$ optical hybrid. The optical signal is then converted to the electrical domain using a pair of Balanced Detectors (BD). The resulting analog electrical signal is converted to the digital domain using a 100 GSample/s real-time oscilloscope with analog bandwidth around 20 GHz (Tektronix MS072004C).

To recover the data information, DSP techniques are applied as follows: Firstly, the digital signal is normalized (unitary average constellation energy) and synchronized to the transmitted symbols. Then, a low-pass filter with bandwidth around $0.8\times$ the symbol rate ($\sim$500 MHz) is applied to remove the information from the neighboring channels. We point out that digital CD compensation is not applied since the temporal effects in such a transmission system is negligible, as discussed in sub-section 2.4.4. The signal is down-sampled to 1 sample per symbol. To recover both phase and frequency, Viterbi and Viterbi algorithm is applied to the QPSK constellation with averaging filter using 4 samples to estimate the phase error. The performance of the network is measured as the root mean squared EVM (EVM_{rms}). The EVM is estimated between a block of 512 recovered symbols at the receiver with respect to the ideal transmitted symbols. Finally, EVM is averaged over 16 independent measurements (totaling nearly 8200 measured symbols) to establish a 95 % confidence interval.

For validation purpose, a set of simulations with the methodologies described in sub-section 2.1.1 has been carried out under similar conditions as the experiments. The propagation model used for simulating the optical fiber is the symmetric SSF with very high spatial and temporal resolutions and 3rd order VSTF. The EVM results obtained from simulations are calculated considering 32 independent simulations.

Fig. 2.6, Fig. 2.7 and Fig. 2.8 show the EVM (center channel) obtained from both measurements and simulations versus input power of 10G–NRZ channel (average optical power) for guard bands equal to 100 GHz (0.8 nm), 150 GHz (1.2 nm) and 200 GHz (1.6 nm), respectively. The measurement results are identified with filled circles ("$\bullet$") whereas the simulation results are represented by open squares (SSF) and open diamonds (VSTF). It is also shown in the figures the cubic interpolation for the simulated data represented by a solid line. Vertical

bars identify the confidence interval for the two methodologies.
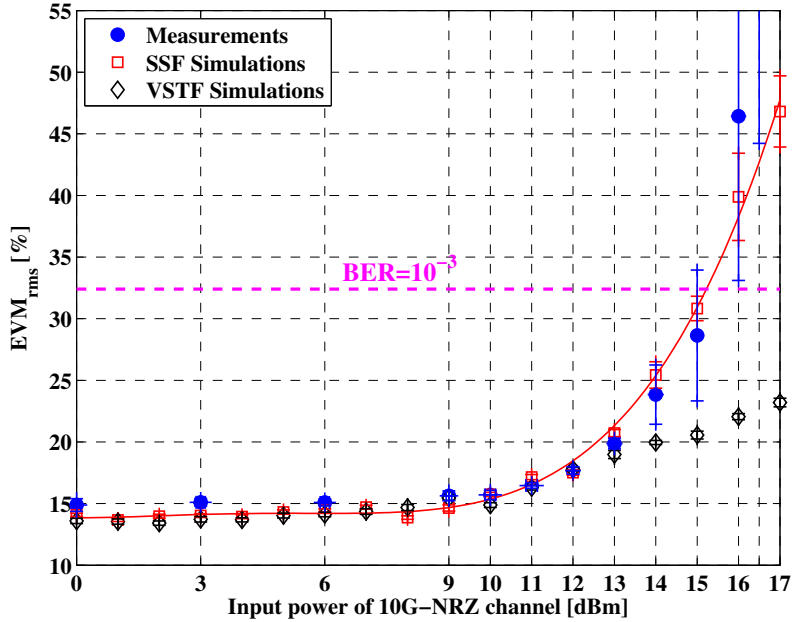
Figure 2.6: EVM versus input power of 10G–NRZ channel for guard bands of 100 GHz (0.8 nm). Filled markers: measurements. Open markers: simulations. Solid lines: interpolation for the simulated results. Vertical bars: confidence interval.

For all tested guard bands shown in Fig. 2.6, Fig. 2.7 and Fig. 2.8 the simulation model (based on SSF simulations), used throughout this work, provides very similar EVM results as the ones obtained from the experiments for input powers of the 10G–NRZ channel up to 16.5 dBm. It is important to highlight that results for 100 GHz and power higher than 15 dBm present a slightly divergence from the average EVM obtained from simulations. In addition, VSTF method is able to estimate accurately EVM results for powers up to 13 dBm, 14 dBm and 15 dBm for 100 GHz, 150 GHz and 200 GHz, respectively.

As expected, the inter-channel nonlinearities play an important role on the system's performance: as the input power increases and the guard band reduces, inter-channel nonlinearities increase. Therefore, as the input power increases higher than 14 dBm, due to inter-channel nonlinearies, the measured EVM results obtained higher uncertainty (represented by the vertical bars) for guard bands of 100 GHz and 150 GHz. For guard band equal to 200 GHz, the uncertainty in the EVM estimation is decreased compared to lower guard bands.

For powers higher than 10 dBm, the EVM increases roughly with the squared input power,
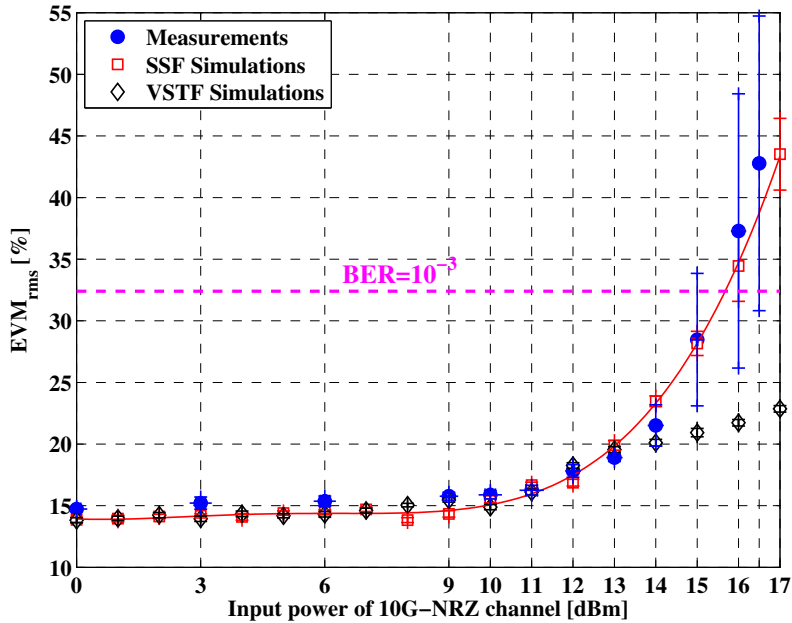
Figure 2.7: EVM versus input power of 10G–NRZ channel for guard bands of 150 GHz (1.2 nm). Filled markers: measurements. Open markers: simulations. Solid lines: interpolation for the simulated results. Vertical bars: confidence interval.

i.e. EVM increases by 2 dB every 1 dB increase in the input power. This power dependence is also confirmed by the results presented in Chapter 4. The EVM dependence on guard band is only noticeable for input powers higher than 15 dBm. Such a high power is particularly relevant since some PON technologies, as some XG-PON transmitter classes for instance, may operate at power as high as 16.5 dBm. See sub-section 2.4.2.

As far as the network performance is concerned, EVM of 32.4 % (SNR$\approx$9.8 dB), which corresponds theoretically to BER=10^{-3}, is achieved for input powers around 15 dBm, 15.6 dBm and 16 dBm at 100 GHz (Fig. 2.6), 150 GHz (Fig. 2.7) and 200 GHz (Fig. 2.8), respectively. Using simple DSP in the ONU provides EVM performance below 20 % (SNR$\approx$14 dB) when the 10G–NRZ input power is limited to 12 dBm even for such narrow guard bands. These results show that coherent UDWDM-PONs can share the same fiber plant with other PON technologies such as 10 Gb/s Ethernet Passive Optical Networks (10G-EPON) and XG-PON that can require optical power nearly to 17 dBm.
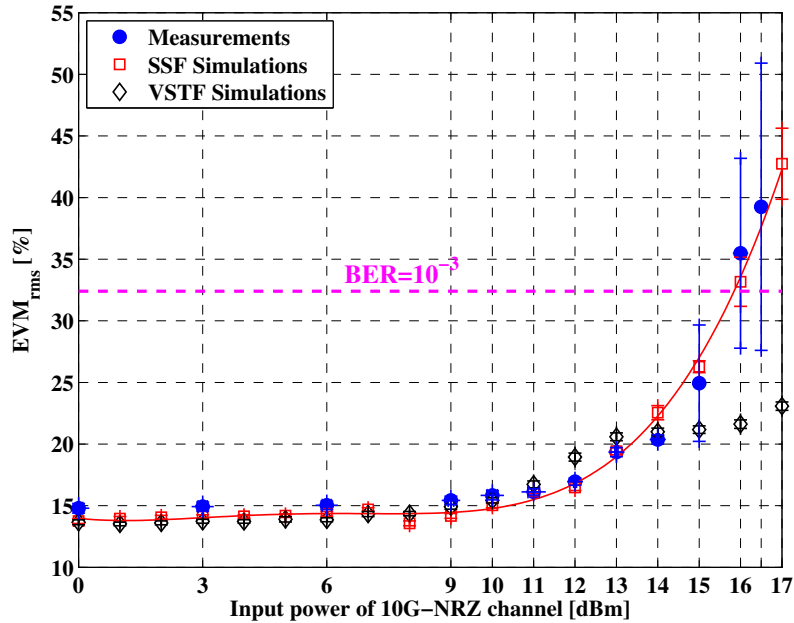
Figure 2.8: EVM versus input power of 10G–NRZ channel for guard bands of 200 GHz (1.6 nm). Filled markers: measurements. Open markers: simulations. Solid lines: interpolation for the simulated results. Vertical bars: confidence interval.

2.3 Optical Line Termination

User density depends on two crucial variables: *channel spacing* and *number of channels* (or wavelengths). In order to maximize the number of users, the channel spacing has to be reduced in order to save the already populated wavelength spectrum. This section discusses the implications of using reduced channel spacing in the OLT, thereby willing to answer the following question.

What should be a compromise minimum bandwidth on coherent UDWDM-PON technologies?

2.3.1 User Density

The results in Fig. 2.9(a) outline the performance of the *homogeneous* coherent scenario in terms of the worst EVM (center channel) among all channels under test as a function of the channel spacing for input powers per channel (average optical power) -6 dBm and -3 dBm in blue solid line and red dash line, respectively. We evaluated the performance of 32 channels at 1.25 Gb/s–QPSK after transmission over 25 km (circles), 60 km (squares) and 100 km

(diamonds) of SSMF fiber. Fig. 2.9(b) highlights the EVM distribution among all tested channels at 3.125 GHz frequency grid. We point out that all fiber spans considered in the simulations (25 km, 60 km and 100 km) have very similar performance for channel spacing higher than 2 GHz indicating that coherent UDWDM-PON can have extended reach as high as 100 km with splitting ratios as high as 1:32.

The system spectral efficiency, as described before, is defined in terms of the aggregated bit rate (32 × 1.25 Gb/s = 40 Gb/s) divided by the total occupied bandwidth (number of channels N_{ch} × channel spacing) decreases as the channel spacing increases. Therefore, lower channel spacing gives better spectral efficiency, e.g. at 1.5625 GHz channel spacing gives spectral efficiency of 0.8 bit/s/Hz. On the other hand, operating at 1.5625 GHz the system is severally impaired by inter-channel nonlinear crosstalk resulting EVM around 15 % even for the -6 dBm per channel case. The solution is to operate at channel spacing higher than 3.125 GHz resulting in spectral efficiency equal to 0.40 bit/s/Hz that assures EVM below the 10 % limit [34]. This limit corresponds to a system error free if the signal is corrupted by Gaussian amplitude and phase noises. Also indicated in the figure is the dash line around EVM=32.4 %, refer to Appendix A.

2.4   Optical Distribution Network

After defining the transmitter specifications that maximize spectral efficiency, this section describes the requirements in the ODN, which includes fiber plus a passive power splitter router. Shared ODN by different technologies, accumulated chromatic dispersion and splitting ratios are investigated in order to maximize the system's spectral efficiency. Therefore, the focus of this section is to address the following questions.

How close can coherent channels coexist with other PON technologies?

How many channels or splitting ratio can we aggregate per band in existing AWG?

Is chromatic dispersion a problem for coherent optical access networks?
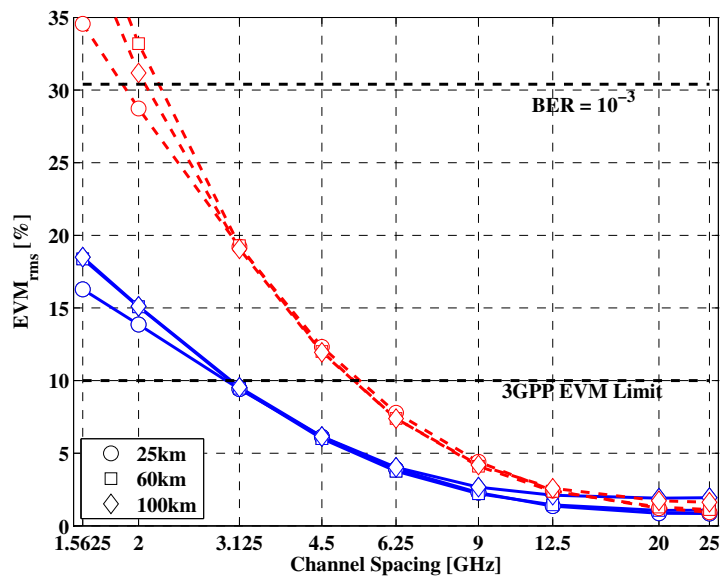
(a)
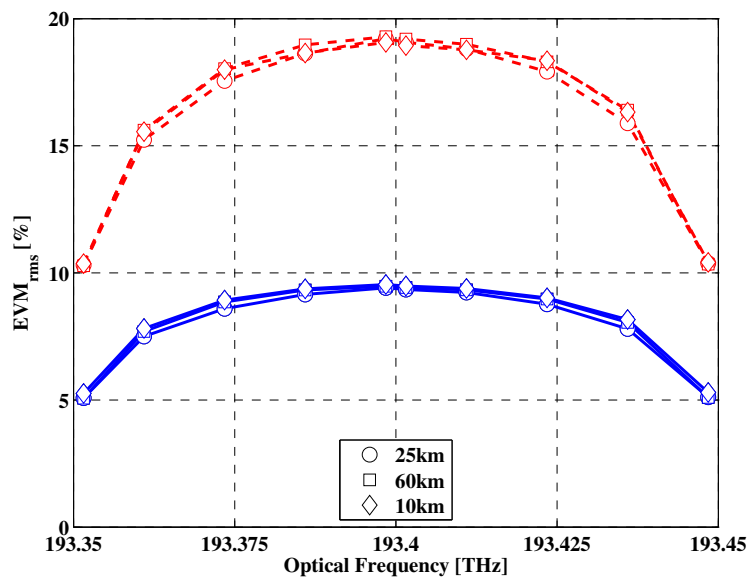
(b)

Figure 2.9: (a) EVM for various channel densities at 32 channels. (b) EVM distribution among tested channels at 3.125 GHz grid. Blue solid lines: -6 dBm per channel; red dash lines: -3 dBm per channel.

2.4.1   Guard Band to GPON

The International Telecommunication Union - Telecommunication Standardization Sector (ITU-T) recommendation G.984.2 [35] specifies the physical layer requirements and characteristics for the physical media dependent layer of GPON deployments. This PON technology offers the integration of voice, Time-Division Multiplexing (TDM), Ethernet (10/100 BaseT), leased lines, wireless extension etc. The main characteristics may include: physical reach of 20 km (60 km logical reach supported by protocol); line rates of 1244.16 Mb/s and 2488.32 Mb/s in the downstream directions and 155.52 Mb/s, 622.08 Mb/s, 1244.16 Mb/s and 2488.32 Mb/s in the upstream direction; operating wavelength for upstream is 1310 nm ±50 nm whereas 1490 nm ±10 nm is reserved for downstream direction for single-fiber systems. Depending on the line rates, there are 3 classes for the operating optical power in the transceiver. Below, it is listed in Table 2.1 [35] the transmitter power classes defined for the downstream at 2488.32 Mb/s and upstream at 1244.16 Mb/s operations:

Table 2.1: Mean launched power for GPON transceivers.

1244.16 Mb/s upstream	A	B	C
Min	-3 dBm	-2 dBm	+2 dBm
Max	+2 dBm	+3 dBm	+7 dBm
2488.32 Mb/s downstream	**A**	**B**	**C**
Min	0 dBm	+5 dBm	+3 dBm
Max	+4 dBm	+9 dBm	+7 dBm

Table 2.1 is the reference for the power levels and bit rates used in this section to address the performance of the *fully transparent heterogeneous* network in Fig. 2.3(b). This scenario consists of 31 coherent QPSK channels coexisting with one NRZ–IMDD channel followed by transmission over 25 km of SSMF. The performance is evaluated in terms of the EVM in % of the 31st QPSK channel as a function of the guard band to the IMDD channel. The coherent -3 dBm–QPSK channels operated in 1.25 Gb/s whereas the IMDD channel operated either at 1.25 Gb/s or 2.5 Gb/s.

Fig. 2.10(a) shows the performance after transmission versus the guard band to the IMDD channel operated at 1.25 Gb/s. The inset in Fig. 2.10 depicts the EVM distribution among all tested channels at 3.125 GHz guard band. The EVM curve in the green dash-dot line represents
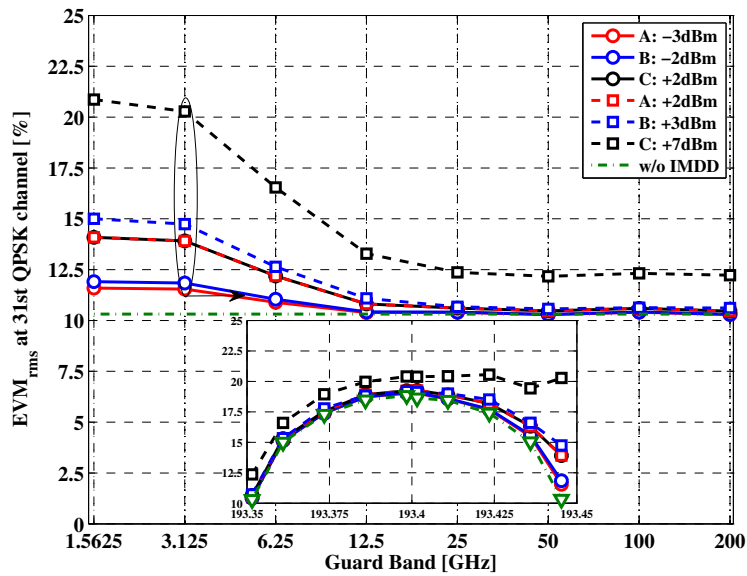
(a)
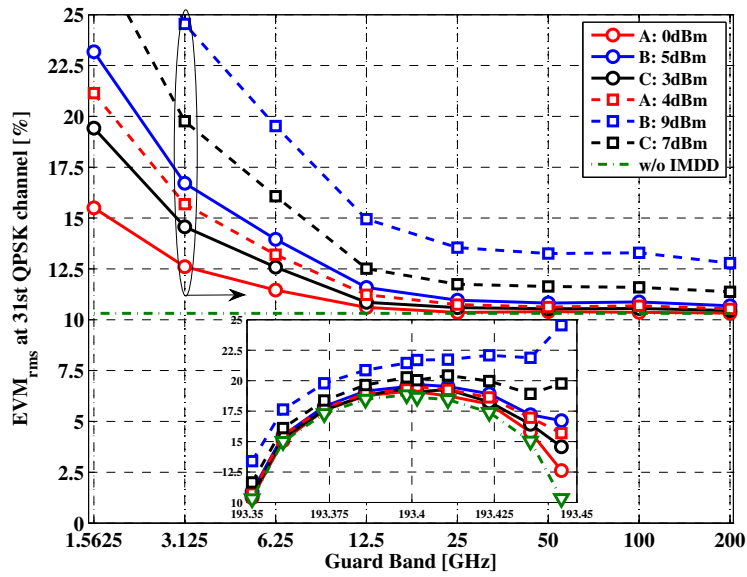
(b)

Figure 2.10: EVM of the received 31st QPSK versus guard band to the IMDD channel with different GPON transmitter powers at (a) 1.25 Gb/s and (b) 2.5 Gb/s. Insets show the EVM distribution among tested channels at 3.125 GHz guard band. Green dash-dot line: reference curve without the IMDD channel.

the performance of the *homogeneous* network without the IMDD channel. The IMDD channel has different laser powers compatible with the specifications for GPON equipment (Table 2.1)

in the ONU transmitters for upstream direction, i.e. from ONU to OLT [35]. The EVM curves point out that guard bands higher than 12.5 GHz is sufficient to minimize the cross effect impact on the system's performance. This results from the fact that the IMDD channel contribution to FWM components starts to be negligible since the phase matching condition stop being satisfied for higher guard bands. Additionally, for guard bands higher than 12.5 GHz the extra penalty on the system's performance is contributed mostly by XPM induced by the IMDD channel up to 200 GHz.

The XPM effect is enhanced for higher power categories of GPON transmitters, i.e. class C with max laser power of 7 dBm. For other classes where the power is below 3 dBm XPM effect is negligible since the EVM converges to the reference system without the IMDD channel, identified by the green line at EVM=10.3 %. It is worth pointing out that crosstalk between the IMDD and 31st QPSK channels is very strong when the guard band is only 1.5625 GHz. In this case, the EVM accounts for both linear and nonlinear crosstalk.

Fig. 2.10(b) shows the performance of the *heterogeneous* scenario when the IMDD channel operates at 2.5 Gb/s. The inset highlights the distribution of the EVM among all tested channels when the guard band is 3.125 GHz. The IMDD power in this case is compatible with GPON classes in the OLT transmitters for downstream direction, i.e. OLT to ONU [35]. As discussed before, 12.5 GHz is sufficient to reduce the FWM impact on the system although these classes require much higher power than the 1.25 Gb/s–IMDD specifications. The overlapping in power occurs for the maximum power of class C at 1.25 Gb/s and 2.5 Gb/s. As such, this overlapping allows analyzing the dependence of XPM on the IMDD bit rate. In the regime where XPM is dominant (guard band > 12.5 GHz) the black dash-lines in Fig. 2.10(a) and 2.10(b) show that its impact is slightly reduced when the IMDD channel operates at 2.5 Gb/s, e.g. $EVM_{1.25\ Gb/s@200\ GHz} = 12.3$ % and $EVM_{2.5\ Gb/s@200\ GHz} = 11.3$ %.

To identify the performance of the IMDD channel impaired by linear and nonlinear crosstalk induced by coherent QPSK channels in the *heterogeneous* scenario, Fig. 2.11 analyzes the Q factor of the IMDD channel as a function of guard band. Classes with lower transmitter powers are more affected by crosstalk (lower Q) since the signal–to–interference ratio is reduced. Guard bands higher than 6.5 GHz assure error free operation (Q>15.5∼dB) without recurring to FEC for both 1.25 Gb/s (Fig. 2.11(a)) and 2.5 Gb/s (Fig. 2.11(b)) systems. On the
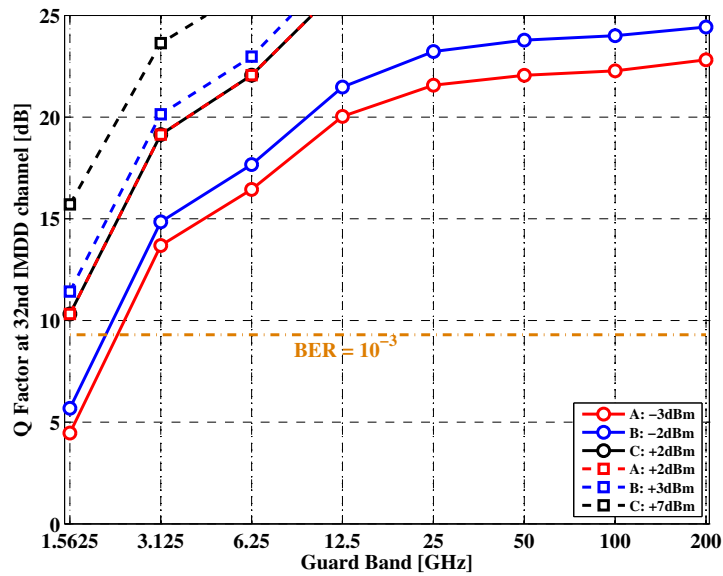
(a)
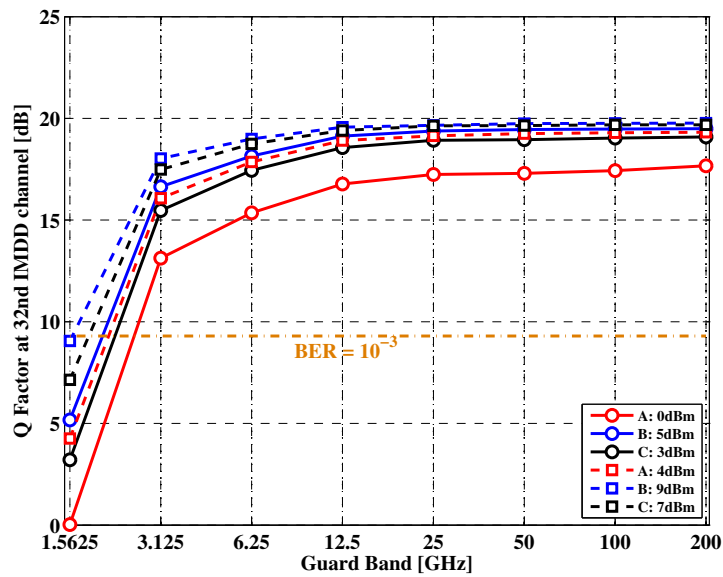
(b)

Figure 2.11: Q factor of the IMDD channel as a function of guard band at (a) 1.25 Gb/s and (b) 2.5 Gb/s with different GPON transmitter powers. The orange dash-dot line theoretically corresponds to a system BER=10^{-3} (FEC limit).

other hand, the system may operate at 3.125 GHz guard band if FEC is employed. The Q factor is limited to around 20 dB when the IMDD channel operates at 2.5 Gb/s. This comes

from that fact that there is a 5 GHz–filter at transmitter and receiver sides, thereby imposing stronger Inter-Symbol Interference (ISI) in 2.5 Gb/s–signal than in 1.25 Gb/s–signal. These filtering effects are highlighted in the received electrical eye diagrams of Fig. 2.12.
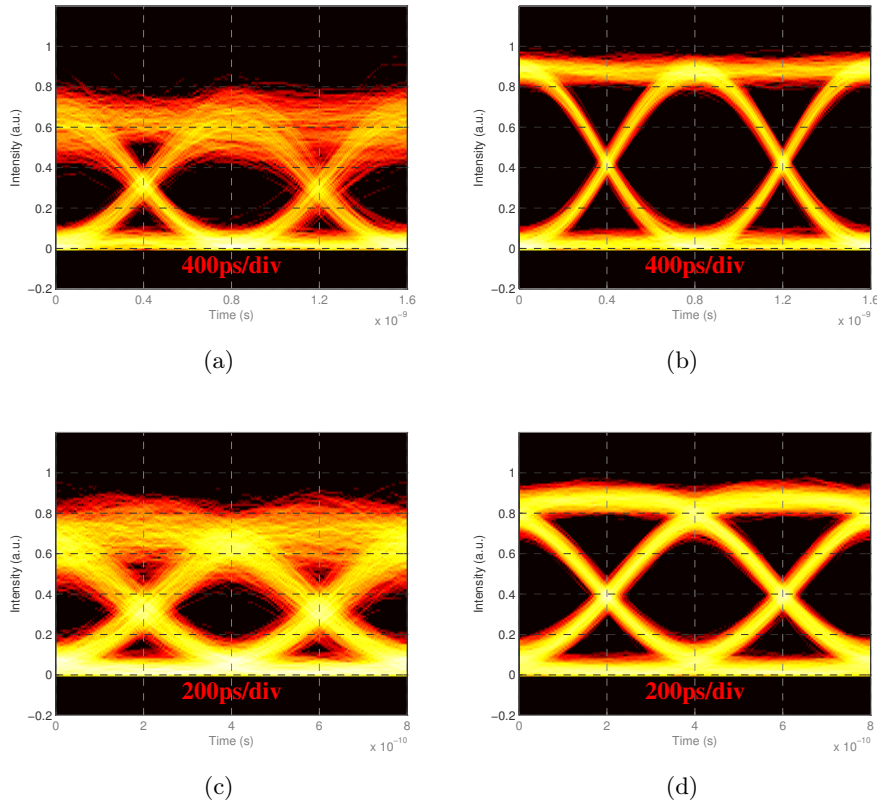
Figure 2.12: Received electrical eye diagrams. (a) 1.25 Gb/s with -3 dBm at 3.125 GHz; (b) 1.25 Gb/s with -3 dBm at 200 GHz; (c) 2.5 Gb/s with 0 dBm at 3.125 GHz; (d) 2.5 Gb/s with 0 dBm at 200 GHz.

2.4.2   Guard Band to XG-PON

ITU-T recently defined an upgraded version of GPON, the so called XG-PON G.987.1 [36], which supports asymmetric 9.95328 Gb/s downstream and 2.48832 Gb/s upstream (XG-PON1). Another version, XG-PON2 is designed to support symmetric 9.95328 Gb/s. This broadband access technology is defined to have full compatibility with GPON and video distribution service thanks to a wavelength plan, blocking filters and loss budget that allow coexistence on a common PON infrastructure. Besides higher bit rates, reach and splitter ratio is extended up to 60 km and 1:128 respectively. The operating wavelength for downstream is 1578 nm ±3

nm whereas the upstream transmission is performed at 1270 nm ±10 nm. The power levels in the XG-PON transceivers are specified in the G.987.2 recommendation [37]. These power levels for both Nominal (N) and Extended (E) classes are listed below in Table 2.2.

Table 2.2: Mean launched power for XG-PON transceivers.

10 Gb/s downstream	N1	N2a	N2b	E1	E2a	E2b
Min	2 dBm	4 dBm	10.5 dBm	6 dBm	8 dBm	14.5 dBm
Max	6 dBm	8 dBm	12.5 dBm	10 dBm	12 dBm	16.5 dBm
2.5 Gb/s upstream	**N1**	**N2**		**E1**	**E2**	
Min	2 dBm	2 dBm		2 dBm	2 dBm	
Max	7 dBm	7 dBm		7 dBm	7 dBm	

In terms of cross effect with next-generation technologies, it is relevant to analyze heterogeneous scenarios in which the XG-PON transceiver operates at classes with higher transmitting power, e.g. classes E in downstream direction. This section, therefore, addresses the dependence of the *heterogeneous* network scenario on the coexistence with XG-PON equipment. Although both PON standards are based on IMDD systems, XG-PON equipment requires much more power than GPON, thereby inducing more nonlinear crosstalk on coherent channels. In Fig. 2.13 is shown the optical spectra after the fiber with the coherent channel under test and the IMDD channel that simulates XG-PON channel at guard band 12.5 GHz (Fig 2.13(a)) and 200 GHz (Fig. 2.13(b)). In this case, the optical filters at transmitter and receiver sides for the IMDD channel were increased to 40 GHz.

Fig. 2.13(c) shows the performance of the *heterogeneous* scenario, consisting of thirty one 2.5 Gb/s–QPSK channels coexisting with one 10 Gb/s–IMDD channel, after transmission over 25 km of SSMF. This performance is evaluated in terms of the EVM in % of the 31st QPSK channel as a function of the guard band to the 10 Gb/s–IMDD channel as illustrated in Fig. 2.13(a) and 2.13(b). Fig. 2.13(d) depicts the EVM distribution among all tested channels at 100 GHz guard band. The IMDD channel has different powers compatible with the specifications for XG-PON equipments (third row of Table 2.2) in the OLT for downstream, i.e. from OLT to ONU [37]. The results depicted by green dash-dot lines represent the system without the presence of the XG-PON equipment. In this case, the performance is essentially limited by FWM among -6 dBm–QPSK channels.

The EVM curves point out that guard bands higher than 100 GHz are sufficient to min-

(a)

(b)

(c)

(d)
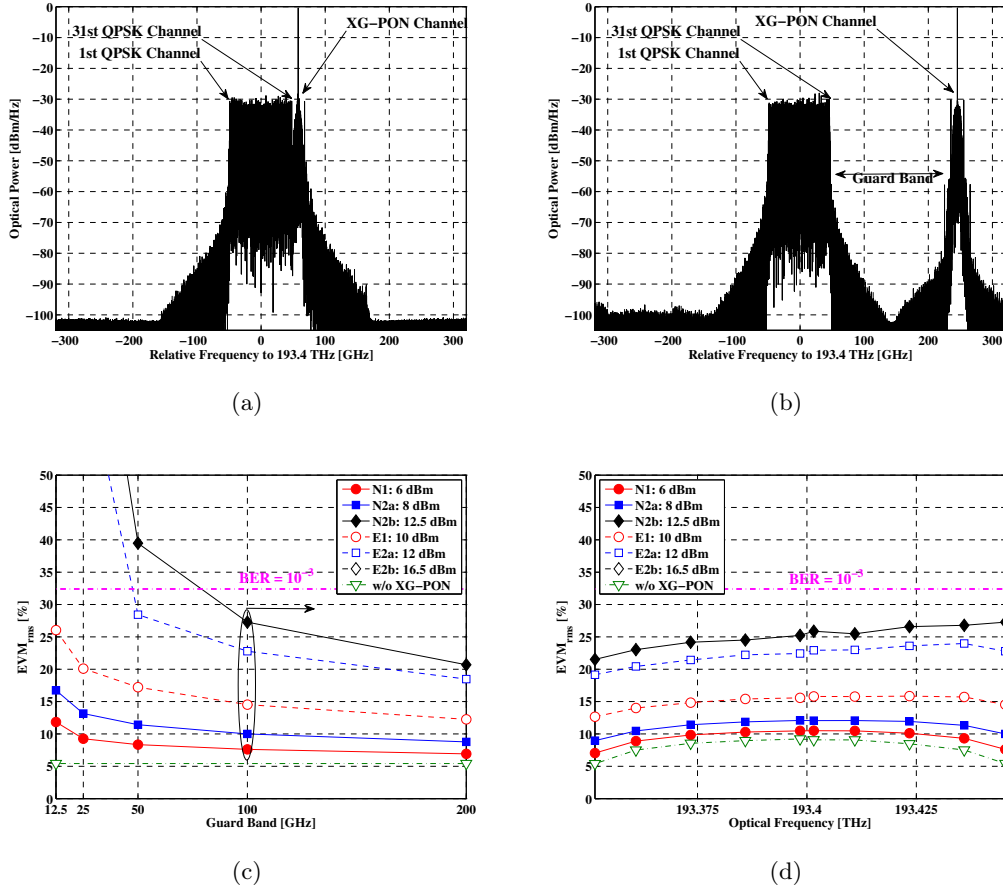
Figure 2.13: 31x2.5 Gb/s–QPSK + XG-PON with variable guard band: (a) 12.5 GHz guard band; (b) 200 GHz guard band. (c) EVM of the received 31st QPSK versus guard band to the 10 Gb/s–IMDD channel with different XG-PON transmitter powers. (d) EVM distribution among all tested channels at 100 GHz guard band. Green dash-dot line: reference curve without the 10 Gb/s–IMDD channel

imize the cross effects due to FWM and XPM in the coherent channel, thus maintaining its performance below the theoretical BER of 10^{-3}. Additionally, for lower XG-PON powers, the performance of the heterogeneous system tends to the reference green line representing the system without the IMDD channel.

For transmitter powers higher than 16 dBm, as in the E_{2b} specification not shown in Fig. 2.13, the guard band to the XG-PON has to be higher than 200 GHz so that the coherent receiver is able to recover the information. Using guard bands not multiple of $\log_2(\Delta f/3.125)$, e.g. 250 GHz, makes the system unequally spaced, thereby mitigating some of the FWM crosstalk as discussed in Chapter 5. The remaining EVM penalty, due to the cross effect with

the XG-PON channel, in the 200 GHz guard band is as follows: 2.1 dB for N_1, 4.1 dB for N_{2a}, 11.6 dB for N_{2b}, 7.0 dB for E_1, 10.6 dB for E_{2a} and 24.8 dB for E_{2b}.

2.4.3   Splitting Ratio versus AWG Band

Since UDWDM-PON uses several channels, it is important to estimate if there is a limit in which the performance for the different architectures discussed in Section 2.1 saturates, thus allowing to increase the number of ultra-dense QPSK channels up to 1000. The methodology is described as follows: the AWG bandwidths vary from 6.25 GHz until 200 GHz for the *homogeneous* network; broader bandwidths allow higher ultra-dense channels aggregated per AWG port; the number of ultra-dense channels per AWG port defines the splitting ratio at ODN. For instance, a 50 GHz–AWG allows multiplex/demultiplex 8 ultra-dense channels (8 × 3.125 GHz = 25 GHz) and distributed via 1:8 power splitter.

Fig. 2.14 shows the overall performance (center channel) of the *filtered* (diamonds), *hybrid* (circles) and *fully transparent* (squares) architectures as a function of average input optical power per channel for different splitting ratios (or ultra-dense channels) and AWG bandwidths. From Fig. 2.14 we can conclude that:
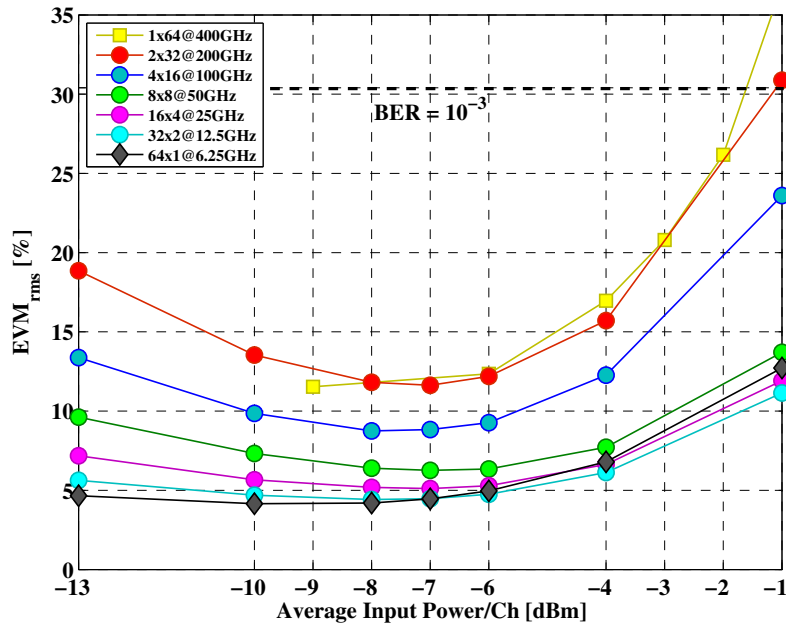
Figure 2.14: EVM in percentage of the center QPSK channel as a function of input power per channel for different AWG ports versus ultra-dense channels (splitting ratio) per AWG bands.

1. for splitting factors up to 8 (8 ultra-dense channels shown by green line plus circles), the system has better overall performance (lower EVM) since nonlinear crosstalk is reduced;

2. for splitting factors higher than 16, the system's performance is severely limited by nonlinear crosstalk as shown by blue, red and yellow curves representing respectively the *hybrid* architecture with 16 channels via 100 GHz–AWG, 32 channels via 200 GHz–AWG and the *fully transparent* with 64 channels equally spaced by 3.125 GHz;

3. upgrading the system from 32 to 64 channels will result in similar performance indicating that we can increase even further the number of channels or users to 128, 256, 512 up to a 1024 × 1 Gb/s with similar performance to the 32–channel case.

The latter can be justified by the fact that the impact of FWM saturates for channel count around 32 channels when transporting only phase-modulated channels. Better performance can be achieved when using unequally channel spacing [C2] to minimize some of the FWM crosstalk, as discussed in Chapter 5.

As discussed in Section 2.1, coherent UDWDM-PON with higher splitting ratios (≥ 16) or broader AWG bandwidths (≥ 100 GHz) provides increased spectral efficiency and flexibility / upgradeability since ultra-dense channels can be trade by channels transporting higher speed technologies such as 10G/40G and 100GbE.

2.4.4   Chromatic Dispersion

One of the advantages of coherent WDM-PON is the DSP in the ONUs to compensate transceivers and some of the transmission impairments. Among the transmission impairments, state of the art DSP effectively compensates for linear effects as the CD and Polarization-Mode Dispersion (PMD). As far as CD is concern, it is important to analyze the effect on the efficiency of fiber nonlinearities as well as the induced ISI on the received signal. Therefore, we simulate the *homogeneous* network without CD compensation transporting 32 ultra-channels modulated either at 1.25 Gb/s–QPSK or 2.5 Gb/s–16-ary Quadrature Amplitude Modulation (16QAM) after transmission over 20 km of SSMF.

The results in Fig. 2.15 show the performance in terms of the EVM of the center channels versus the CD for various input powers per channel. By analyzing these results we can conclude that CD plays an important role on the efficiency of fiber nonlinearities rather than
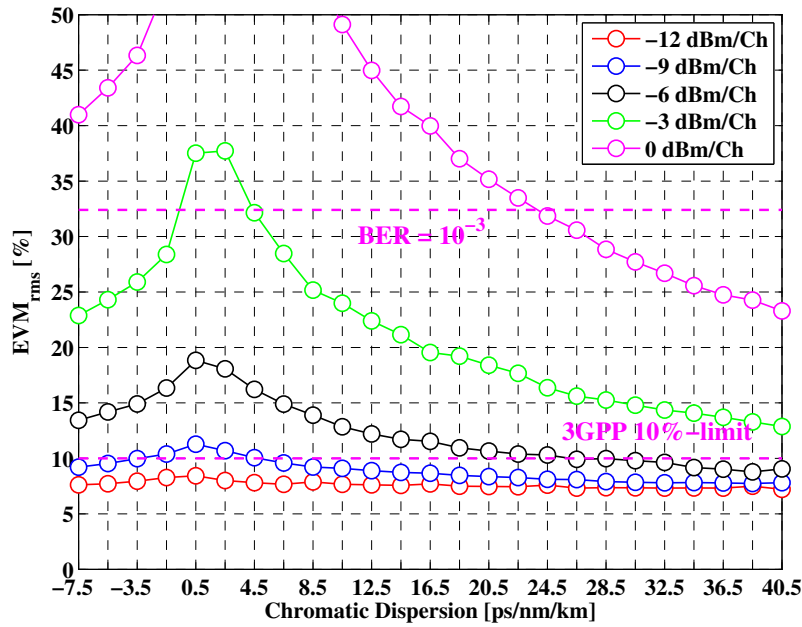
(a)
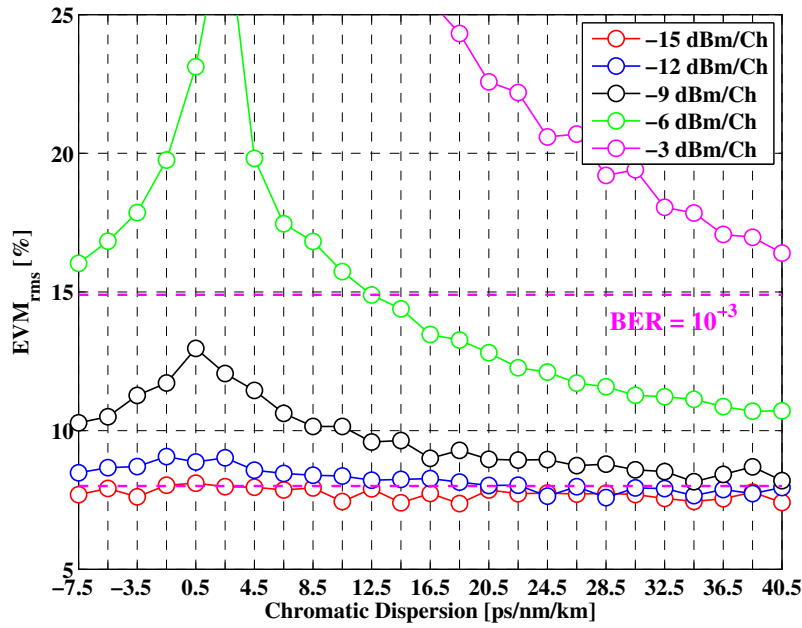
(b)

Figure 2.15: EVM in percentage of the center channel after 20 km as a function of Chromatic Dispersion for: (a) 1.25 Gb/s–QPSK; (b) 2.5 Gb/s–16QAM.

by inducing ISI in the received signal at 625 Mbaud over one span of SSMF. For instance, in the high power regime (higher than -6 dBm per channel), decreasing dispersion increases the efficiency of FWM; thus the system's performance is strongly limited by nonlinear crosstalk. For lower power regime, the system's performance does not depend on Chromatic Dispersion although neither electrical nor optical compensation was performed in the receiver side.

2.5   Optical Network Unit

This section addresses the network limitations imposed by the coherent receiver in the ONUs when the upgrade of the user's data rate is considered. On that matter, two questions have to be asked:

What if 1 Gb/s per subscriber per polarization is not enough?

How to compensate for the phase noise induced by the local oscillator in the ONUs?

2.5.1   ADC Resolution

Current works have been describing UDWDM-PON systems targeting 1.25 Gb/s per subscriber [28, 29, 10]. On the other hand, one may argue that some future applications can require even higher data rates per channel. Therefore, it is quite challenging to deliver 10 Gb/s per wavelength/subscriber (single polarization) in a 3 GHz frequency grid using QPSK only. One solution is to (i) increase the baud rate to 1.25 Gbaud and (ii) use higher order modulation formats such that the net data rates increase to 3.75 Gb/s, 5 Gb/s, 7.5 Gb/s and 10 Gb/s employing 8-ary Phase-Shift Keying (8PSK), 16QAM, 64-ary Quadrature Amplitude Modulation (64QAM) and 256-ary Quadrature Amplitude Modulation (256QAM), respectively.

If we assume the electronics required at both transmitter and receiver for 625 Mbaud is about the same as for 1.25 Gbaud, the optical counterpart does not change significantly from the model depicted in Fig. 2.3(a). Since the signals are generated electrically at the transmitter side and processed digitally at the receiver side, the coding/decoding process for recovering the digital information is very easily adapted allowing different signal constellations. One of the limiting factors is related to the ADC characteristics.

In access networks applications where the accumulated dispersion is not an issue for signals
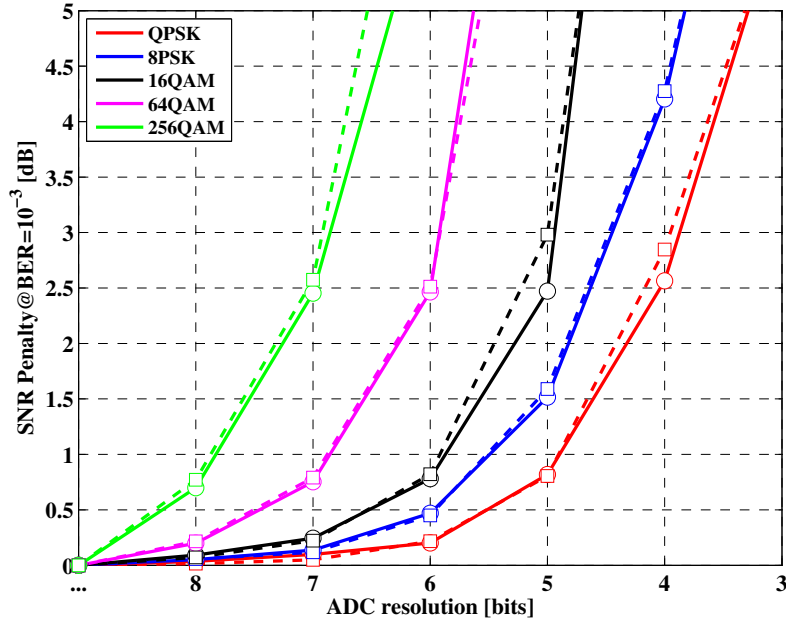
Figure 2.16: SNR Penalty at BER=10^{-3} versus ADC resolution in bits for different modulation formats: 625 Mbaud – solid lines + circles; 1.25 Gbaud – dash lines + squares.

at 625 Mbaud / 1250 Mbaud (see 2.4.4), sampling the signal at twice the baud rate may be sufficient, in most cases, for performing phase/carrier recovery and channel equalization (linear and nonlinear eventually). Thus ADC sampling rate is perfectly transparent to modulation formats at 625 Mbaud (1.25 GSample/s) or 1250 Mbaud (2.5 GSample/s) assuming electrical bandwidth broad enough to avoid distortion. On the other hand, different signal constellations require different ADC resolution (in bits) since higher order constellations are more sensitive to quantization errors. In this work we focus on the amplitude resolution of the ADC, remaining the time resolution subject for further studies.

We evaluate the SNR penalty for a system BER=10^{-3} as a function of ADC resolution for various modulation formats. In this case, the *fully transparent homogeneous* network scenario was evaluated in back–to–back for 4 ultra-dense channels at 625 Mbaud (256 steps of 2048 symbols = 524288 simulated symbols) and 1250 Mbaud (128 steps of 4096 symbols 524288 simulated symbols) in which the coherent receivers have similar algorithms for phase sync/re-timing as well as amplitude normalization (6 % of pilot symbols) for a fair comparison. The SNR was estimated from the actual root mean squared EVM, between received symbols $s_i^{'} = a_i^{'} + j * b_i^{'}$ and ideal transmitted symbols $s_i = a_i + j * b_i$ as defined in equation (2.1). We

used the closed expressions to relate EVM or SNR to BER for M-ary Quadrature Amplitude Modulation (QAM) [33] and M-ary Phase-Shift Keying (PSK) [38] signals as discussed in Appendix A.

From Fig. 2.16, we can draw the following conclusions:

- considering the 1 dB margin as the tolerable SNR penalty we found that QPSK at 1.25–2.5 Gb/s, 8PSK at 1.875–3.75 Gb/s, 16QAM at 2.5–5 Gb/s, 64QAM at 3.75–7.5 Gb/s and 256QAM at 5–10 Gb/s signals require ADC resolutions of 5, 6, 6, 7, and 8 bits, respectively;

- operating at 1.25 Gbaud imposes minimal penalty when compared to the system at 625 Mbaud assuming sufficient electrical bandwidths.

Those results are in agreement with the work in [39], i.e. the ADC resolution increases in 1 bit every time the levels in each signal's components (in-phase or quadrature) are doubled up. Furthermore, it is also included in Fig. 2.16 the results for 8PSK constellation (6 bits ADC resolution). This modulation format may be relevant when considering the upgradeability of the users' data rate from 1.25 Gb/s (QPSK) to 1.875 Gb/s (8PSK) keeping almost the same nonlinear transmission characteristics. The transmission impairment affecting the system's performance is mostly FWM as it will be detailed in Chapter 4.

2.5.2   Laser Linewidth

The advantage of using ONU as a coherent receiver is that the phase noise is mitigated digitally using well-known Carrier Phase Estimation/Recovery techniques. In this section we evaluate the phase noise in terms of the required linewidth to provide minimal SNR penalty with respect to BER=10^{-3}.

We used the same *fully transparent homogeneous* network described before operating at 625 Mbaud and 1.25 Gbaud per channel after 25 km of SSMF with the following input power per channel: -2 dBm/channel for QPSK, -4 dBm/channel for 8PSK and -6 dBm/channel for 16QAM. As a result, the system is entirely limited by inter-channel nonlinearities. In our simulations, 32 runs of 512 (625 Mbaud) and 1024 (1.25 Gbaud) symbols per channel were used for SNR estimation. After coherent detection at the ONU, we applied the Feed Forward M-th power block scheme described in [30] (field averaging) for phase estimation considering a

block size of 8 symbols for phase estimation. Fig. 2.17 depicts the SNR penalty at BER=10^{-3} of the received center channel as a function of linewidths per laser sources, i.e. the transmitter and local oscillator lasers have the same linewidths. Solid curves plus circles describe the system's performance operating at 625 Mbaud per channel whereas dash curves plus squares describe the system operation at 1.25 Gbaud per channel.
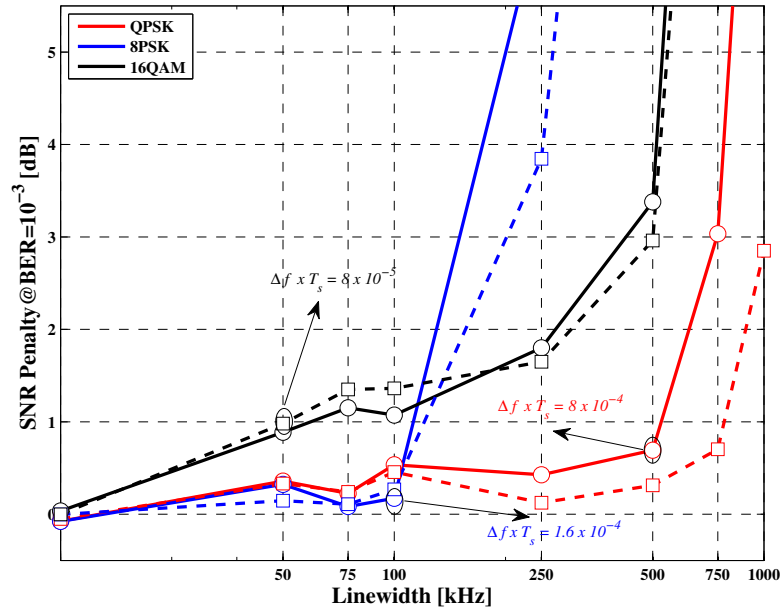
Figure 2.17: SNR Penalty at BER=10^{-3} versus linewidth per laser for different modulation formats: 625 Mbaud – solid lines + circles; 1.25 Gbaud – dash lines + squares. $\Delta f \times T_s = 8 \times 10^{-4}$ (QPSK); 1.6×10^{-4} (8PSK); 8×10^{-5} (16QAM).

The results for phase-modulated signals in red for QPSK (M=4) and black for 8PSK (M=8) show similar performance for the system operating either at 625 Mbaud or 1.25 Gbaud for lower linewidths. Allowing 1 dB penalty, QPSK is able to operate with linewidth per channel around 500 kHz whereas 8PSK should be around 100 kHz. On the other hand, 625 Mbaud–16QAM and 1.25 Gbaud–16QAM systems operate with 1.1 dB and 1.4 dB penalty at 100 kHz, respectively. In terms of the effective linewidth, defined as the linewidth per laser Δf times symbol duration T_s, we obtained the following values within the 1 dB margin: $\Delta f \times T_s = 8 \times 10^{-4}$ for QPSK, $\Delta f \times T_s = 1.6 \times 10^{-4}$ for 8PSK and $\Delta f \times T_s = 8 \times 10^{-5}$ for 16QAM. Note that the 16QAM transmission, on average only half of the 8 symbols is used for phase estimation, i.e. the inner and outer rings symbols used as for QPSK phase estimation.

The challenge on the UDWDM-PON system is the increased symbol duration (decreased symbol rate), which effectively reduces significantly the maximum tolerable linewidth. With symbol duration around $800 \sim 1600$ ps (symbol rates $1250 \sim 625$ Mbaud), the tested network should require linewidths ranging from only 500 kHz (625 Mbaud) to 1 MHz (1.25 Gbaud) if transporting QPSK ($\Delta f \times T_s \approx 8 \times 10^{-4}$) for instance. On the other hand, higher symbol rates alleviate the needs for narrower linewidths as in [39] where the authors found $\Delta f \times T_s \approx 4.1 \times 10^{-4}$, which gives maximum linewidth of 4.1 MHz for the system at 10 Gbaud–QPSK. Although we used fixed block-symbol (8 symbols) for different symbol rates we obtained slightly lower penalty for the system at 1.25 Gbaud compared to 625 Mbaud, as would be expected. This can be seen on the red curves (QPSK) in Fig. 2.17 for linewidths higher than 100 kHz. For the other modulation formats, the penalty was prohibitively high to see the benefit of increased symbol rate. We point out that those results present the effects of the laser linewidth as well as its interaction with Chromatic Dispersion and Kerr nonlinearities. Furthermore, this tolerance can be improved by optimizing the block length [40, 21]; by improving the field averaging filter for phase estimation in each block of symbols [41]; or by using more sophisticated schemes that take into account all symbols inside a block for phase estimation on QAM signals such as in [42, 21].

2.6   Conclusions

In this chapter we addressed some of the most relevant technical aspects and network sub-systems related to high data rate aggregate PONs at both simulation and experimental levels. In addition, an experimental validation of the simulation model is presented for a fully transparent heterogeneous network. Besides architectural aspects, several parameters in the OLT, ODN and ONUs were addressed to fulfill user requirements and cross effect among different PON technologies sharing the same fiber infrastructure. Coherent UDWDM based PON is a promising solution for Next-Generation all-Optical Access Networks capable of delivering over a 1000 users broadband connections at minimal occupied bandwidth. We concluded that coherent transceivers employing high-order modulation formats and digital signal processing gather the required conditions for tackling the needs for broadband in Optical Access Networks. The main advantages of this solution include wide wavelength tuning range ONUs, extended reach, high splitting ratios and simple data rate upgradeability.

One of the challenges related to this technology is the need for higher-order modulations to increase the net data rate. As demonstrated in this work, higher-order modulations are more sensitive to transceiver imperfections such as quantization errors, induced phase noise and filtering effects. Nevertheless, by employing advanced digital signal processing techniques may alleviate the needs for more expensive transceiver components. As far as the fiber channel is concerned, chromatic dispersion plays an important role on the nonlinear performance rather than inducing inter-symbol interference. Furthermore, the launched input power per channel and guard band to legacy PON technologies have to be optimized to avoid inter-channel fiber nonlinearities (cross-phase modulation and four-wave mixing) in both heterogeneous and homogeneous network scenarios. Modeling fiber nonlinearities is the subject of the following chapters.

Chapter 3

Volterra Series Transfer Function

As discussed in previous chapters, it is expected that strong fiber nonlinearities limit the system's performance when the channel spaced is reduced to only a few Gigahertz and the channel count is increased to 32, for instance. The launched power into the fiber and transmission distance are key variables to describe the nonlinear fiber's performance. Therefore, it is crucial to develop mathematical tools capable of analyzing and simulating the nonlinear propagation over the optical fiber.

SSF is the worldwide reference for emulating the light propagation over the optical fiber. It is a relatively fast numerical method for solving the Nonlinear Schrödinger Equation (NLSE) when the total field propagation is considered. It might be challenging, however, to model all different contributions of fiber nonlinearities for a multi-channel transmission system with very high channel count. Specifically, SSF has to be applied to every combination of a nonlinear term represented by a coupled NLSE. The number of nonlinear terms (each represented by a coupled equation) is proportional to the third power of channel count, thus over 32000 equations for a 32 channel system have to be solved using SSF to identify all the contributions of nonlinear effects.

One interesting methodology to model the nonlinear performance is based on perturbation approaches. They have been used for describing the performance for different fiber optic transmission systems, either with direct detection [43, 44] or coherent detection [45, 46, 47, 48]. Among them, Volterra theory has gained a lot of attention from the optical communication community due to its versatility in modeling the total field propagation, separate fiber nonlinearities or as a nonlinear filter in the digital domain. Volterra series has been proposed for modeling the nonlinear propagation over the optical fiber [25], modeling the nonlinear behav-

ior of laser diodes [49], post-processing fiber nonlinearities on coherent optical transmission systems [26], [J8]; analysis of fiber nonlinearities on direct detection systems [27] and coherent optical systems [J3, J1].

This chapter, based on Journals [J1], [J3] and [J4] and Conference papers [C9], [C11], [C14] and [C15], firstly discusses in Section 3.1 Volterra theory for the analysis of the overall system's performance. Section 3.2 shows how Volterra series calculate fiber nonlinearities in WDM transmission system. Section 3.3 presents an effective algorithm for solving numerically the integral in the nonlinear Volterra solution. Section 3.4 outlines the coherent UDWDM-PON scenario in which the overall system's performance is investigated. Section 3.5 validates the Volterra series method against Split-Step Fourier simulations in a UDWDM-PON scenario. Section 3.6 concludes the topics discussed in this chapter.

3.1   Volterra Theory

The goal of this chapter is to apply Volterra theory firstly to estimate the overall system's performance and secondly to identify the most relevant fiber nonlinear effects. The identification of fiber nonlinear effects requires a versatile model capable of analyzing the most relevant effects even for UDWDM transmission systems with the number of channel as high as 32. In addition, it should be able to analyze the nonlinear effects in phase-modulated and/or amplitude modulated channels. A deeper discussion on nonlinearities is given in sub-section 3.2. The overall system's performance is simply estimated after the total signal is propagated over the fiber followed by detection and down-sampling to recover constellation information. The total signal propagation over the optical fiber is governed by the Nonlinear Schrödinger (NLS) equation defined in (3.1) as [31]

$$\frac{\partial A}{\partial z} + \beta_1 \frac{\partial A}{\partial t} - j\frac{\beta_2}{2}\frac{\partial^2 A}{\partial t^2} - \frac{\beta_3}{6}\frac{\partial^3 A}{\partial t^3} + \frac{\alpha}{2}A =$$
$$-j\gamma\left[|A|^2 A + \frac{j}{\omega_c}\frac{\partial\left(|A|^2 A\right)}{\partial t} - T_R A\frac{\partial\left(|A|^2\right)}{\partial t}\right], \tag{3.1}$$

where z is the propagation distance, $A = A(t, z)$ is the scalar version of the optical field, α is the attenuation coefficient, β_1 is the pulse group velocity, β_2 is the second order dispersion

coefficient, β_3 is the third order dispersion coefficient, γ is the nonlinear coefficient (Kerr), γ/ω_c accounts for the strength of SS (ω_c is the reference optical frequency in rad/s) and T_R is the SRS coefficient. Alternatively, (3.1) can be simplified if the effects of SS and SRS are not relevant for the transmission system at hand. In addition, the term with β_1 can be omitted If the reference frame is moving at the group velocity of the pulse (i.e. retarded frame). As a result, equation (3.1) is rewritten as

$$\frac{\partial A}{\partial z} - j\frac{\beta_2}{2}\frac{\partial^2 A}{\partial t^2} - \frac{\beta_3}{6}\frac{\partial^3 A}{\partial t^3} + \frac{\alpha}{2}A = -j\gamma|A|^2 A. \tag{3.2}$$

Equation (3.2) defined in the time domain may also be represented in the frequency domain. Taking the Fourier Transform (FT) in both sides and using the following relations given by equations (3.3)-(3.6), one can easily obtain equation (3.7).

$$FT\left[\frac{\partial A(t,z)}{\partial t}\right] = j\omega A(\omega, z). \tag{3.3}$$

$$FT\left[\frac{\partial^2 A(t,z)}{\partial t^2}\right] = -\omega^2 A(\omega, z). \tag{3.4}$$

$$FT\left[\frac{\partial^3 A(t,z)}{\partial t^3}\right] = -j\omega^3 A(\omega, z). \tag{3.5}$$

$$FT\left[|A(t,z)|^2 A(t,z)\right] = \frac{1}{4\pi^2}\int\int A(\omega_1,z) A^*(\omega_2,z) A(\omega - \omega_1 + \omega_2, z) d\omega_1 d\omega_2. \tag{3.6}$$

$$\frac{\partial A(\omega,z)}{\partial z} = -\frac{\alpha}{2}A(\omega,z) - j\frac{\beta_2}{2}\omega^2 A(\omega,z) - j\frac{\beta_3}{6}\omega^3 A(\omega,z) -$$
$$\frac{1}{4\pi^2}\int\int j\gamma A(\omega_1,z) A^*(\omega_2,z) A(\omega - \omega_1 + \omega_2, z) d\omega_1 d\omega_2. \tag{3.7}$$

Where $A(\omega, z)$ is the FT of the optical signal $A = A(t,z)$, ω is the angular frequency, ω_i are auxiliary angular frequencies that scan the optical signal $A(\omega)$ in the double integral of (3.7) and $(.)^*$ is the complex conjugate operator. From (3.7), the quantities G_1 and G_3 are defined as follow

$$G_1(\omega) = -\frac{\alpha}{2} - j\frac{\beta_2\omega^2}{2} - j\frac{\beta_3\omega^3}{6}, \tag{3.8}$$

$$G_3\left(\omega_1, \omega_2, \omega_3\right) = -j\gamma. \tag{3.9}$$

$G_1(\omega)$ accounts for the linear effects whereas $G_3(\omega_1, \omega_2, \omega_3)$ accounts for the nonlinear effects. It is important to mention that G_1 and G_3 should be represented in their complete versions as $G_1(\omega) = -\frac{\alpha}{2} - j\beta_1\omega - j\frac{\beta_2\omega^2}{2} - j\frac{\beta_3\omega^3}{6}$ and $G_3(\omega_1, \omega_2, \omega_3) = -j[\gamma + \frac{\gamma}{\omega_c}(\omega_1 - \omega_2 + \omega_3)] - \gamma T_R(\omega_1 - \omega_2)$ if the NLSE in equation (3.1) is employed [50]. By doing the appropriate substitutions of G_1 and G_3 in equation (3.7), the NLSE in the frequency domain is expressed as

$$\frac{\partial A\left(\omega, z\right)}{\partial z} = A\left(\omega, z\right) G_1\left(\omega\right) + \frac{1}{4\pi^2} \int \int G_3\left(\omega_1, \omega_2, \omega - \omega_1 + \omega_2\right) \times$$
$$A\left(\omega_1, z\right) A^*\left(\omega_2, z\right) A\left(\omega - \omega_1 + \omega_2, z\right) d\omega_1 d\omega_2. \tag{3.10}$$

Volterra series expansion is used to model any nonlinear systems by relating the input signal $X(.)$ with the output signal $Y(.)$. In optical communications, it has been used mostly in the frequency domain as defined below in equation (3.11).

$$Y\left(\omega\right) = \sum_{n=1}^{\infty} \int \cdots \int H_n\left(\omega_1, \cdots, \omega_{n-1}, \omega - \omega_1 - \cdots - \omega_{n-1}\right) \times$$
$$X\left(\omega_1\right) \cdots X\left(\omega_{n-1}\right) \times X\left(\omega - \omega_1 - \cdots - \omega_{n-1}\right) d\omega_1 \cdots d\omega_{n-1}, \tag{3.11}$$

where $H_n(\omega - \omega_1 - \cdots - \omega_{n-1})$ is the nth order frequency domain Volterra kernels that have to be identified for the system at hand. It is well known that in silica optical fibers, 2nd order nonlinearities are not present [31]. Therefore, from the definition of the Volterra series given in equation (3.11), one can replace $X(\omega)$ and $Y(\omega)$ by the corresponding A in the frequency domain to find the 3rd VSTF method as follows [25]

$$A\left(\omega, z\right) = A\left(\omega\right) H_1\left(\omega, z\right) + \frac{1}{4\pi^2} \int \int H_3\left(\omega_1, \omega_2, \omega - \omega_1 + \omega_2, z\right) \times$$
$$A\left(\omega_1\right) A^*\left(\omega_2\right) A\left(\omega - \omega_1 + \omega_2\right) d\omega_1 d\omega_2, \tag{3.12}$$

where $A(\omega) = A(\omega, z = 0)$ is the FT of the input optical signal $A(t, z = 0)$, $H_1(\omega, z)$ is the linear transfer function (1st order Volterra kernel) whereas $H_3(\omega_1, \omega_2, \omega - \omega_1 + \omega_2, z)$ is the nonlinear transfer function (3rd order Volterra kernel). In WDM system where $A(\omega)$ is of the form $A(\omega) = \sum_i A_i(\omega)$, the numerical evaluation of the double integral in (3.12) accounts for SPM (intra-channel), XPM and FWM (inter-channel) effects. The VSTF solution includes the signal distortion due to linear and nonlinear effects as well as the signal interaction with Amplified Spontaneous Emission (ASE) in case the system employ optical amplification.

The definition of VSTF given in (3.12) needs the analytic expressions for the linear and nonlinear transfer functions. One possible solution to find H_1 and H_3 is to firstly substitute $A(\omega, z)$ given by equation (3.12) in equation (3.10), as the authors in [25] presented. This procedure results in expression (3.13) defined below.

$$
\frac{\partial \left[A(\omega) H_1(\omega, z) \right]}{\partial z} + \frac{1}{4\pi^2} \int \int \frac{\partial}{\partial z} \left[H_3(\omega_1, \omega_2, \omega - \omega_1 + \omega_2, z) \right] \times
$$

$$
A(\omega_1) A^*(\omega_2) A(\omega - \omega_1 + \omega_2) d\omega_1 d\omega_2 = G_1(\omega) H_1(\omega, z) A(\omega) + \frac{G_1(\omega)}{4\pi^2}
$$

$$
\int \int H_3(\omega_1, \omega_2, \omega - \omega_1 + \omega_2, z) \times A(\omega_1) A^*(\omega_2) A(\omega - \omega_1 + \omega_2) d\omega_1 d\omega_2 +
$$

$$
\frac{1}{4\pi^2} \int \int G_3(\omega_1, \omega_2, \omega - \omega_1 + \omega_2) \times \left\{ \left[A(\omega_1) H_1(\omega_1, z) + \frac{1}{4\pi^2} \right. \right.
$$

$$
\int \int H_3(\omega_1', \omega_2', \omega_1 - \omega_1' + \omega_2', z) \times A(\omega_1') A^*(\omega_2') A(\omega_1 - \omega_1' + \omega_2') d\omega_1' d\omega_2' \right]
$$

$$
\left[A(\omega_2) H_1(\omega_2, z) + \frac{1}{4\pi^2} \right.
$$

$$
\left. \int \int H_3(\omega_1', \omega_2', \omega_2 - \omega_1' + \omega_2', z) \times A(\omega_1') A^*(\omega_2') A(\omega_2 - \omega_1' + \omega_2') d\omega_1' d\omega_2' \right]^*
$$

$$
\left[A(\omega - \omega_1 + \omega_2) H_1(\omega - \omega_1 + \omega_2, z) + \frac{1}{4\pi^2} \right.
$$

$$
\int \int H_3(\omega - \omega_1 + \omega_2 - \omega_1' + \omega_2') \times A(\omega_1') A^*(\omega_2') A(\omega - \omega_1 + \omega_2 - \omega_1' + \omega_2')
$$

$$
\left. \left. d\omega_1' d\omega_2' \right] \right\} d\omega_1 d\omega_2.
$$

$$
(3.13)
$$

By comparing the two terms in the left-hand and right-hand sides of the equation (3.13) and replacing $\omega_3 = \omega - \omega_1 + \omega_2$ and $\omega = \omega_3 + \omega_1 - \omega_2$, one can obtain the following pair of

differential equations.

$$\frac{\partial H_1\left(\omega, z\right)}{\partial z} = G_1\left(\omega\right) H_1\left(\omega, z\right). \tag{3.14}$$

$$\frac{\partial H_3\left(\omega_1, \omega_2, \omega_3, z\right)}{\partial z} = G_1\left(\omega_1 - \omega_2 + \omega_3\right) H_3\left(\omega_1, \omega_2, \omega_3, z\right) +$$
$$G_3\left(\omega_1, \omega_2, \omega_3\right) H_1\left(\omega_1, z\right) H_1^*\left(\omega_2, z\right) H_1\left(\omega_3, z\right). \tag{3.15}$$

The solution of (3.14) is of the form $\frac{dy}{dz} = ay \rightarrow y = e^{az}$, thus $H_1(\omega, z)$ is given by

$$H_1\left(\omega, z\right) = e^{G_1(\omega)z}. \tag{3.16}$$

Replacing (3.16) in (3.15), one can have

$$\frac{\partial H_3\left(\omega_1, \omega_2, \omega_3, z\right)}{\partial z} = G_1\left(\omega_1 - \omega_2 + \omega_3\right) H_3\left(\omega_1, \omega_2, \omega_3, z\right) +$$
$$G_3\left(\omega_1, \omega_2, \omega_3\right) e^{H_1(\omega_1)z} e^{H_1^*(\omega_2)z} e^{H_1(\omega_3)z}. \tag{3.17}$$

The solution of (3.17) is of the form $\frac{dy}{dz} = ay + be^{cz} \rightarrow y = b\frac{e^{cz}-e^{az}}{c-a}$. Therefore, $H_3(\omega_1, \omega_2, \omega_3, z)$ is given by

$$H_3\left(\omega_1, \omega_2, \omega_3, z\right) = G_3\left(\omega_1, \omega_2, \omega_3\right) \times$$
$$\frac{e^{\left[G_1(\omega_1)+G_1^*(\omega_2)+G_1(\omega_3)\right]z} - e^{G_1(\omega_1-\omega_2+\omega_3)z}}{G_1\left(\omega_1\right) + G_1^*\left(\omega_2\right) + G_1\left(\omega_3\right) - G_1\left(\omega_1 - \omega_2 + \omega_3\right)}. \tag{3.18}$$

Equations (3.16) and (3.18) may also be defined as a function of the physical parameters of the fiber (α, β_i and γ) and the angular frequencies ω_i. This can be performed by firstly substituting equations (3.8) in (3.16) to obtain H_1 rewritten in equation (3.19). Secondly, by using $\omega_3 = \omega - \omega_1 + \omega_2$ and including equations (3.8) and (3.9) in (3.18) result in two terms of the form $\exp\{z[G_1(\omega_1) + G_1^*(\omega_2) + G_1(\omega - \omega_1 + \omega_2)]\} - \exp\{z[G_1(\omega)]\} = \exp\{z[-\frac{3\alpha}{2} - j\frac{\beta_2}{2}(\omega_1^2 - \omega_2^2 + (\omega - \omega_1 + \omega_2)^2) - j\frac{\beta_3}{6}(\omega_1^3 - \omega_2^3 + (\omega - \omega_1 + \omega_2)^3)]\} - \exp\{z[-\frac{\alpha}{2} - j\frac{\beta_2}{2}\omega^2 - j\frac{\beta_3}{6}\omega^3]\}$ and $G_1(\omega_1) + G_1^*(\omega_2) + G_1(\omega - \omega_1 + \omega_2) - G_1(\omega) = -\frac{\alpha}{2} - j\frac{\beta_2}{2}[\omega_1^2 + \omega_2^2 - (\omega - \omega_1 + \omega_2)^2 -$

$\omega^2] - j\frac{\beta_3}{6}[\omega_1^3 - \omega_2^3 + (\omega - \omega_1 + \omega_2)^3 - \omega^3]$. After manipulating these two terms and evaluating $[\omega_1^2 - \omega_2^2 + (\omega - \omega_1 + \omega_2)^2 - \omega^2]$ and $[\omega_1^3 - \omega_2^3 + (\omega - \omega_1 + \omega_2)^3 - \omega^3]$ associated with β_2 and β_3, respectively, one may easily arrive at equation (3.20).

$$H_1(\omega, z) = e^{\left(-\frac{\alpha}{2} - j\frac{\beta_2 \omega^2}{2} - j\frac{\beta_3 \omega^3}{6}\right)z}. \tag{3.19}$$

$$H_3(\omega_1, \omega_2, \omega, z) = -j\gamma \exp\left((-\frac{\alpha}{2} - j\frac{\beta_2 \omega^2}{2} - j\frac{\beta_3 \omega^3}{6})z\right)$$
$$\times \frac{1 - \exp(-\alpha z - j\beta_2(\omega_1 - \omega)(\omega_1 - \omega_2)z - j\frac{\beta_3}{2}(\omega + \omega_2)(\omega_1 - \omega)(\omega_1 - \omega_2)z)}{\alpha + j\beta_2(\omega_1 - \omega)(\omega_1 - \omega_2) + j\frac{\beta_3}{2}(\omega + \omega_2)(\omega_1 - \omega)(\omega_1 - \omega_2)}. \tag{3.20}$$

If the dispersion slope is neglected, i.e. $\beta_3 = 0$, equation (3.20) ends up exactly as equation (4) of [27] defined here for convenience.

$$H_3(\omega_1, \omega_2, \omega, z) = -j\gamma \exp\left((-\frac{\alpha}{2} - j\frac{\beta_2 \omega^2}{2})z\right)$$
$$\times \frac{1 - \exp(-\alpha z - j\beta_2(\omega_1 - \omega)(\omega_1 - \omega_2)z)}{\alpha + j\beta_2(\omega_1 - \omega)(\omega_1 - \omega_2)} \tag{3.21}$$

The VSTF solution is truncated by the 3rd kernel, thereby it is expected that an error on the estimation of $A(\omega, z)$ occurs. This error is proportional to $P^{(n+2)/2}$, where P is the peak power of the optical field and n is the highest order kernel in the series, i.e. $P^{5/2}$ for the 3rd order solution [25]. If P is not properly chosen, the solution of $A(\omega, z)$ diverges from the actual value, thus requiring higher-order kernels to mitigate the error. Without recurring to higher-order kernels, which impose a huge computational effort, the *Modified Version* of the 3rd order VSTF was proposed by the authors in [51] to improve the accuracy of the method. This method is based on a phase correction included to the solution of $A(t, z)$ after calculating both the linear and nonlinear solutions of $A(\omega, z)$. This method is defined below.

$$A(t, z) = \begin{cases} A_{LI} \cdot e^{\left(\frac{A_{NL}}{A_{LI}}\right)}, & \text{if } |A_{NL}| < |A_{LI}| \\ A_{NL} + A_{LI}, & \text{otherwise,} \end{cases} \tag{3.22}$$

where A_{LI} and A_{NL} is the time domain linear (first right-hand term) and nonlinear solution

(second right-hand term) of $A(\omega, z)$ in (3.12), respectively. In section 3.5, the 3rd order VSTF solution is compared to SSF for various powers, distances and modulation formats in coherent UDWDM-PON network scenarios.

3.2 Calculating Nonlinearities

VSTF can be used either as a propagation model or an analytic mathematical tool in order to quantify independently the contributions of nonlinear effects. For instance, if one considers the interactions inside the double integral in (3.12) of the input modulated signals as $A_i(\omega_1)A_j^*(\omega_2)A_k(\omega - \omega_1 + \omega_2)$, where $i, j, k = 1, 2, \cdots, N_{ch}$, with N_{ch} being the number of channels, correspond to the indexes of any WDM channel, then we have the following relations:

- if $[i = j = k]$, then (3.12) accounts for SPM at ith channel as

$$H_3(\omega_1, \omega_2, \omega - \omega_1 + \omega_2, z)A_i(\omega_1)A_i^*(\omega_2)A_i(\omega - \omega_1 + \omega_2) \tag{3.23}$$

- if $[i = j \neq k]$, then (3.12) accounts for XPM at kth channel as

$$H_3(\omega_1, \omega_2, \omega - \omega_1 + \omega_2, z) \times \left\{ A_k(\omega - \omega_1 + \omega_2) \times \left[\sum_{i \neq k} A_i(\omega_1)A_i^*(\omega_2) \right] + \right.$$
$$\left. A_k(\omega_1) \times \left[\sum_{i \neq k} A_i(\omega_2)A_i^*(\omega - \omega_1 + \omega_2) \right] \right\} \tag{3.24}$$

- if $[i \neq j = k]$, then (3.12) accounts for XPM at ith channel as

$$H_3(\omega_1, \omega_2, \omega - \omega_1 + \omega_2, z) \times \left\{ A_i(\omega_1) \times \left[\sum_{k \neq i} A_k^*(\omega_2)A_k(\omega - \omega_1 + \omega_2) \right] + \right.$$
$$\left. A_i(\omega - \omega_1 + \omega_2) \times \left[\sum_{k \neq i} A_k(\omega_1)A_k^*(\omega_2) \right] \right\} \tag{3.25}$$

- if $[i \neq k \ or \ k \neq j]$, then (3.12) accounts for FWM at $[i + j - k]$th channel as

$$\sum_{i,j,k} H_3(\omega_1, \omega_2, \omega - \omega_1 + \omega_2, z) A_i(\omega_1) A_k^*(\omega_2) A_j(\omega - \omega_1 + \omega_2) \tag{3.26}$$

Note that the calculation of the nonlinear effects does not consider the pump–probe analysis in which the channel under test is approximated by a Continuous Wave signal. Instead, the VSTF enables the calculation of these effects for any type of input signal such as intensity–modulated, phase–modulated or both. Additionally, estimating the system's performance, either in terms of SNR or EVM associated with SPM, XPM and FWM effects only requires to apply the matrix of WDM channels (being the columns representing the channels and the rows representing the samples) prior multiplexing to the VSTF method described before.

Calculating FWM effect, as expressed in (3.2), requires a huge computation effort as the number of mixing products estimated by $(N_{ch}^3 - N_{ch}^2)/2$ for a 32–channel system exceeds 15000. To avoid extra calculations, we evaluate the phase mismatch condition and efficiency of each new FWM frequency component considering the Continuous Wave (CW) approach presented by the authors in [52]. As such, any FWM component whose efficiency is below 20% of its maximum is not considered for calculation in the double integral of equation (3.12). As a result, we evaluated 61 instead of 360 FWM products falling on the center channel under test. Our calculations indicated a penalty on the total FWM power below 1.2 dB after removing products whose efficiency is below the 20%–threshold. A graphical representation of such approach is given in Fig. 3.1 for 32 CW signals (spaced by 3.125 GHz) after 25 km of SSMF. Fig. 3.1(a) depicts the calculation of the FWM efficiency where all FWM products (15872 products) are represented by diamonds whereas the ones whose efficiency is higher than 20% (3212 products) are represented by squares. Fig. 3.1(b) shows the calculation of FWM crosstalk in each signal bandwidth considering the two aforementioned approaches: the results depicted by diamond markers consider all FWM products falling on the signal bandwidth whereas square markers neglect FWM components with efficiency below 20%. Therefore, faster and attainable calculations can be obtained with minimal impact on the crosstalk estimation.
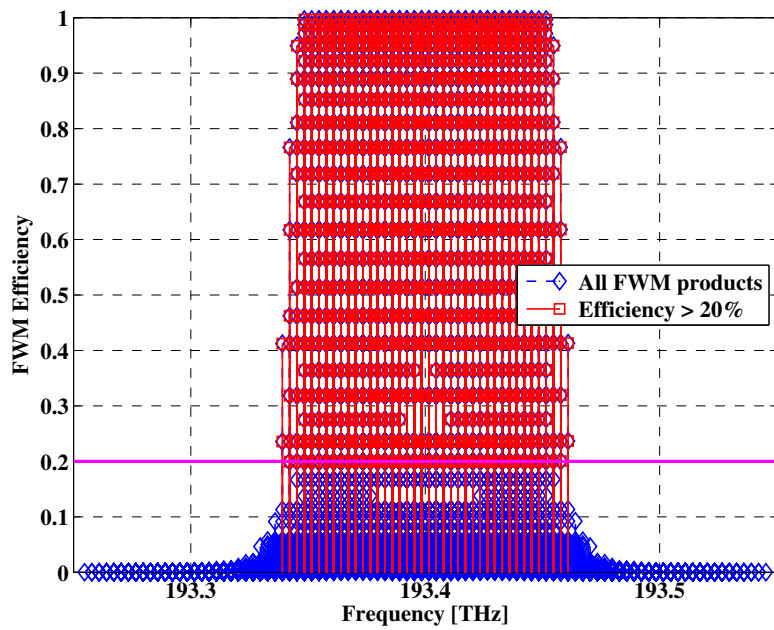
(a)
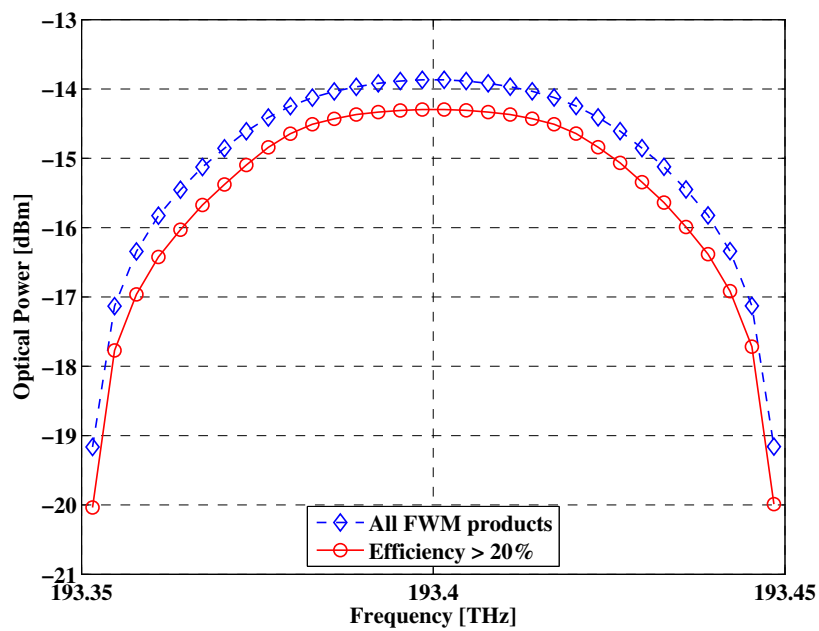
(b)

Figure 3.1: (a) FWM efficiency. (b) FWM crosstalk calculated in each signal bandwidth. Diamonds: FWM products. Squares: FWM products with Efficiency > 20%.

3.3   Numerical Solution of the VSTF Double Integral

The complexity of the 3rd VSTF method can be minimized depending on the approach to numerically solve the double integral in (3.12). One strategy can be based on a direct sum or more accurately using trapezoidal rule to perform the integration. Since it is usual to work with discrete signals, the right term (nonlinear part) of this equation can be rewritten as follows in (3.27)

$$A_{NL}[n]_z = \sum_l \sum_m H_3 \left[\omega_l, \omega_m, \omega_n - \omega_l + \omega_m, z\right]_z A\left[l\right] A^*\left[m\right] A\left[n - l + m\right] \tag{3.27}$$

where the integer indexes (n, l, m) represent the signal sample points at the discrete angular frequencies $(\omega_n, \omega_l, \omega_m)$. Assuming the input discrete signal in the time domain has N symbols and SP samples per symbol spaced by the sampling period T_s (sampling frequency $F_s = 1/T_s$) gives a total of $NFFT = SP \times N$ points in the time/frequency window.

In the frequency domain, these samples are spread on the interval $[-F_s/2, F_s/2[$ centered at $NFFT/2$. We will consider that each channel has the same bandwidth roughly similar to the channel spacing, Δf. Thus, the WDM total signal bandwidth is defined as $N_{ch} \times \Delta f$.

The next step is to translate the channel bandwidth Δf in the integer number of frequency points per channel denoted as SP_c. This quantity is approximately given by Δf divided by the frequency resolution, which is $F_s/NFFT = (T_s \times NFFT)^{-1}$. As a result, $SPc = \lceil \Delta f \times T_s \times NFFT \rceil$ where the operator $\lceil \cdot \rceil$ stands for the largest integer greater or equal to. The total frequency points in the WDM total signal, NF, is the sample points per channel SP_c times the number of channels N_{ch}, or:

$$NF = SP_c \times N_{ch} \tag{3.28}$$

Therefore, we define the vector of integer indexes (l, m), to control both $A[l, m]$ and $\omega_{l,m}$, as

$$l,\ m = [-NF/2 : NF/2 - 1] + NFFT/2 \tag{3.29}$$

or

$$l, \, m = [-N_{ch} \times SP_c/2 : N_{ch} \times SP_c/2 - 1] + NFFT/2 \tag{3.30}$$

Let $k = 1, 2, ..., N_{ch}$ represents each channel index, then

$$
\begin{aligned}
n &= l\left(1 + SP_c \times (k-1) : k \times SP_c\right), & \text{solves (3.27) only for channel } k; \\
n &= [-NF/2 : NF/2 - 1] + NFFT/2, & \text{solves (3.27) for all channels } k = N_{ch}.
\end{aligned}
\tag{3.31}
$$

To avoid implementation errors when calling $A[n - l + m]$, we need to guarantee that $1 \leq n - l + m \leq NFFT$. Equivalently, $\max[l, m] + NF = SP_c \times N_{ch}/2 - 1 + NFFT/2 + SP_c \times N_{ch} \leq NFFT$ arrives at (3.32),

$$N_{ch} \leq \lfloor \frac{NFFT + 2}{3 \times \Delta f \times T_s \times NFFT} \rfloor \tag{3.32}$$

where the operator $\lfloor \cdot \rfloor$ denotes the largest integer less than or equal to. This expression shows the maximum allowable number of channels that we can simulate using VSTF based on the size of the Fast Fourier Transform (FFT) to represent the input signal in the frequency domain and the sampling period. One pseudo code for solving (3.27) is as follows:

1. If the condition in (3.32) stands, then

    - Create the square matrices $\mathbf{l}$ and $\mathbf{m}$ with dimension NF by NF where each column is the vector l and m, respectively

    - Evaluate matrices $\mathbf{A}[\cdot]$ and $\Omega_{l,m}$ in indexes given by matrices $\mathbf{l}$ and $\mathbf{m}$

2. Define the desirable range of n, given by either the first or the second equation in (3.31)

3. For each n, evaluate

    - $\mathbf{A}_{l,m} = \sum_l \sum_m H_3 \left[\Omega_l, \Omega_m, \Omega_n - \Omega_l + \Omega_m, z\right]_z \mathbf{A}\left[\mathbf{l}\right] \mathbf{A}^*\left[\mathbf{m}\right] \mathbf{A}\left[n - \mathbf{l} + \mathbf{m}\right]$

    - $A_{NL}\left[n\right]_z = \sum_l \sum_m \mathbf{A}_{l,m}$

4. Calculate the VSTF complete solution: $A\left[n\right]_z = A_{LI}\left[n\right]_z + A_{NL}\left[n\right]_z$

(a)

(b)

(c)
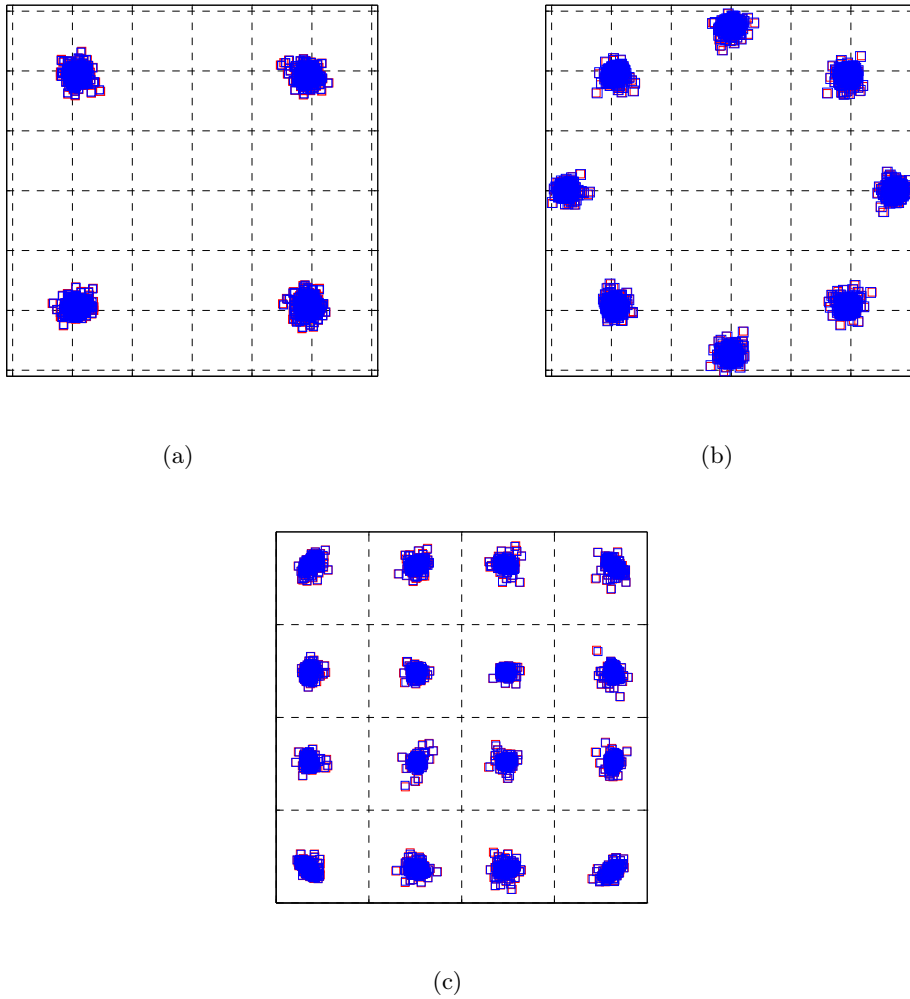
Figure 3.2: Received constellation of the center channel after 100 km–NZDSF for (a) 16 × 50 Gb/s–QPSK, (b) 16 × 75 Gb/s–8PSK and (c) 16 × 100 Gb/s–16QAM. Blue squares: SSF; Red squares: VSTF.

As an example, we performed a simple comparison between SSF and VSTF to confirm that VSTF can be used as a transmission model for optical fiber communication systems. We used a system with 16 channels, spaced by 50 GHz with fixed symbol rate at 25 Gbaud, transmitted over a single Non Zero Dispersion Shifted Fiber (NZDSF) span with 100 km. The digital information is recovered after a conventional coherent detection used in optical communication systems. The simulated symbols, after propagation using these two models, are depicted in figures 3.2. Clearly, the symbols are coincident for both in phase and quadrature components for QPSK, 8PSK and 16QAM modulation formats. In section 3.5, it is presented

a more detailed comparative analysis between VSTF and SSF in UDWDM-PON scenario.

3.4   System Scenario

The numerical validation of the proposed Volterra series approach is carried out in this section for the *fully transparent homogeneous* network. The UDWDM-PON scenario used in this work for simulations is comprised by 32 channel wavelengths (or users) and the transmission system is evaluated in the downstream direction, i.e. from OLT to ONU. The transmission model, depicted in Fig 3.3 is outlined as follows: 32 CW laser sources (without any intensity and phase noises), spaced by 3.125 GHz (0.025 nm), are each independently modulated using an optical IQ modulator driven by electrical signals. Each IQ modulator has two MZM in push-pull configuration with one of the arms having an additional Phase Modulator (PM) to set a phase shift of $\pi/2$. The electrical signals are 625 Mb/s–NRZ shaped by a 5th order Bessel filter with electrical bandwidth of 1.25 GHz. Each electrical signal is a 2^9–long PRBS in which the resulting modulated optical signal, with fixed symbol rate at 625 Mbaud and time window equivalent to 512 symbols per channel (sampled at 512 samples per symbol), has the following properties: 1024 bits at 1.25 Gb/s–QPSK via 2 encoded bits per symbol; 1536 bits at 1.875 Gb/s–8PSK via 3 bits encoded per symbol; 2048 bits at 2.5 Gb/s–16QAM via 4 bits encoded per symbol; 3072 bits at 3.75 Gb/s–64QAM via 6 bits encoded; 4096 bits at 5 Gb/s–256QAM via 8 bits encoded per symbol. The transmitter structures [30] for each modulation format along with the constellation in back-to-back corresponding to a system BER=10^{-3} are depicted in the insets of Fig. 3.3. We point out that all optical subsystems such as Electrical to Optical (E/O) or Optical to Electrical (O/E) devices are assumed to be ideal if not otherwise stated.

The resulting independently-encoded modulated channels are then multiplexed via an ideal lossless AWG modeled as a 2nd order super-Gaussian filter with 3 dB bandwidth around 2.5 GHz. The total optical signal is transmitted over 25 km, 60 km and 100 km of SSMF with the following physical parameters:

- The reference optical frequency between center channels 16th and 17th is 193.4 THz ($\sim$1550 nm);

- Fiber attenuation $\alpha = 0.20\ dB/km$;
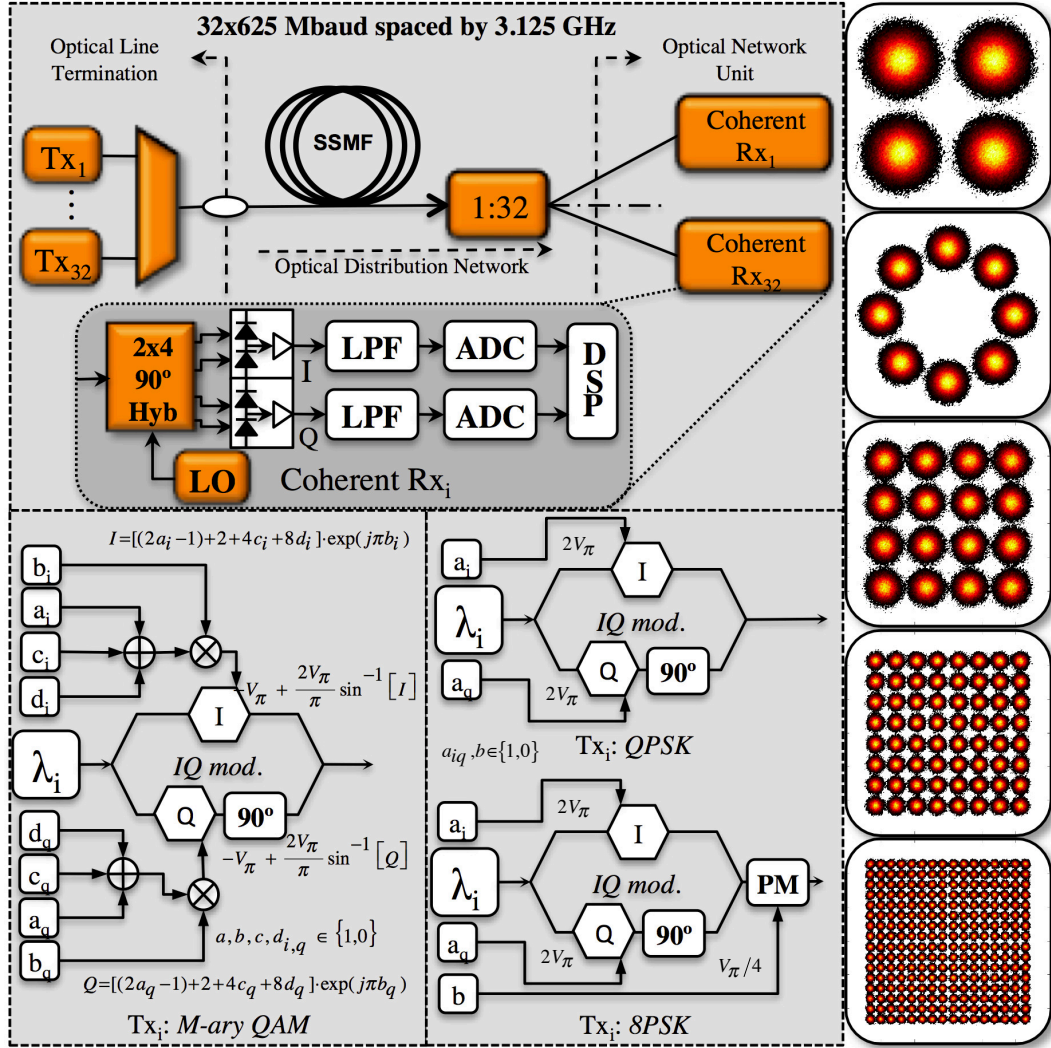
Figure 3.3: UDWDM-PON scenario employing coherent detection and complex modulation formats. LO: local oscillator; LPF: low-pass filter; ADC: analog to digital converter; DSP: digital signal processing; CW: continuous wave; PM: phase modulator.

- Chromatic dispersion $D = 16.5 \ ps/(nm.km)$;

- Dispersion slope $S = 0.07 \ ps^2/nm.km$;

- Nonlinear parameter $\gamma = 1.35 \ (W \cdot km)^{-1}$.

The total optical signal propagation (complex envelope) through the fiber is modeled using the symmetric version of the Split-Step Fourier method with very high temporal and spatial resolution. To guarantee very accurate results symmetric step-size has been dynamically set to prevent a phase change higher than 1×10^{-6} rad. In Fig. 3.4 is shown the optical spectrum
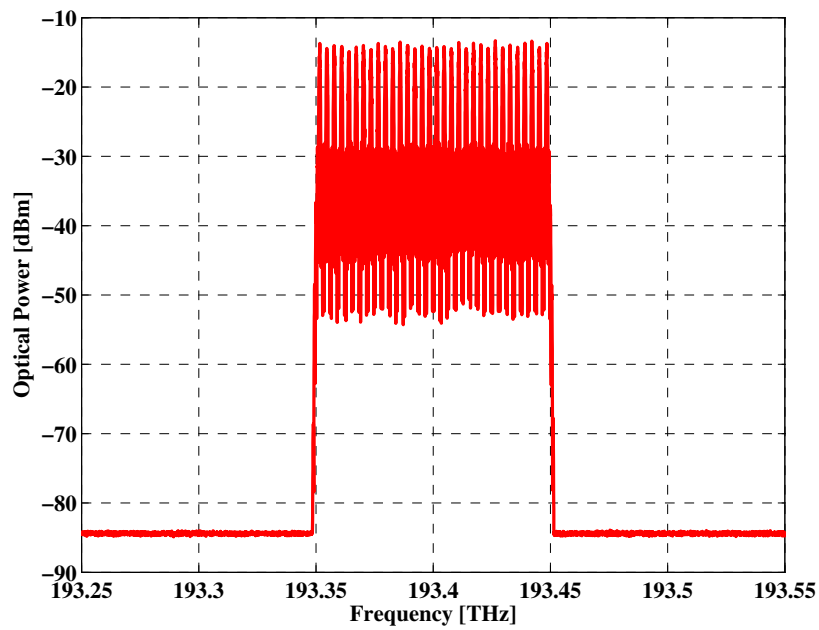
(a)
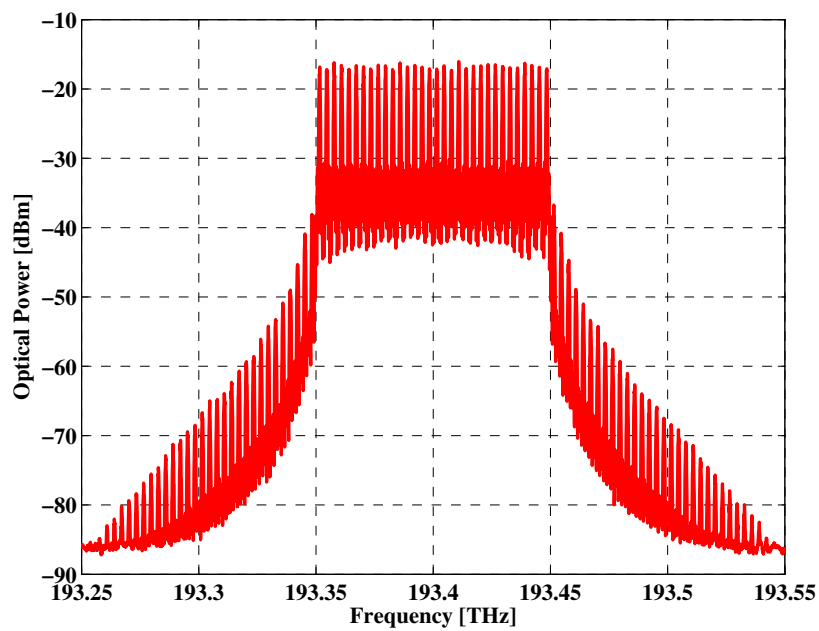
(b)

Figure 3.4: Optical spectra for the UDWDM-PON with 32×625 Mbaud spaced by 3.125 GHz (0.025 nm) (a) before and (b) after the fiber.

before (Fig. 3.4(a)) and after (Fig. 3.4(b)) transmission over 25 km of SSMF. At the coherent receiver depicted in the inset of Fig. 3.3 intradyne detection [53] is performed in which the optical phase is recovered digitally and the local oscillators are tuned to the corresponding UDWDM channel under test as follows in Table 3.1.

Table 3.1: Channel under test and corresponding optical frequencies.

1st	193.3515 THz
4th	193.3609 THz
8th	193.3734 THz
12th	193.3859 THz
16th	193.3984 THz
17th	193.4015 THz
20th	193.4109 THz
24th	193.4234 THz
28th	193.4359 THz
32nd	193.4484 THz

Firstly, the optical signal from the 1:32 splitter is mixed along with the 0 dBm local oscillator through $2 \times 4 - 90^o$ optical hybrid. Since the local oscillator laser does not have phase noise, phase/carrier techniques such as in [21] is not employed at the ONU. Secondly, both in-phase and quadrature components of the resulting optical signal is optical-to-electrical down-converted using two pairs of balanced photo detectors shown in the inset of Fig. 3.3, i.e. one for in-phase and the other for quadrature signals components. Note that both thermal noise of the receiver circuitry (front-end impedance of 50 Ω) and photocurrent shot noises are considered in the coherent receiver at ONU. The electrical signal is then filtered using a 5th order low-pass Bessel filter with 3 dB bandwidth around $0.7 \times$ symbol rate ($\sim$450 MHz). The analog signal is further down sampled at symbol rate (625 MSample/s or one sample per symbol) and converted to the digital domain using an ADC (analog to digital converter) with 8 bits resolution to minimize any quantization errors as discussed in Section 2.5.1. Thus, the recovered symbols are normalized to 1 (average constellation energy) and the phase synchronization is performed as follows:

- 6.25 % of transmitted symbols (32/512) are assigned as pilot symbols with phases ϕ_i;

- The pilot symbols with ϕ_i are known at receiver;

- The phase difference of the received symbols with $\phi_i^{'}$ and pilot symbols with ϕ_i at each time instant is calculated as $\Delta\phi_i = \phi_i - \phi_i^{'}$;

- The expected value of the phase difference is estimated over the 32 pilot symbols: $\Delta\phi = E\{\Delta\phi_i\}$;

- The average phase difference $\Delta\phi$ is then feed back to the actual symbol as $\exp^{j(\phi_i^{'}-\Delta\phi)}$ being $j = \sqrt{-1}$.

It is worth emphasizing that digital chromatic dispersion compensation was not performed since the temporal effect of the total accumulated dispersion has negligible effect in 625 Mbaud signals in typical access network links with fiber lengths up to 100 km. See the discussion in Section 2.4.4.

To measure the system's performance it is calculated the root mean squared EVM between received symbols $s_i^{'} = a_i^{'} + j*b_i^{'}$ and ideal transmitted symbols $s_i = a_i + j*b_i$ as

$$EVM_{dB} = 20 \cdot \log_{10}\left[\sqrt{\frac{\sum_{i=1}^{512}|s_i - s_i^{'}|^2}{\sum_{i=1}^{512}|s_i|^2}}\right] \tag{3.33}$$

over 512 transmitted symbols per channel. The resulting EVM is averaged over 32 independently transmissions with a total of 16384 simulated symbols or 32768 bits for QPSK; 49152 bits for 8PSK; 65536 bits for 16QAM; 98304 bits for 64QAM; 131072 bits for 256QAM. Throughout this work we used the closed expressions that relate EVM or SNR to BER for M-ary QAM [33] and M-ary PSK [38] signals. Therefore, the EVM corresponding to a system BER around 10^{-3} is calculated. For more detail, see Appendix A.

3.5 Volterra Series Transfer Function versus Split-Step Fourier

The first part of the simulated results comprises the comparative analysis of the modified version of VSTF and SSF for UDWDM systems transporting either phase-modulated or amplitude-modulated signals.

The results in Fig. 3.5 and 3.6 show the overall system's performance calculated in terms of EVM in dB, which is mathematically equal to the inverse square root of SNR, of the received center channel (16th channel) of the transmitted comb as a function of input power per channel (average optical power). We refer to the overall system's performance, using either SSF or

VSTF, as the total field formulation that jointly takes into account all the linear (dispersion and attenuation) and nonlinear (SPM, XPM and FWM) fiber effects. Furthermore, we refer to the nonlinear regime as the values of power from which the EVM of a specific effect (SPM, XPM, FWM, or the overall system's performance) is increased.
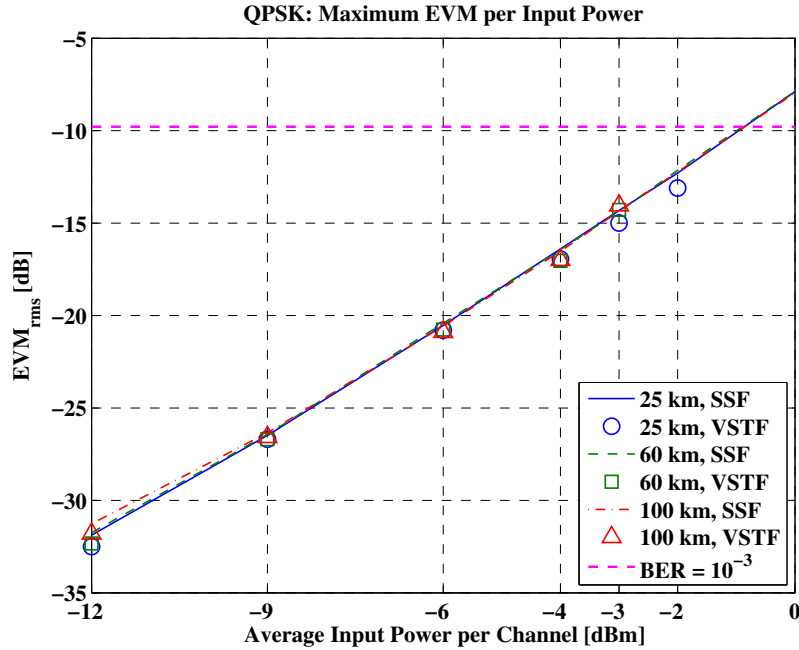
Figure 3.5: EVM of the received center channel versus input power per channel for $32 \times$ 1.25 Gb/s–QPSK. Solid lines: 25 km; Dash lines: 60 km; Dash-dot lines: 100 km.

By analyzing the results both in Fig. 3.5 and Fig. 3.5, the EVM grows by 6 dB every time the power increases by 3 dB meaning that the performance is degraded with the square power in the nonlinear regime, i.e. $EVM_{dB} = 10 \cdot \log_{10}(P^2) + c$ where c is a constant. In addition, theses curves show that the performance is about the same for all transmission distances, i.e. EVM does not change significantly when transmitting 1.25 Gb/s–QPSK or 1.875–8PSK over 25 km, 60 km or 100 km in a UDWDM-PON scenario.

As far as the accuracy of the VSTF method is concerned, for both modulation formats, QPSK in Fig. 3.5 and 8PSK in Fig. 3.6, the method shows similar EVM results (markers) as the SSF (lines) for different transmission distances up to 100 km with power limited to -3 dBm per channel. The power can scale to -2 dBm per channel if the the distance is kept at 25 km as depicted by the blue circles. For higher power regimes, VSTF suffers from energy convergence problems that should be solved by including higher order kernels (5th order for
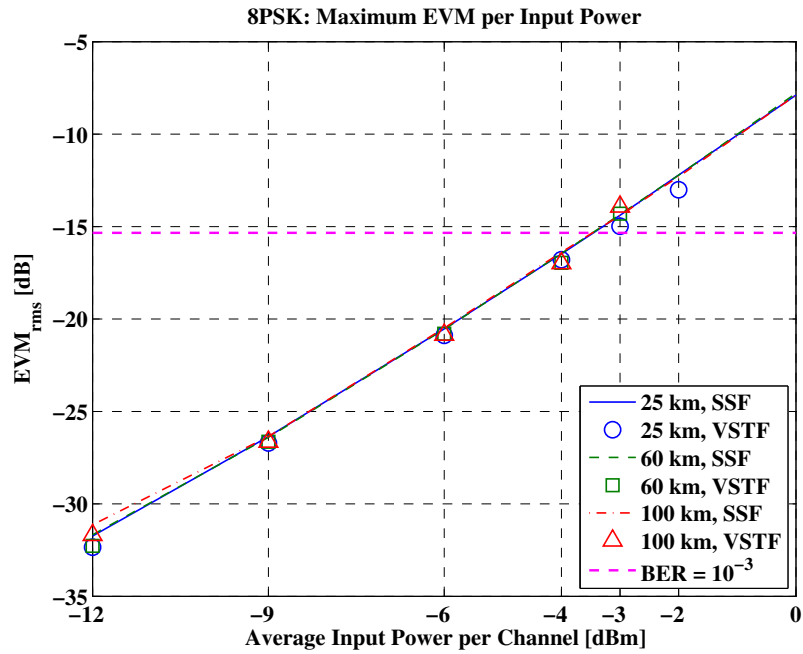
Figure 3.6: EVM of the received center channel versus input power per channel for $32 \times$ 1.875 Gb/s–8PSK. Solid lines: 25 km; Dash lines: 60 km; Dash-dot lines: 100 km.
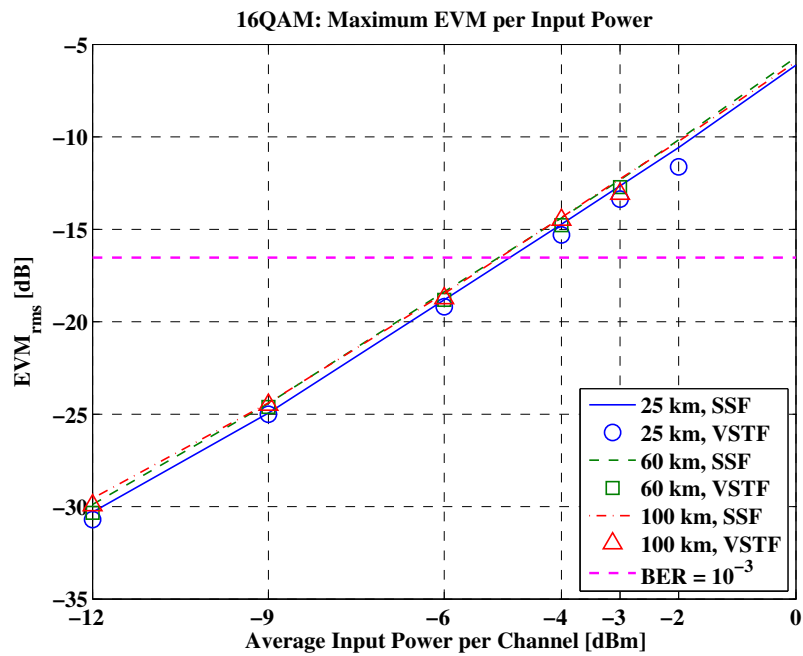
Figure 3.7: EVM of the received center channel versus input power per channel for $32 \times$ 2.5 Gb/s –16QAM. Solid lines: 25 km; Dash lines: 60 km; Dash-dot lines: 100 km.
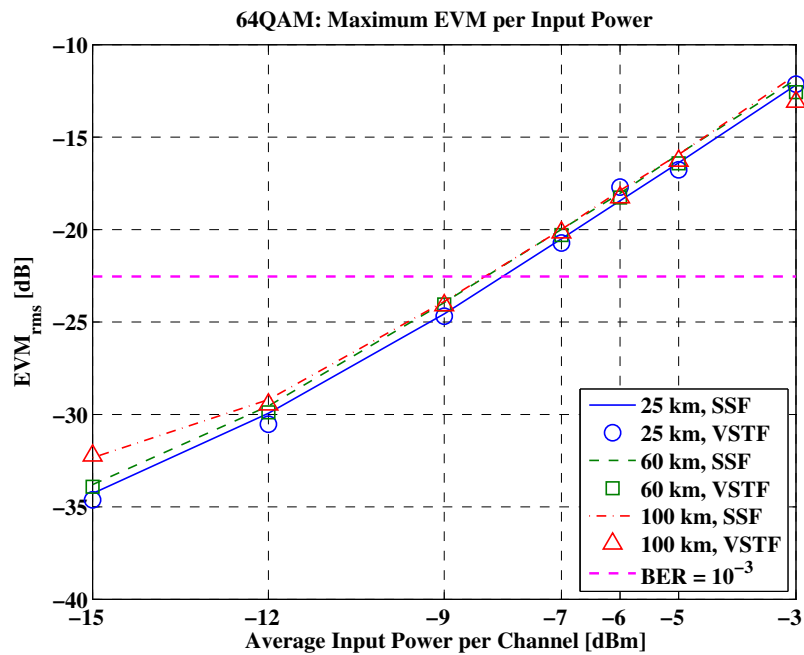
Figure 3.8: EVM of the received center channel versus input power per channel for $32 \times$ 3.75 Gb/s–64QAM. Solid lines: 25 km; Dash lines: 60 km; Dash-dot lines: 100 km.
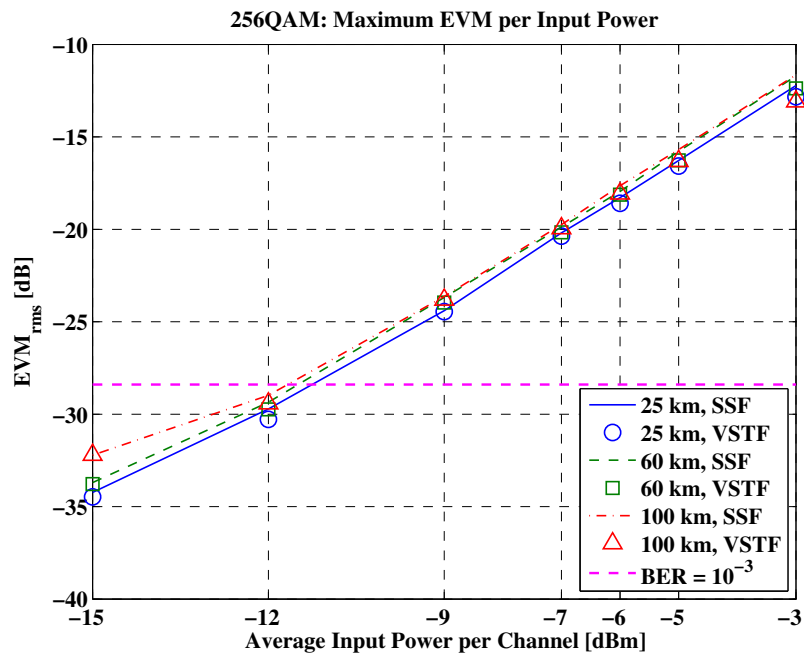
Figure 3.9: EVM of the received center channel versus input power per channel for $32 \times$ 5 Gb/s–256QAM. Solid lines: 25 km; Dash lines: 60 km; Dash-dot lines: 100 km.

instance) in the solution in equation (3.12). On the other hand, this may not be practical in terms of numerical complexity since the system studied in this thesis requires input power below -2 dBm per channel and -4 dBm per channel for QPSK (EVM $\approx$ -9.8 dB) and 8PSK (EVM $\approx$ -15.4 dB) so that EVM represents BER<10^{-3}. Therefore, these results validate the VSTF application to model accurately the fiber propagation even for such a high density of WDM channels in the nonlinear regime operation.

Fig. 3.7, 3.8 and 3.9 show the EVM in dB of the center channel under test for the UDWDM system carrying M-ary QAM signals. As in the previous system with phase-modulated signals, VSTF (colored markers) matched the SSF (style lines) simulations for transmission distances up 100 km when limited to -3 dBm per channel. -2 dBm per channel is also accurate if the transmission distance is limited to 25 km of fiber.

The EVM obtained from the overall system's performance via SSF simulations indicated that BER $<$ 10^{-3} is achievable with input powers per channel below -6 dBm, -9 dBm and -12 dBm after 100 km for 16QAM (EVM $\approx$ -16.53 dB), 64QAM (EVM $\approx$ -22.54 dB) and 256QAM (EVM $\approx$ -28.4 dB), respectively. In addition, the EVM variation with power per channel follows the same quadratic rule, i.e. EVM increases with square power.

Regarding the fiber length L, there is slightly variation of EVM with distance. Specifically, the system's performance when transporting amplitude–modulated channels decreases as the distance increases with $L^{0.053}$, $L^{0.091}$ and $L^{0.101}$ for 16QAM, 64QAM and 256QAM, respectively. This quantity can be found by simply performing $\log_{10}[EVM_{100\ km}/EVM_{25\ km}]/6$ for a target power. Therefore, the overall system's performance can be summarized by the expression below as follows:

$$EVM_{dB} = 10 \cdot \log_{10} \left(a_{nl} P^2 \cdot L^{\varepsilon} \right) \tag{3.34}$$

where a_{nl} is a parameter in $W^{-2} \cdot m^{-\varepsilon}$ that depends on system configuration, modulation formats and fiber parameters and ε is 0.053 for 16QAM, 0.091 for 64QAM and 1.01 for 256QAM.

3.6   Conclusion

This chapter addressed Volterra theory for modeling the total field propagation into the optical fiber on coherent ultra-dense WDM based passive optical networks.

By using transfer functions to represent linear and nonlinear fiber effects, VSTF is a powerful mathematical tool which provides both phase and amplitude of fiber channel. We presented a very efficient method for evaluating the double integral in the frequency domain of the 3rd order VSTF. This algorithm essentially avoids zero amplitude frequency components outside the bandwidth of the optical signal.

As far as the overall system's performance is concerned, the modified version of the 3rd order VSTF matched SSF results for UDWDM systems. In that case for 32 channel spaced by 3.125 GHz, accurate EVM results were found to input powers limited to -3 dBm/channel over a single SSMF link with 100 km. Furthermore, estimates for the maximum input power per channel, when the bit rate scales using high–order modulation formats, were found to be -2 dBm (1.25 Gb/s–QPSK), -4 dBm (1.875 Gb/s–8PSK), -6 dBm (2.5 Gb/s–16QAM), -9 dBm (3.75 Gb/s–64QAM) and -12 dBm (5 Gb/s–256QAM) so that the performance was within the limit of current 7 % overhead FEC employed in coherent optical communication systems.

Next chapter investigates the main contributions of nonlinearities that limit the feeder optical power for coherent UDWDM-PON.

Chapter 4

Impact of Fiber Nonlinearities

Data transmission over the optical fiber channel has been continuously increasing in a very fast pace [54, 55]. Furthermore, the transmission distance between source and destination never reaches a limit [56]. As a result, the performance of the optical communication system has been strongly limited by fiber nonlinearities as the channel density and power increases, thereby pushing the system towards nonlinear Shannon's limit of the optical fiber. Fiber nonlinearities have been widely investigated in two contexts. Firstly, great effort has been put in developing analytic models to estimate the system's performance in both linear and nonlinear regimes. Secondly, tacking advantage of both in-phase and quadrature components of the received signal being detected in current coherent optical systems, DSP is applied in the receiver so that the performance is optimized. For that reason, it is of great significance to gather prior knowledge about transmission aspects such as intra-channel and inter-channel nonlinearities and their dependence on link length, launch power and modulation formats to identify compensation schemes so that the network conveys information in a reliable way.

Most of the work in literature, concerning analysis and compensation of fiber nonlinear effects, applies to long-haul transmission systems where the symbol rate is as high as 30 Gbaud and the transmission distance goes beyond thousands of kilometers of fiber. In that case, intra-channel nonlinearities are dominant or in some cases of WDM transmission, inter-channel XPM is dominant. If the symbol rate is further increased to higher than 60 Gbaud, the dominant physical impairment is intra-channel SPM, even when WDM is used as demonstrated in [57]. FWM is not relevant in such scenarios with channel spacing of 50 GHz or 100 GHz (Dense Wavelength-Division Multiplexing (DWDM)) when SSMF is employed. Some research works have used reduced channel spacing as low as 33 GHz as in [48] using Nyquist WDM (symbol

rate divided by channel spacing around 0.9) or 9 GHz as in [58] (channel spacing is scaled as 1.79 of symbol rate). However, inter-channel FWM still with minimal impact on the system's performance in the aforementioned works. On the other hand, the fiber nonlinear behavior is uncertain in the context of NG-OAN where the network may operate at reduced symbol rate (e.g. 625 Mbaud), reduced channel spacing (e.g. 3 GHz), reduced transmission distance (e.g. 100 km) and increased channel count (e.g. higher than 32). As such, it is expected that nonlinear crosstalk induced by both FWM and XPM are the dominant transmission impairments. For this specific application, there is not a closed solution as the analysis of the system's performance is mostly carried out through brute force simulations. Thereby, from simulated or experimental results numerical expressions relating performance, power and distance for instance, can be extrapolated to determine the system's nonlinear performance. Usually, polynomial interpolation applied to the data results is used for this purpose.

This chapter, based on Journals [J1], [J3] and [J4] and Conference papers [C1], [C11], [C14] and [C15], firstly discusses in Section 3.2 the impact of fiber nonlinearities such as SPM, XPM and FWM in a ultra-dense WDM based PON employing both digital phase modulated (sub-section 4.1.1) and quadrature amplitude modulated (sub-section 4.1.2) channels. Secondly, the dependence of the number of channels on the network performance for various modulation formats is investigated in Section 4.2.

4.1   Impact of Nonlinearities on the System's Performance

This section discusses the impact of nonlinearities on the performance of *fully transparent homogeneous* network described in Section 3.4. In this case, the Volterra models described in Chapter 3 are applied for various network capacity (bit rate per user times channel count) and coverage (distance) to identify the range of dominance of SPM, XPM and FWM. The network has 32 coherent channels spaced by 3.125 GHz, each operated at 625 Mbaud. Via 1:32 transparent splitter, the information reaches the coherent optical receiver in the ONU. The performance is estimated in terms of the EVM of the received symbols for 32 independent transmission. The transmission is performed over a single span of SSMF with 25 km, 60 km and 100 km.

4.1.1 M-ary phase-modulated signals

The first part of the results covers UDWDM-PON employing digital phase-modulated channels. The blue style curves in Fig. 4.1 and 4.2, i.e. solid lines for 25 km (filled markers), dash lines for 60 km (partially filled markers) and dash-dot lines for 100 km (open markers), show the overall performance, estimated in terms of EVM of the center channel, as a function of input power per channel (average optical power). As discussed in Section 3.5, the network has similar performance for all the transmission distance and the modified version of the 3rd–VSTF (diamonds markers) matches the SSF (circles markers) up to -3 dBm per channel. Furthermore, the style lines represent the polynomial interpolation following the fiber nonlinearities dependence of power and distance for single-span propagation discussed in Chapter 3. For QPSK and 8PSK, the EVM curves can be represented by the following expressions:

Figure 4.1: EVM of the received center channel versus input power per channel for 32×1.25 Gb/s–QPSK. Solid lines: 25 km; Dash lines: 60 km; Dash-dot lines: 100 km.

$$EVM_{total}^{QPSK} = 10 \cdot \log_{10} \left(a_{nl} P^2 \cdot L^{-0.0014} \right) \qquad (4.1)$$

$$EVM_{total}^{8PSK} = 10 \cdot \log_{10} \left(a_{nl} P^2 \cdot L^{0.0013} \right) \qquad (4.2)$$

Figure 4.2: EVM of the received center channel versus input power per channel for 32×1.875 Gb/s–8PSK. Solid lines: 25 km; Dash lines: 60 km; Dash-dot lines: 100 km.

where P is the input power per channel, L is the length of the fiber and a_{nl} is a constant which depends on the system's characteristics. As can be seen from the equations, the EVM basically depends on power as the distance has negligible impact on the performance.

Fig. 4.1 and 4.2 also depicts the contributions of SPM (green upward-pointing triangles), XPM (black downward-pointing triangles) and FWM (red squares) in the coherent network. One important conclusion from these figures is that XPM degradation increases for longer transmission distances whereas FWM is slightly reduced for shorter links. For instance, the EVM difference in dB from the black solid line (XPM effect at 25 km) to the black dash line (XPM effect at 60 km) in Fig. 4.1 (QPSK transmission) indicates that XPM effect is increased by 0.7 dB in the nonlinear regime (power $\geq$ -4 dBm), i.e. $QPSK : XPM_{25\ km \rightarrow 60\ km} = +0.7\ dB$. We point out that the effect of thermal and shot noise is only noticeable for input powers below -7 dBm per channel over 100 km and for the single channel case, i.e. when only intra-channel SPM effect is considered. The same criteria may be applied to the red lines representing FWM effect in way that we find its variation with transmission distance; for instance, increasing the distance from 25 km (red solid lines) to 60 km (red dash lines) decreases FWM by -0.7 dB using QPSK signals, i.e. $QPSK : FWM_{25\ km \rightarrow 60\ km} = -0.7\ dB$.

By extending this concept to all combinations of fiber lengths (from 25 km to 100 km, 60 km to 100 km), nonlinear effects and modulation formats, we arrive at the values summarized in the second and third columns of Table 4.1.

Besides the variation with power and distance of XPM and FWM, the EVM results also indicate how much FWM dominates XPM. This relation can be characterized by the FWM to XPM ratio (F/X), which ranges from 25 dB to 30 dB for phase-modulated channels, as depicted in Fig. 4.3 for various distances. The analysis is similar to the previous cases where the EVM differences in dB are calculated from the red lines to the black lines for a given fiber length instead; e.g. at 25 km of fiber (solid line) the F/X for QPSK signaling is around 30 dB in the nonlinear regime, i.e. $QPSK : F/X_{25\ km} = 30\ dB$. The fourth column of Table 4.1 outlines F/X values for 60 km and 100 km links as well. By comparing the two modulation formats, XPM effect on 8PSK signals is slightly higher than the XPM noise induced by QPSK signals as shown in Fig. 4.1 and 4.2. This is also justified from the F/X results in which for QPSK this value ranged from 30 dB to 26.6 dB whereas for 8PSK the F/X ranged from 28.6 dB to 25 dB.

Table 4.1: Inter-channel nonlinearities on M-ary PSK.

QPSK	XPM	FWM	F/X
$25\ km \rightarrow 60\ km$	+0.7 dB	-0.7 dB	25 km: 30 dB
$25\ km \rightarrow 100\ km$	+1.76 dB	-0.9 dB	60 km: 28 dB
$60\ km \rightarrow 100\ km$	+1.3 dB	-0.2 dB	100 km: 26.6 dB
8PSK	**XPM**	**FWM**	**F/X**
$25\ km \rightarrow 60\ km$	+0.5 dB	-1 dB	25 km: 28.6 dB
$25\ km \rightarrow 100\ km$	+1.6 dB	-1.1 dB	60 km: 26 dB
$60\ km \rightarrow 100\ km$	+1 dB	-0.1 dB	100 km: 25 dB

The style curves that interpolate the EVM results for FWM and XPM are obtained from the distance variation from 25 km to 100 km listed in Table 4.1. This factor of 4 (or 6 dB) for the distance variation is used to characterize the EVM as a function of the length of the fiber L, or the accumulated dispersion for single span propagation as discussed in [59]. As an example considering the QPSK transmission, the XPM grows by +1.76 dB when the distance grows from 25 km to 100 km (+6 dB), thus the resulting slope is 1.76/6=0.29 dB/dB. Extending
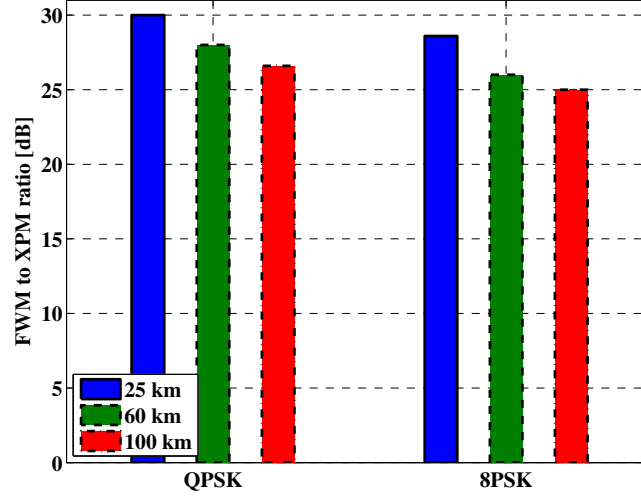
Figure 4.3: FWM to XPM ratio (F/X) for phase-modulated channels and transmission distances. Solid lines: 25 km; Dash lines: 60 km; Dash-dot lines: 100 km.

for FWM and 8PSK, one finds the EVM predictions in the nonlinear regimes as

$$EVM_{XPM}^{QPSK} = 10 \cdot \log_{10} \left(a_{xpm} P^2 \cdot L^{1.76/6} \right) \tag{4.3}$$

$$EVM_{FWM}^{QPSK} = 10 \cdot \log_{10} \left(a_{fwm} P^2 \cdot L^{-0.9/6} \right) \tag{4.4}$$

$$EVM_{XPM}^{8PSK} = 10 \cdot \log_{10} \left(a_{xpm} P^2 \cdot L^{1.6/6} \right) \tag{4.5}$$

$$EVM_{FWM}^{8PSK} = 10 \cdot \log_{10} \left(a_{fwm} P^2 \cdot L^{-1.1/6} \right) \tag{4.6}$$

The summary from Fig. 4.1 and 4.2 is that coherent UDWDM-PON employing phase-modulated signals are mainly limited by FWM (red lines plus squares) since XPM (black lines plus diamonds) and SPM (green lines plus triangles) impose negligible impact on the system's performance for transmission distances up to 100 km. This is justified by the fact that the nearly constant intensity nature of phase-modulated signals (power profile) does not impose effectively modulation of the fiber refractive index via Kerr effect. In addition, those types of signals along with close channel spacing enhance the phase matching condition for improving

the efficiency of FWM generation. Therefore, the occurrence of very strong FWM crosstalk limits the system's performance to operate below -1 dBm and -4 dBm per channel ensuring BER below 10^{-3} for QPSK ($EVM \approx -9.8\ dB$) and 8PSK ($EVM \approx -15.3\ dB$), respectively.

4.1.2   M-ary amplitude-modulated signals

This section analyzes the performance of the network when bit rate is scaled to 2.5 Gb/s, 3.75 Gb/s and 5 Gb/s using high-order QAM constellations. Fig. 4.4, 4.5 and 4.6 show the EVM in dB of the center channel under test versus power per channel for the coherent UDWDM-PON system carrying M-ary QAM signals.

As in the previous system with phase-modulated signals, VSTF (blue circles) matched the SSF (blue diamonds) simulations for transmission distances up 100 km limited to -3 dBm per channel. The EVM obtained from the overall system's performance via SSF simulations indicated that BER $< 10^{-3}$ is achievable with input powers per channel below -6 dBm, -9 dBm and -12 dBm at 100 km for 16QAM ($EVM \approx -16.53\ dB$), 64QAM ($EVM \approx -22.54\ dB$) and 256QAM ($EVM \approx -28.4\ dB$), respectively. The blue style lines that best interpolate
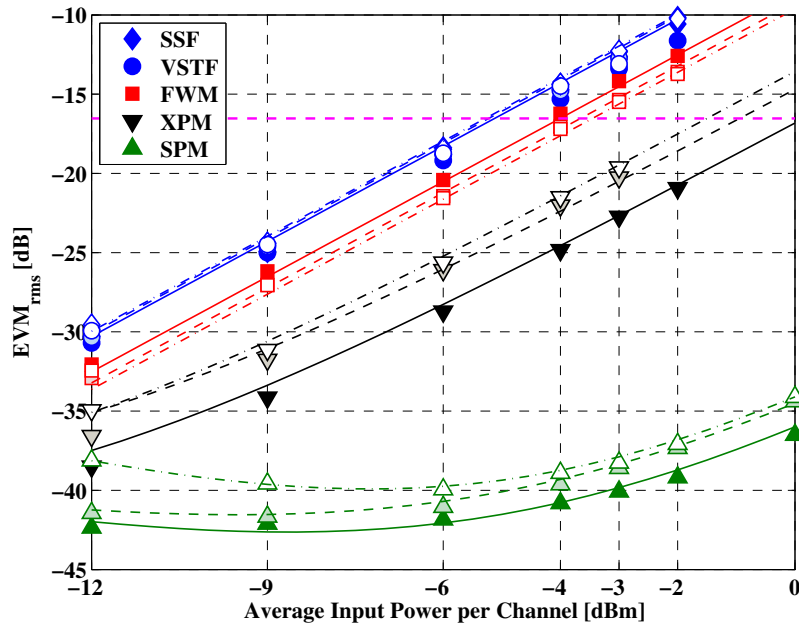
Figure 4.4: EVM of the received center channel versus input power per channel for 32 $\times$ 2.5 Gb/s–16QAM. Solid lines: 25 km; Dash lines: 60 km; Dash-dot lines: 100 km.
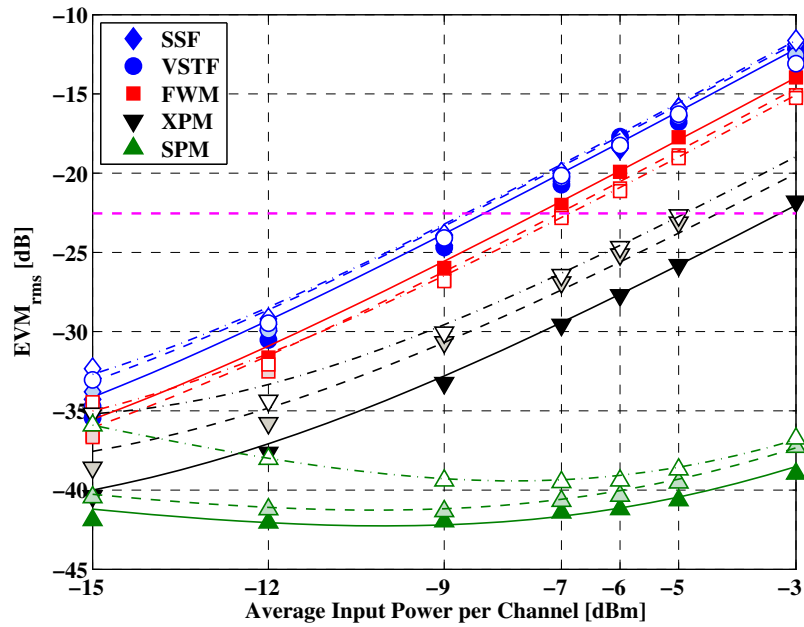
Figure 4.5: EVM of the received center channel versus input power per channel for 32 × 3.75 Gb/s–64QAM. Solid lines: 25 km; Dash lines: 60 km; Dash-dot lines: 100 km.
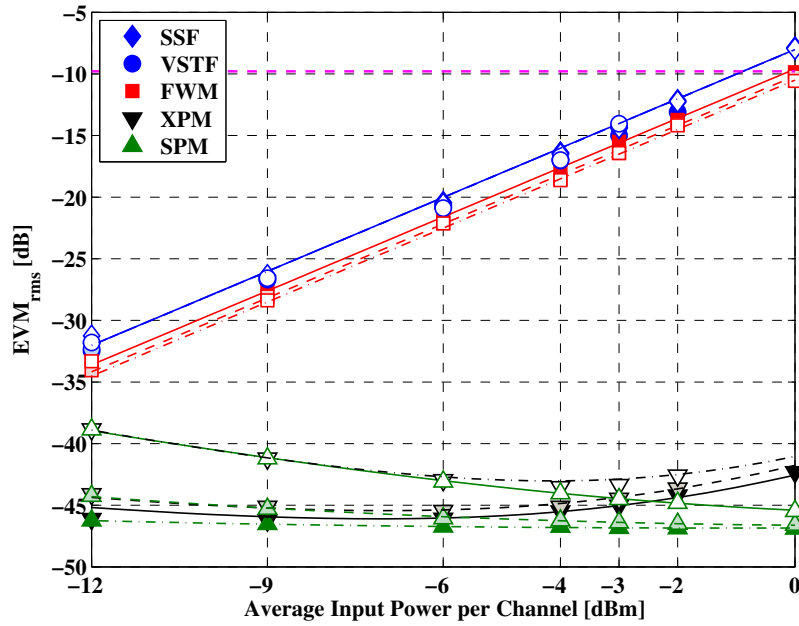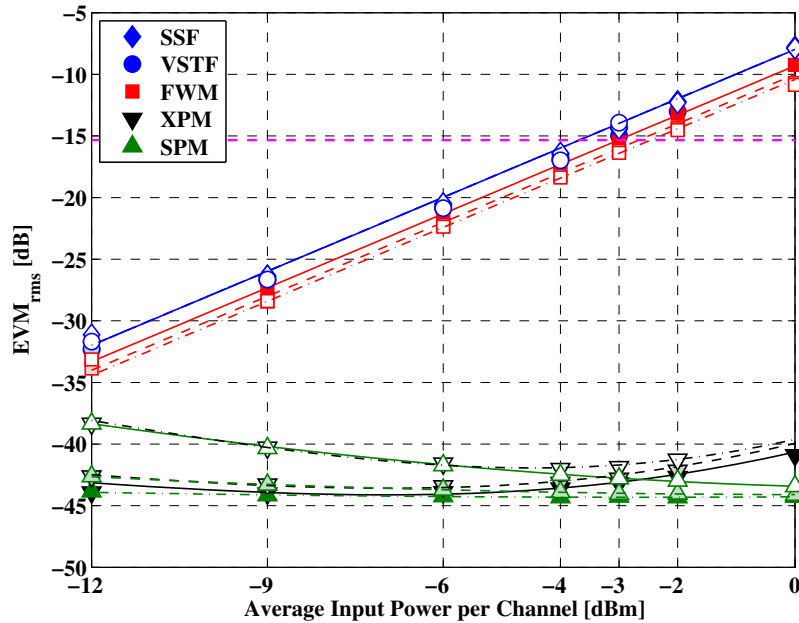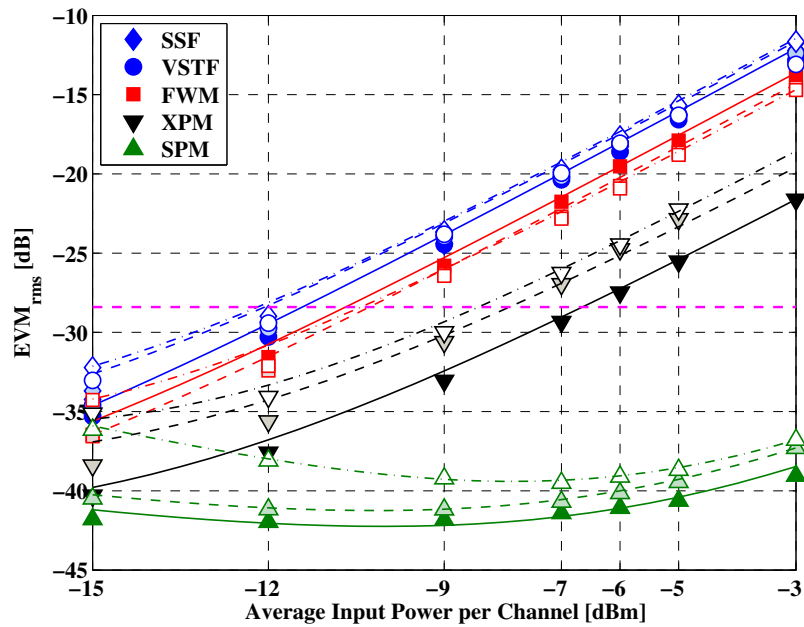

Figure 4.6: EVM of the received center channel versus input power per channel for 32 × 5 Gb/s–256QAM. Solid lines: 25 km; Dash lines: 60 km; Dash-dot lines: 100 km.

the overall performance is given by

$$EVM_{total}^{16QAM} = 10 \cdot \log_{10}\left(a_{nl}P^2 \cdot L^{0.053}\right) \tag{4.7}$$

$$EVM_{total}^{64QAM} = 10 \cdot \log_{10}\left(a_{nl}P^2 \cdot L^{0.0906}\right) \tag{4.8}$$

$$EVM_{total}^{256QAM} = 10 \cdot \log_{10}\left(a_{nl}P^2 \cdot L^{0.1005}\right) \tag{4.9}$$

Regarding the fiber nonlinearities, the intensity modulation nature of M-ary QAM signals boosts the nonlinear phase noise through both SPM (green lines) and XPM (black lines). This nonlinear behavior is highlighted in the received constellations after 100 km transmission shown in Fig. 4.8(a) and 4.8(b) for M-ary PSK and 4.8(c), 4.8(d) and 4.8(e) for M-ary QAM. In addition, the variation with distance is much stronger than the observed when the network transported purely phase-modulated channels. For the system at hand, the SPM effect on M-ary QAM is solely higher than the XPM effect on phase-modulated signals. As a result, the SPM effect outperforms the receiver noise where the EVM is increased for higher values of power. This increasing of EVM when considering SPM only is not evident in the previous results for phase-modulated channels.

By carrying out the same analysis as in Section 4.1.1 about nonlinearities and their dependence on transmission distances and modulation formats, we ended up in the values in Table 4.2 in the nonlinear regime (power $\geq$ -12 dBm for both FWM and XPM). Table 4.2 also shows the F/X quantities from which Fig. 4.7 is generated for QAM signaling over several distances.

The coefficients for the expressions that best interpolates the EVM predictions are obtained from Table 4.2. We emphasize that the expressions below account only for the noise induced by fiber nonlinearities. Furthermore, the SPM predictions for 16QAM (4.12), 64QAM (4.15) and 256QAM (4.18) are also included below.

$$EVM_{XPM}^{16QAM} = 10 \cdot \log_{10}\left(a_{xpm}P^2 \cdot L^{3.3/6}\right) \tag{4.10}$$

Table 4.2: Inter-channel nonlinearities on M-ary QAM.

16QAM	XPM	FWM	F/X
$25\ km \rightarrow 60\ km$	+2.9 dB	-0.9 dB	25 km: 7.4 dB
$25\ km \rightarrow 100\ km$	+3.3 dB	-1.1 dB	60 km: 3.6 dB
$60\ km \rightarrow 100\ km$	+0.4 dB	-0.1 dB	100 km: 3 dB
64QAM	**XPM**	**FWM**	**F/X**
$25\ km \rightarrow 60\ km$	+2.6 dB	-0.9 dB	25 km: 6.8 dB
$25\ km \rightarrow 100\ km$	+3.1 dB	-1.1 dB	60 km: 3.2 dB
$60\ km \rightarrow 100\ km$	+0.5 dB	-0.1 dB	100 km: 2.4 dB
256QAM	**XPM**	**FWM**	**F/X**
$25\ km \rightarrow 60\ km$	+2.6 dB	-0.9 dB	25 km: 6.8 dB
$25\ km \rightarrow 100\ km$	+3.1 dB	-1.1 dB	60 km: 3.2 dB
$60\ km \rightarrow 100\ km$	+0.5 dB	-0.1 dB	100 km: 2.4 dB
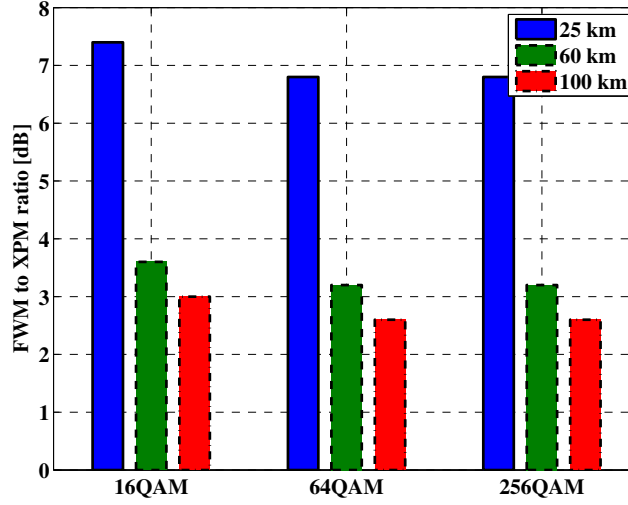
Figure 4.7: FWM to XPM ratio (F/X) for amplitude-modulated channels and transmission distances. Solid lines: 25 km; Dash lines: 60 km; Dash-dot lines: 100 km.

$$EVM_{FWM}^{16QAM} = 10 \cdot \log_{10} \left(a_{fwm} P^2 \cdot L^{-1.1/6} \right) \tag{4.11}$$

$$EVM_{SPM}^{16QAM} = 10 \cdot \log_{10} \left(a_{spm} P^2 \cdot L^{2.1/6} \right) \tag{4.12}$$

$$EVM_{XPM}^{64QAM} = 10 \cdot \log_{10}\left(a_{xpm}P^2 \cdot L^{3.1/6}\right) \tag{4.13}$$

$$EVM_{FWM}^{64QAM} = 10 \cdot \log_{10}\left(a_{fwm}P^2 \cdot L^{-1.1/6}\right) \tag{4.14}$$

$$EVM_{SPM}^{64QAM} = 10 \cdot \log_{10}\left(a_{spm}P^2 \cdot L^{2.09/6}\right) \tag{4.15}$$

$$EVM_{XPM}^{256QAM} = 10 \cdot \log_{10}\left(a_{xpm}P^2 \cdot L^{3.1/6}\right) \tag{4.16}$$

$$EVM_{FWM}^{256QAM} = 10 \cdot \log_{10}\left(a_{fwm}P^2 \cdot L^{-1.1/6}\right) \tag{4.17}$$

$$EVM_{SPM}^{256QAM} = 10 \cdot \log_{10}\left(a_{spm}P^2 \cdot L^{2.06/6}\right) \tag{4.18}$$

The summary of the results presented in Fig. 4.4–4.6 is that FWM is slightly reduced for longer links whereas XPM is increased, which keeps the overall system's performance almost the same for 25 km, 60 km and 100 km spans. For instance, increasing the transmission distance by a factor of 1.7, 2.4 and 4 effectively increases the XPM effect on average by 0.5, 2.6 and 3 dB, respectively; whereas FWM is slightly reduced by 0.1, 1 and 1.1 dB. Essentially, the phase noise through both SPM and XPM accumulates for longer links whereas FWM crosstalk has maximum efficiency around the effective fiber length, i.e. 21 km of SSMF. For links longer than the effective length, the optical fiber works as a dispersive media only. As a result, the F/X ranged from 7.4 dB (longer links) down to only 2.6 dB (shorter links) as shown in Fig. 4.7. The constellation diagrams, depicted in Fig. 4.8 with blue symbols from SSF simulations and red ones from the Volterra XPM model described in Chapter 3, show that the phase noise is more accumulated in the outermost symbols. This increased phase noise results in a increased overall EVM, thereby indicating that coherent UDWDM-PON transporting high-order QAM is not only limited by FWM but also by XPM.

(a)

(b)

(c)

(d)

(e)
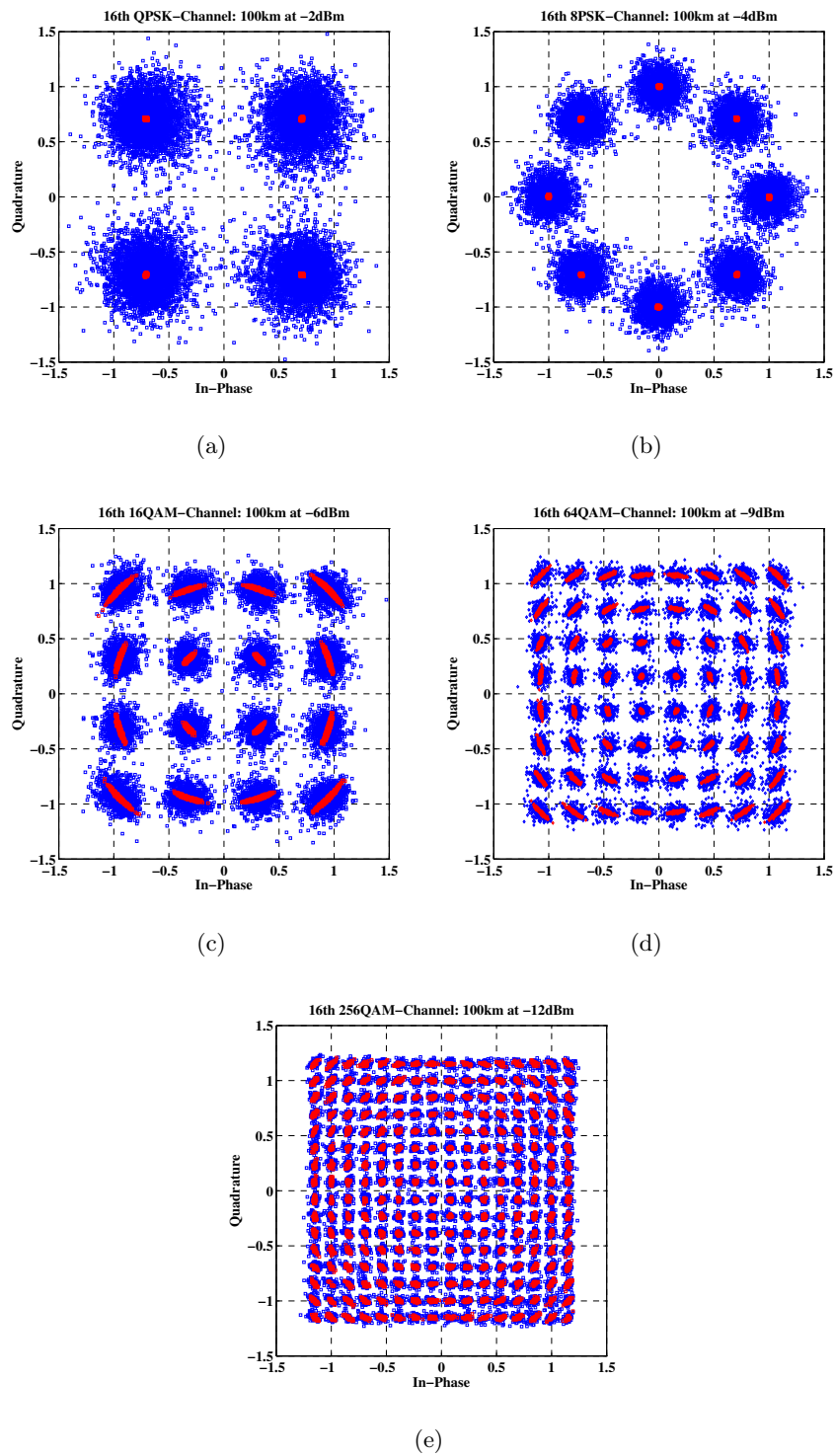
Figure 4.8: Received constellations of the center channel after 100 km of SSMF: $32 \times$ 1.25 Gb/s–QPSK (a); 32×1.875 Gb/s–8PSK (b); 32×2.5 Gb/s–16QAM (c); 32×3.75 Gb/s– 64QAM (d); 32×5 Gb/s–256QAM (e). Blue squares: SSF; Red squares: XPM.

4.2 Impact of The Number of Channels on the System's Performance

The previous results analyzed coherent UDWDM-PON when the network transported 32 channels (or user). On the other hand, it is relevant to identify the overall performance when higher number of channels are transmitted in the same fiber.

The *fully transparent homogeneous* scenario is similar to the previous case where, we simulate in this case 2, 4, 8, 16, 32, 64, 128, 200, 256 coherent channels. The split ratio was simply updated to $1 : N_{ch}$ where N_{ch} is the number of transmitted channels. The symbol rate was increased to 1.25 Gbaud to obtain 2.5 Gb/s, 5 Gb/s and 10 Gb/s per channel/wavelength using QPSK, 16QAM and 256QAM, respectively. In addition, both transmitter lasers and local oscillators were set to 100 kHz–linewidth for QPSK and 16QAM simulations. Thus, carrier/phase estimation was performed based on the Viterbi and Viterbi algorithm. We point out that for 256QAM transmission, the lasers linewidths were set to 0 kHz. We optimized the input power per channel so that at 32 channels after 25 km of fiber the performance is close to the theoretical BER=10^{-3}. Specifically, we used $\sim$-1 dBm per channel for QPSK, $\sim$-5 dBm per channel for 16QAM and $\sim$-11 dBm per channel for 256QAM as shown in Fig. 4.1, Fig. 4.4 and Fig. 4.6, respectively.

The performance was calculated in terms of the EVM in dB, shown in Fig. 4.9 and SNR penalty at BER=10^{-3}, depicted in Fig. 4.10 of the center channel. Fig. 4.9(a), Fig. 4.9(b) and Fig. 4.9(c) show how the performance dependence with number of channels for various distances and bit rates. From these results, it is possible to validate the dependence with distance at 32 channels expressed in equations 4.1, 4.7 and 4.9 as: $\sim L^0$, $\sim L^{0.05}$ and $\sim L^{0.1}$ for QPSK, 16QAM and 256QAM respectively.

At the maximum aggregate data rate in the same ODN extending up to 100 km, the SNR penalty in Fig. 4.10 compared to the 32 channel case is always below 1 dB, 2 dB and 4 dB for 640 Gb/s (256×2.5 Gb/s–QPSK), 1.28 Tb/s (256×5 Gb/s–16QAM) and 2.56 Tb/s (256×10 Gb/s–256QAM), respectively.

When the network transports only QPSK channels (squares), the performance worsens when the number of channels scales up to 32. Higher than 32 channels, the performance remains unchanged due to the fact that the sole effect of FWM is limited within a $\sim$100 GHz

(a)

(b)

(c)
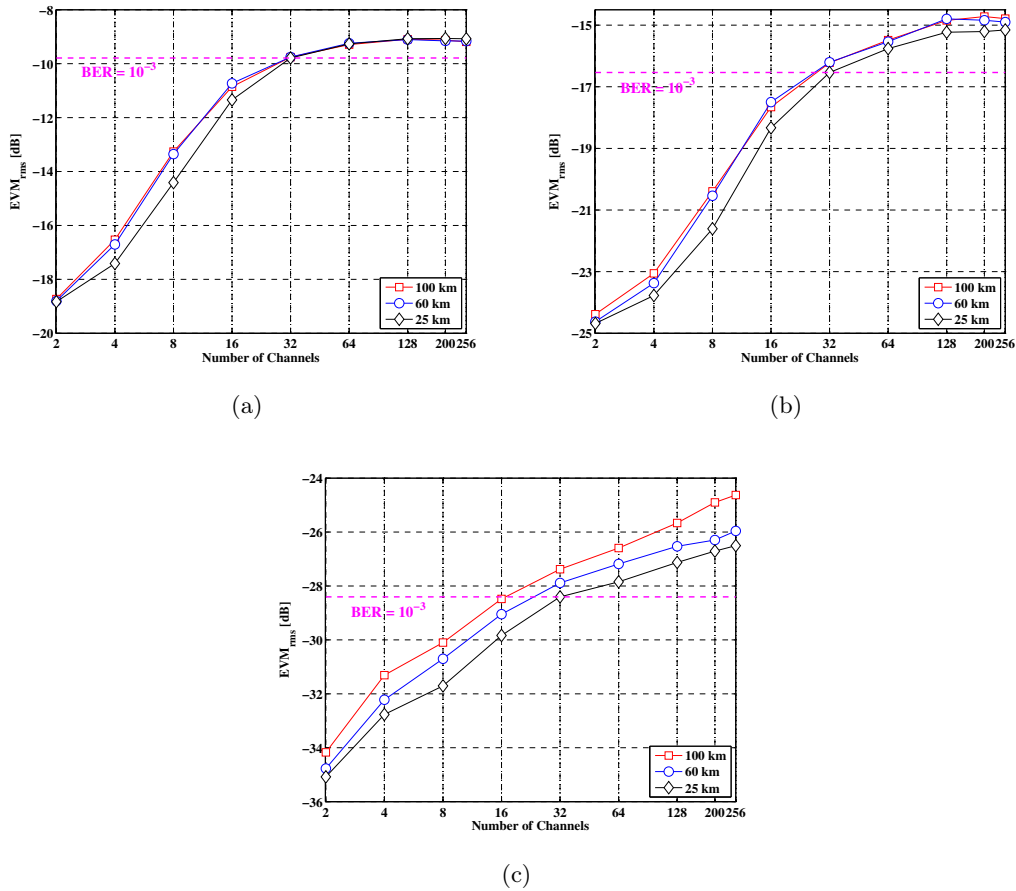
Figure 4.9: EVM of the received center channel versus number of channels ($\log_2$ scale) for: (a) 2.5 Gb/s–QPSK; (b) 5 Gb/s–16QAM; (c) 10 Gb/s–256QAM.

bandwidth ($\sim$32$\times$3.125 GHz). This indicates that in terms of nonlinearities, transmitting 1024 QPSK channels gives the same nonlinear performance as transmitting nearly 32 QPSK channels. Since XPM does not affect QPSK over a single SSMF span as FWM overpowers XPM by 25 dB, the performance does not change significantly with transmission distance. As discussed in Section 4.1.1, the SNR due to nonlinearities slightly decreases with distance as $L^{-0.0014}$ for QPSK transmission.

If the network employs 16QAM (circles) or 256QAM (diamonds) modulated channels, the intensity nature of QAM signaling enhances the impact of XPM and the variation with distance is highlighted, i.e. due to nonlinearities the SNR decreases as the transmission distance increases. The performance worsens by 0.5 dB and 1.5 dB when the link length increases from 25 km to 100 km for 16QAM and 256QAM, respectively. This variation with distance ($L^{0.05}$
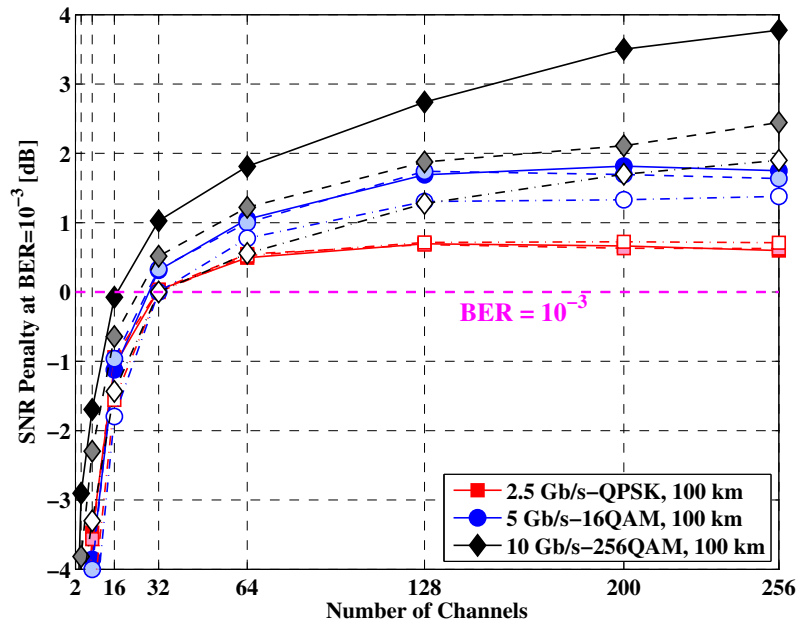
Figure 4.10: SNR penalty at BER=10^{-3} versus number of channels for 2.5 Gb/s–QPSK (squares), 5 Gb/s–16QAM (circles) and 10 Gb/s–256QAM (diamonds). Dash dot lines: 25 km. Dash lines: 60 km; Solid lines: 100 km.

and $L^{0.1}$) is much more evident as a result of FWM overcoming XPM by only 3 dB according to the previous discussions in Section 4.1.2. Besides the FWM saturation at 32 channels, due to XPM the SNR penalty continues to increase up to 128 channels for 16QAM, whereas the performance does not stop worsening before 256 channels for the 256QAM. This is justified by the broader bandwidth of XPM compared to the 100 GHz of FWM.

4.3   Conclusion

This chapter addressed the impact of nonlinearities in the *fully transparent homogeneous* network for various bit rates, obtained with high-order constellations with fixed symbol rate.

For the 32 channel-UDWDM-PON, the network is mostly limited by FWM (25<F/X<30 dB) when transmitting only M-ary PSK channels. On the other hand, the network is impaired by both FWM and XPM (2.5<F/X<7.5 dB) when transmitting M-ary QAM channels. The main advantage of transmitting M-ary PSK is the flexibility to scale the number of users in the same optical distribution network as high as 1024 keeping similar nonlinear performance as the 32 users case. In terms of user's data rate upgradeability, the modulation format is limited to provide 8 Gb/s per channel if the 3 GHz frequency grid is employed.

Since M-ary QAM transmission system enhances induced-XPM nonlinear phase noise, the performance degradation keeps increasing as the number of QAM channels increases. Thereby, it is preferable to maintain lower number of channels, e.g. 64 users (or wavelength channels). However, these signaling offers great possibilities to upgrade the user's data rate up to 24 Gb/s per user, i.e. 8 bits/symbol × 3 Gsymbols/s in the 3 GHz optical bandwidth. In summary, if the ODN in coherent UDWDM-PON is deigned to provide the highest number of users (e.g. 1000) at 1 Gb/s, QPSK signaling provides the best robustness against fiber impairments. If the ODN is designed to provide data rate per users as high as 10 Gb/s, QAM is the best format if the number of users does not exceed 64.

Chapter 5

System's Performance Optimization

The amount of data information over all-optical networks has been continuously increasing as never before [54, 55]. As a result, more and more WDM channels are physically multiplexed and transmitted in the same optical fiber plant to reduce the overall cost of the network deployment. As the number of channels (or users in the case of purely WDM networks) conveying data information increases in a narrower optical bandwidth, the power launched into the fiber increases pushing the system's performance towards the nonlinear Shannon's limit. As such, the network upgradeability in terms of user data rate and number of users is compromised if no optimization scheme to minimize the fiber nonlinear impact on the system's performance is employed.

From the studies carried out in Chapter 4, it is clear that fiber nonlinear effects play an important role on the performance of coherent ultra-dense WDM based PON. Inter-channel nonlinearities, i.e. due to the nonlinear interaction among the several channels co-propagating in the fiber, are the dominant transmission impairments in the network. Specifically, inter-channel FWM accounts for the majority of the nonlinear noise accumulated in the received signal. This effect is particularly enhanced for coherent UDWDM-PON, which uses very narrow channel spacing when transporting QPSK modulated channels. Although the transmission distance might be limited to 100 km of fiber, inter-channel XPM is also an important source of noise that has to be analyzed when M-ary QAM modulated channels are transported. In either cases, the impact of FWM overpowers at least by 2.5 dB the impact of XPM in coherent UDWDM-PON limited to 32 channels.

How to mitigate FWM has been a topic of research in previous versions of WDM optical transport networks in which the system operates really close to the zero dispersion wavelengths,

i.e. by using Dispersion Shifted Fiber (DSF) or NZDSF [60]. Besides the fact that the channel spacing values used in previous versions were in the range of hundreds of Gigahertz, e.g. 400/200/100 GHz, the operation near the zero dispersion wavelengths boosted the FWM generation [61, 52].

One very interesting solution proposed to mitigate FWM crosstalk considered to use un-equally spaced channels that showed to be more effective compared to equally spaced channel [62]. The main idea of this technique is divide the available bandwidth into frequency slots and then finding the vector which best represents these slots in order to minimize the num-ber of FWM products falling into the WDM channels. This technique was firstly reported in [63, 62] for up to twelve WDM channels based on exhaustive computer search whereby the channel spacing must be greater than or equal to the pulse separation slot. The main ad-vantage is that no FWM is allowed to fall in the signal bandwidth, thus the resulting FWM crosstalk is almost zero. On the other hand, the operating bandwidth has to be expanded to accommodate all WDM channels for this allocation strategy to be successful. Another solution relies on obtaining unequally spaced channels that permits a few FWM products in the signal bandwidth where the operating bandwidth is not penalized. In that case, unequally spaced channels is achievable by performing small frequency tuning in the WDM channels. For in-stance, the maximum frequency tuning ($\pm$10 GHz) lesser than 10 % of the channel separation (100 GHz) was used in [J5] for 6 CW channels.

As far as inter-channel XPM is concerned, this effect is particularly relevant in the context of NG-OAN limited to 100 km of fiber when high-order QAM signaling is employed. For QPSK signaling, XPM (multi-channel) and SPM (single channel) are relevant when the transmission goes beyond hundreds of kilometers of fiber. In current coherent optical systems, SPM/XPM has been tackled by using DSP techniques [64, 65], [J8, J7].

This chapter, based on Journals [J1], [J5], [J6], [J7] and [J8], Conference papers [C3], [C5], [C12], [C13], [C17] and [C18] and Patent [P1], focuses on how to minimize inter-channel FWM in a coherent UDWDM-PON by employing unequally channel spacing. We studied different strategies to obtain unequally spaced channels keeping the overall bandwidth unchanged com-pared to equally spaced channels. The frequency tuning strategy is based either on Genetic Algorithm (GA) optimized frequency coefficients or by randomly set frequency coefficients. The chapter is organized as follows. Section 5.1 discusses how to obtain unequally spaced

channels by using GA (sub-section 5.1.1) and random frequency tuning (sub-section 5.1.2). Section 5.2 gives the directions toward the minimization of SPM and XPM.

5.1 Minimization of FWM

This section discusses two strategies to obtain unequally spaced channels for the minimization of FWM in coherent UDWDM-PON. The main focus is to mitigate some of the FWM crosstalk ($\pm$ 3 dB) without penalize the overall bandwidth. The approach considered in this work is based on performing small frequency tuning among all the WDM channels so that they are unequally spaced keeping the overall bandwidth unchanged. This is a realistic approach since most of the laser sources in the transmitters/receivers are tunable by a few nanometers. In coherent UDWDM-PON, a tunability of only a few Gigahertz are required since the channel spacing is below 25 GHz for instance. Fig. 5.1 illustrates the principal of the frequency tuning strategy to obtain unequally spaced channels. In WDM networks, the available optical bandwidth per channel (BW) is limited by an optical filter in the AWGs. This bandwidth BW has to be broad enough for allocating the optical signal which occupies $2 \times R_s$ with R_s being the symbol rate. Therefore, the remaining bandwidth Γ given by the difference $BW - 2 \times R_s$ can be used to perform small frequency tuning ($\Gamma = BW - 2 \times R_s$).
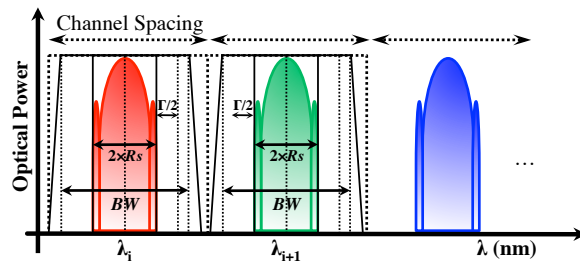
Figure 5.1: Frequency tuning scheme to obtain unequally spaced channels in UDWDM-PONs.

In the coherent UDWDM-PON analyzed in this work, which uses channel spacing of only 3.125 GHz, BW usually is around 2.5 GHz and the symbol rate is either 500 Mbaud or 625 Mbaud. In the case of 1.25 Gbaud signaling is used, $\Gamma \approx 1.25\ GHz$ or $\Gamma/2 \approx 625\ MHz$.

It is important to emphasize that the minimization of FWM improves as the available Γ increases, i.e. for the same BW the reduction of FWM improves as the R_s is decreased. The main advantage of this technique is that the bandwidth expansion is limited to maximum

$2 \times \Gamma/2 = \Gamma$. In the 32 channels case, the overall bandwidth is expanded by only $100 \times (2 \times \Gamma/2)/(32 \times 3.125 \ GHz) = 0.6 \ \%$.

In the following sections, two schemes for obtaining unequally spaced channels are discussed. Firstly, frequency and power coefficients optimized by a GA are found in a traditional WDM network. Secondly, a randomly set frequency coefficients are applied for the coherent UDWDM-PON.

5.1.1 Genetic Algorithm Approach

One strategy to obtain unequally spaced channels consists in optimizing the frequency coefficients $Gamma_i$ of all the available WDM channels. These optimized coefficients can be obtained by using GA for instance. In addition, power coefficients can also be found so that the generated FWM products that interfere with the WDM channels have lesser intensity. This power variation among the WDM channels is relevant in hybrid WDM rings / TDM trees network scenarios where some earlier dropped channels may need lesser energy than others [8], [C5, C4].

Power allocation is obtained by multiplying the initial channel power (P_i) by a coefficient (Θ) ranging from 0 to 1 ("1" means maximum power and "0" means channel turned off), i.e. $P'_i = P_i \times \Theta_i$. In order to avoid the channel deactivation one can simply bound those coefficients between 0.5 and 1.0 (3 dB variation). The frequency allocation (Γ) consists in adding values to the initial channel frequencies (f_i), i.e. $f'_i = f_i + \Gamma_i$. Therefore, GA finds the best set of parameters that minimizes the in–band FWM crosstalk vector given by $\|P_{FWM}(P'_i, f'_i)\|$, where $\|.\|$ stands for the norm. The calculation of P_{FWM} is found in [J5]. This approach considers the constraint that the final allocated power should be greater or equal to half of the total available power (P_T); i.e. the power summation of all WDM channels should be greater than half of the initial total power. The optimization problem can be defined as follows:

$$min \, \|P_{FWM}\left(P_i', f_i'\right)\|$$

$$P_i' = P_i \times \Theta_i^{GA}; f_i' = f_i + \Gamma_i^{GA}; i = 1 \cdots N_{ch};$$

$$S.T.: |\Gamma_i^{GA}| \leq 10 \, GHz$$

$$0 < \Theta_i^{GA} \leq 1$$

$$\sum_i P_i \geq P_T/2 \qquad\qquad (5.1)$$

where, P_i and f_i (c/λ_i) are the initial WDM power and frequency for ith channel, respectively.

The GA optimization scheme is demonstrated experimentally for a DWDM system consisting of 6 CW Distributed Feedback (DFB) lasers in C spectral band (0.8 nm or 100 GHz spacing). The transmitter lasers are multiplexed by an AWG with typical loss of $\approx$ 8 dB and transmitted into 9 km of DSF fiber in order to emphasize the impact of FWM and better demonstrate the effectiveness of the proposed algorithm. The fiber was previously characterized by an Optical Network Analyzer (ONA) in order to evaluate the attenuation, chromatic dispersion and dispersion slope values. In addition, 3 optical bands at 1553.33 nm, 1554.13 nm and 1554.94 nm were considered for monitoring the FWM power. Each transmitter laser allows a frequency variation of $\pm$120 GHz achieved by thermal tuning and a power variation between 3 dBm and 13 dBm. For a channel spacing of 100 GHz and considering the AWG filter of 40 GHz, the maximum allowable frequency tuning is $\pm$ 10 GHz. The output optical power spectrum was obtained by a high resolution OSA. The nonlinear refractive index and effective area were also computed indirectly using a single–objective Genetic Algorithm.

Firstly, a non-optimized power spectrum (P_i=7 dBm) was obtained in order to assess the FWM crosstalk and to compare it to the expected theoretical results. The simulation and experimental results showed a good agreement. Those values are depicted in Fig. 5.2(a). Fig. 5.2(b) displays a zoomed version of the power spectrum of the first 3 channels. By looking at the spectrum, we verify the existence of FWM interference in all the 6 channels ranging from -40 dBm to -37 dBm. The FWM crosstalk in the monitoring bands varies from -61 dBm to -43 dBm.

For the best optimization case (P_i=10 dBm), the obtained parameters were $\Gamma_i^{GA} = [9.5, -4.6, -8.2, 10.0, 7.4, -8.3] \, GHz$; $\Theta_i^{GA} = [0.914, 0.400, 0.400, 0.400, 0.400, 0.486]$. In that

situation none of the channels was deactivated. Fig. 5.2(c) depicts a zoom of the optimized
power spectrum of the first 3 channels. We pointed out that the interfering FWM products
were shifted away the vicinity of the channels which obviously reduces the effect of crosstalk.
For instance, using a 25 GHz electrical filter (typical for IMDD–10 Gb/s transmission) those
products would be fully removed. Fig. 5.2(d) shows the total FWM power crosstalk in the
9 channels obtained experimentally for the non-optimized (squares) and optimized (circles)
situations. Clearly, the FWM crosstalk reduction obtained by the GA optimization scheme
ranged from 3 dB to 10 dB for all the propagating channels.
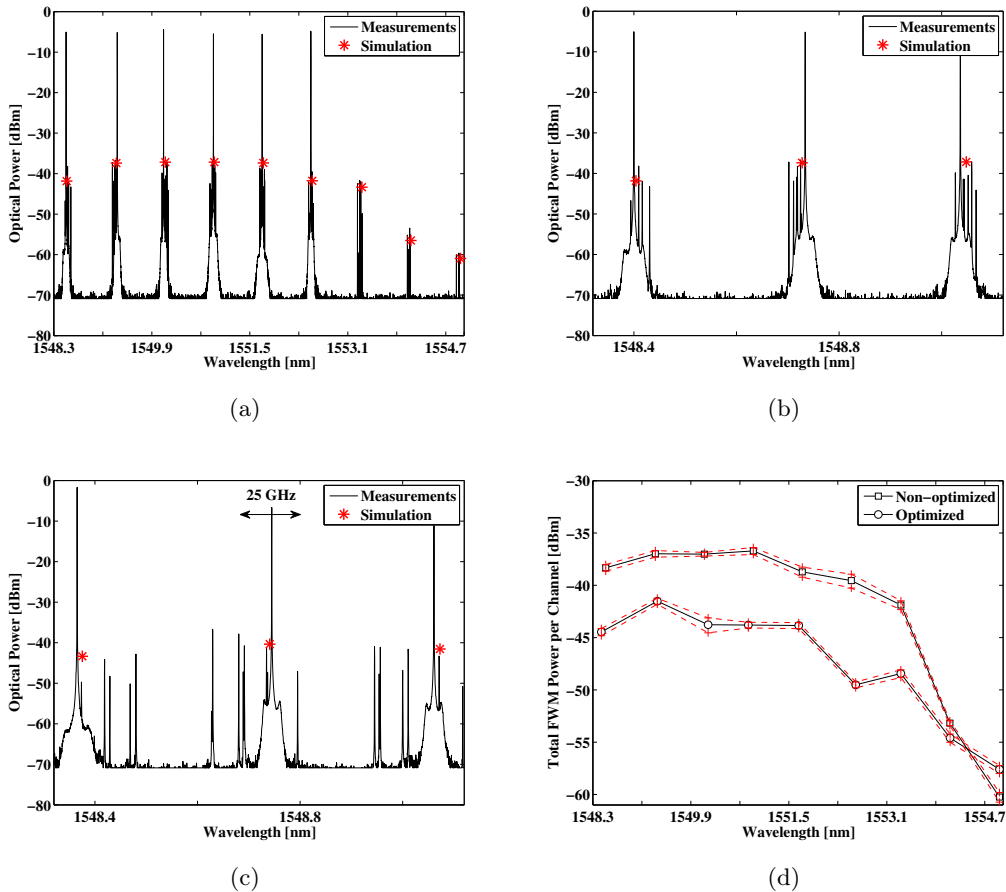
Figure 5.2: (a) Optical power spectrum for the non-optimized situation. Solid lines: experi-
mental; "∗": simulation. (b) Zoom of the first 3 non-optimized channels (equally spaced). (c)
Zoom of the first 3 optimized channels (unequally spaced). (d) Measured FWM power in each
channel. Squares: without optimization; circles: with optimization.

5.1.2 Randomly Set Frequency Coefficients

Optimizing all WDM channel coefficients may require a huge computation effort if the objective function has to be calculated for a very high number of channels, e.g. 1000 channels. Another strategy is simply set random frequency coefficients for all the WDM channels instead of running a multi-objective GA. This strategy is particularly interesting for coherent UDWDM-PON that can transport over 32 channels in a single fiber plant.

The *Randomly Set Frequency Coefficient* scheme is defined as follows for the coherent UDWDM-PON carrying 64×1 Gb/s–QPSK channels:

1. each QPSK channel occupies around 1.5 GHz optical bandwidth (sufficient for either 500 Mbaud or 625 Gbaud operations) out of the 2.5 GHz available optical bandwidth limited by the ideal AWG filter;

2. we considered that each optical carrier can be tuned at maximum $\Gamma \leq |500|\ MHz$. This approach ensures the signal will be inside the optical filter bandwidth without interfering with neighboring channels;

3. For each transmission, the optical carriers at the transmitters are updated as follows: $f_i' = f_i + \Gamma_i$ such that Γ_i assumes randomly any value in the vector $[-500, -250, 0 + 250, +500]\ MHz$. As a result, unequally channel spacing is obtained in a way that the majority of the FWM frequency components will fall outside the signal bandwidths; then those components are removed by electrical filtering (low-pass filter or digital filter in the coherent receiver) improving the SNR of the received constellation.

Fig. 5.3 shows the overall system performance in terms of maximum EVM among tested channels as a function of the input optical power per channel with (solid + circles) and without (dash + squares) the optimized channel frequency coefficients. In terms of nonlinear performance, the impact of FWM is relevant for network scenarios transporting number of channels higher than 16, i.e. splitting ratios higher than 16 (or *hybrid* for $K \leq 4$ and *fully transparent*). The network scenarios with lower splitting ratios (*hybrid* $K > 4$ and *filtered*) obtained the best overall performances since the reduced density of channels decreases the effectiveness of inter–channel FWM crosstalk. The *fully transparent* scenario (64 channels spaced by 3.125 GHz) and *hybrid* 2×200 GHz $\times$ 32–AWG ($K = 2$) obtained similar performance indicating that
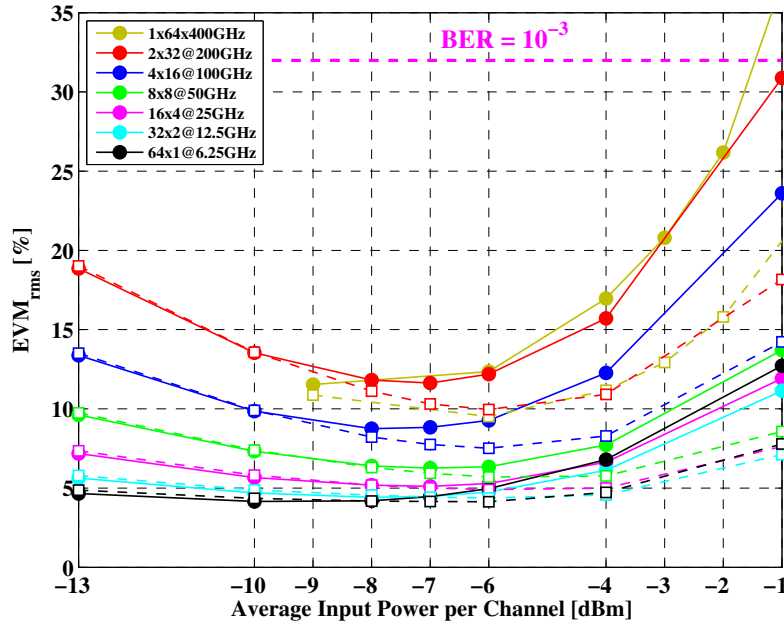
Figure 5.3: Overall system's performance (maximum EVM among tested channels) after transmission without (solid lines + circles) and with (dash lines + squares) randomly set frequency coefficients.

upgrading the network from 32 to 64 channels at 3.125 GHz has similar inter-channel FWM impact. This conclusion is in agreement with the discussion in Chapter 4, Section 4.2.

As far as the minimization of FWM is concerned, the optimization gain in terms of the EVM reduction is on average 4.4 dB with a lower endpoint of 3.2 dB and upper endpoint of 5.5 dB within the 95 % confidence interval. It is worth pointing out that the tested network scenarios with optimized parameters through the frequency tuning algorithm achieved on average an improvement of 3 dB in the optimal input power with EVM below the 10 % limit.

Both methods, *Genetic Algorithm* and *Randomly Set Frequency Coefficients* for optimizing the WDM channels are very effective frequency tuning schemes to obtain unequally channel spacing, which minimizes the FWM impact and improves the SNR up to 4.5 dB. The later is highly suitable for network scenarios with high channel count. Therefore, it is relevant to study the effectiveness of the *Randomly Set Frequency Coefficients* for the coherent UDWDM-PON transporting high-order QAM signaling. Here, we apply this technique, considering a maximum tuning of ± 500 MHz in the fully transparent homogeneous network to validate the analysis of nonlinearities dependence on power, link length and modulation formats discussed

in Chapter 4. Besides the fact that this technique is tested in systems (amplitude-modulated signals) where SPM/XPM is enhanced, it is worth pointing out that lower SNR improvements are expected in the following results since the symbol rate (R_s) is slightly higher, i.e. currently 625 Mbaud against previously 500 Mbaud per channel. This increased signal bandwidth basically decreases the out of band available for allocating FWM components thus worsening the ability of the coherent receiver in filtering these crosstalk components out.

Fig. 5.4 (32 × 1.25 Gb/s–QPSK), 5.5 (32 × 1.875 Gb/s–8PSK), 5.6 (32 × 2.5 Gb/s–16QAM), 5.7 (32 × 3.75 Gb/s–64QAM) and 5.8 (32 × 5 Gb/s–256QAM) show the EVM in dB of the center channel as a function of input power per channel measured with (solid lines plus circles) and without (dash line plus squares) optimized channel frequencies using the *Randomly Set Frequency Coefficients*. Note that both transmitter and local oscillator lasers in the OLT/ONU have the same random coefficient which does not exceed ± 500 MHz, i.e. intradyne detection in the receiver is performed.
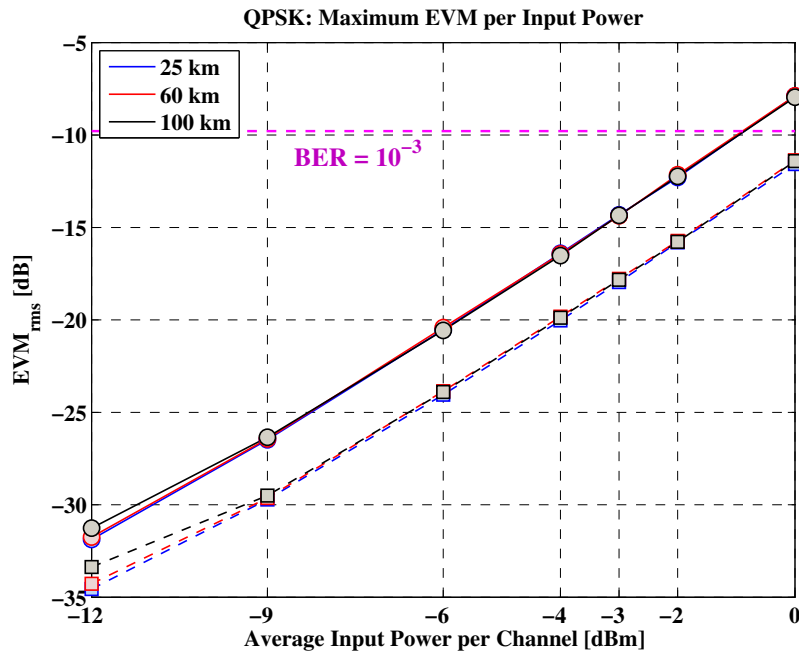
Figure 5.4: EVM of the received center channel versus input power/channel for 32 × 1.25 Gb/s–QPSK. Solid lines plus circles: non-optimized; Dash lines plus squares: optimized.

For all the transmitted modulation formats, the frequency tuning scheme reduced the overall EVM at least by 2.3 dB. Table 5.1 shows the EVM difference in dB, which gives an estimation of the SNR improvements, obtained from the solid lines and the dash lines in
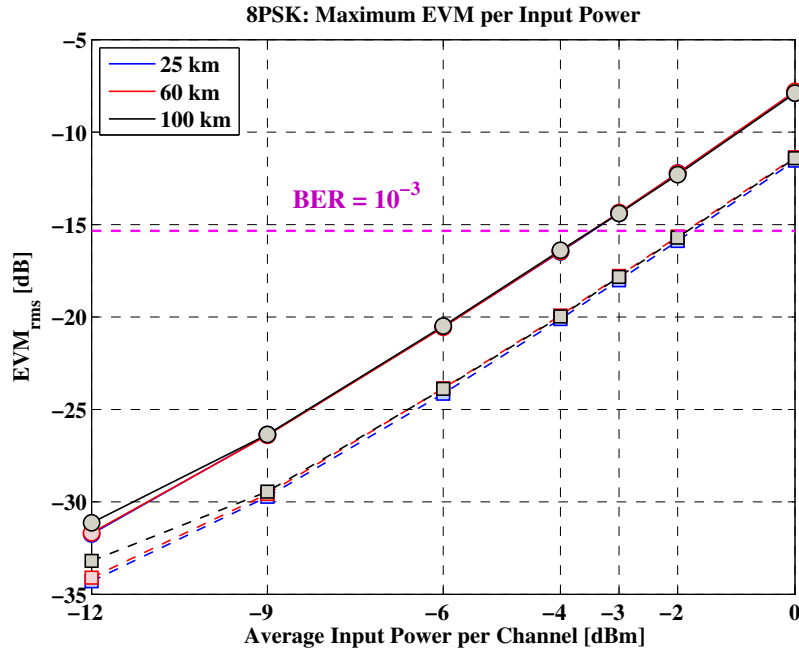
Figure 5.5: EVM of the received channel versus input power/channel for 32×1.875 Gb/s–8PSK. Solid lines plus circles: non-optimized; Dash lines plus squares: optimized.

Fig. 5.4, 5.5, 5.6, 5.7 and 5.8. Since the system with phase-modulated (QPSK and 8PSK) channels has negligible SPM/XPM impact, the frequency tuning scheme manages to reduce FWM by 3.5 dB. This SNR improvement hardly changed for different transmission distances.

Nevertheless when the UDWDM-PON system transported amplitude-modulated signals (16QAM, 64QAM and 256QAM) the reductions were decreased to 3.2 dB and 2.4 dB for shorter and longer links, respectively. Furthermore, the SNR improvement slightly decreases as the order of the QAM constellation increases, e.g. the SNR improvement at 25 km of fiber is reduced by 0.4 dB when the QAM order increases from 16 to 256 ($+SNR_{16QAM@25\ km} = 3.19\ dB$ and $+SNR_{256QAM@25\ km} = 2.83\ dB$). This comes from the fact that performing small frequency tuning in the transmitter lasers effectively minimizes solely FWM with minimal effect on the XPM.

Recalling the values of F/X (FWM to XPM ratio) in Tables 4.1 and 4.2 in Section 4.1, one can recalculate these values by taking into account the reductions of FWM in Table 5.1. This is particularly interesting to evaluate the relevance of both FWM and XPM for a given transmission distance and user's data rate. As an example, consider a UDWDM-PON with 100 km–links carrying M-ary QAM and employing *Randomly Set Frequency Coefficients*, the

Table 5.1: SNR improvements after optimizing the channel frequencies.

Modulation	25 km	60 km	100 km
$QPSK$	3.53 dB	3.41 dB	3.39 dB
$8PSK$	3.59 dB	3.39 dB	3.40 dB
$16QAM$	3.19 dB	2.81 dB	2.52 dB
$64QAM$	2.95 dB	2.51 dB	2.35 dB
$256QAM$	2.83 dB	2.44 dB	2.37 dB
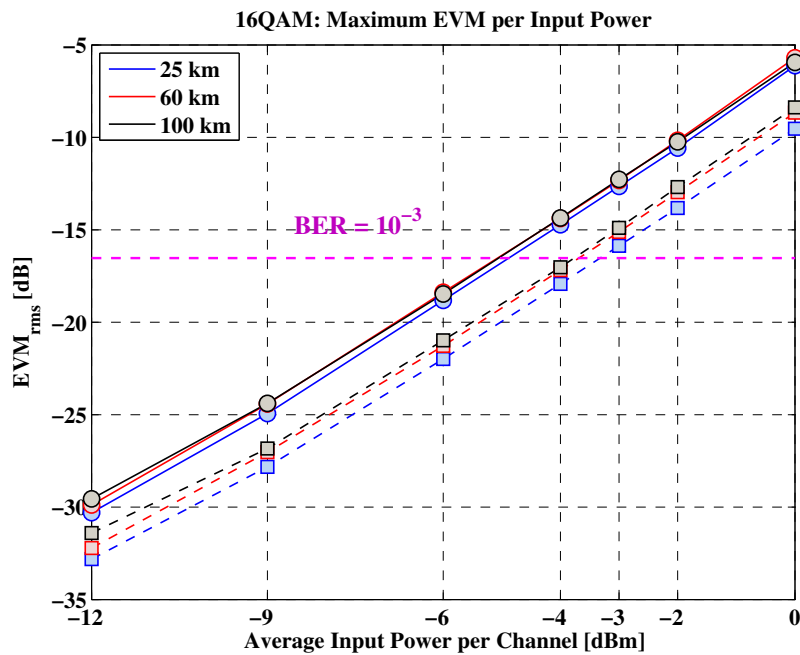
Figure 5.6: EVM of the received center channel versus input power/channel for 32×2.5 Gb/s–16QAM. Solid lines plus circles: non-optimized; Dash lines plus squares: optimized.

system's performance is limited equally by XPM and FWM since the F/X is reduced to only 0.2 dB (256QAM at 100 km). The chart in Fig. 5.9 gives all the F/X values versus modulation formats before (top figure) and after (bottom figure) minimizing FWM in the coherent UDWDM-PON. This chart confirms the conclusions in Chapter 4 that phase-modulated channels are mostly limited by FWM whereas amplitude-modulated channels are impaired by both FWM and XPM. In addition, unequally spaced channels mitigate most of the FWM crosstalk among WDM channels.
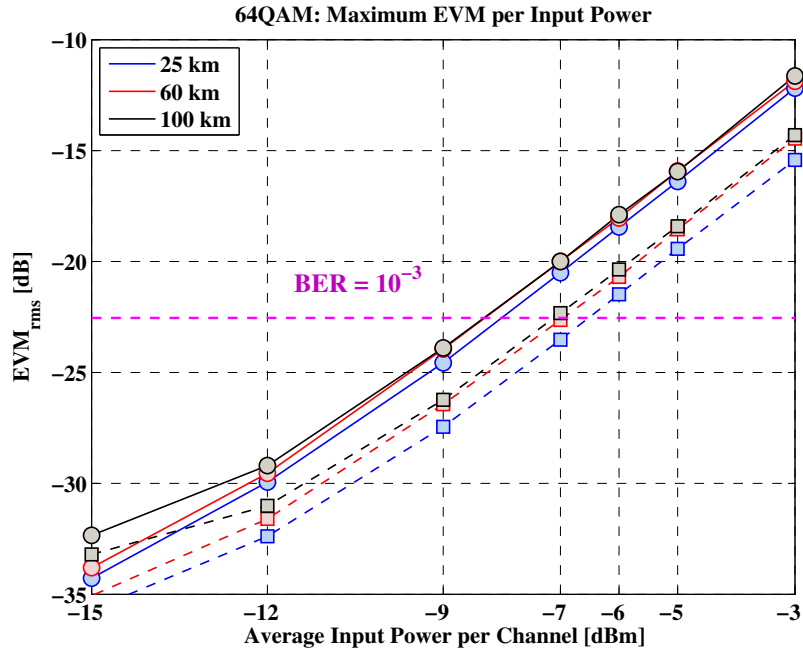
Figure 5.7: EVM of the received center channel versus input power/channel for $32 \times$ 3.75 Gb/s–64QAM. Solid lines plus circles: non-optimized; Dash lines plus squares: optimized.
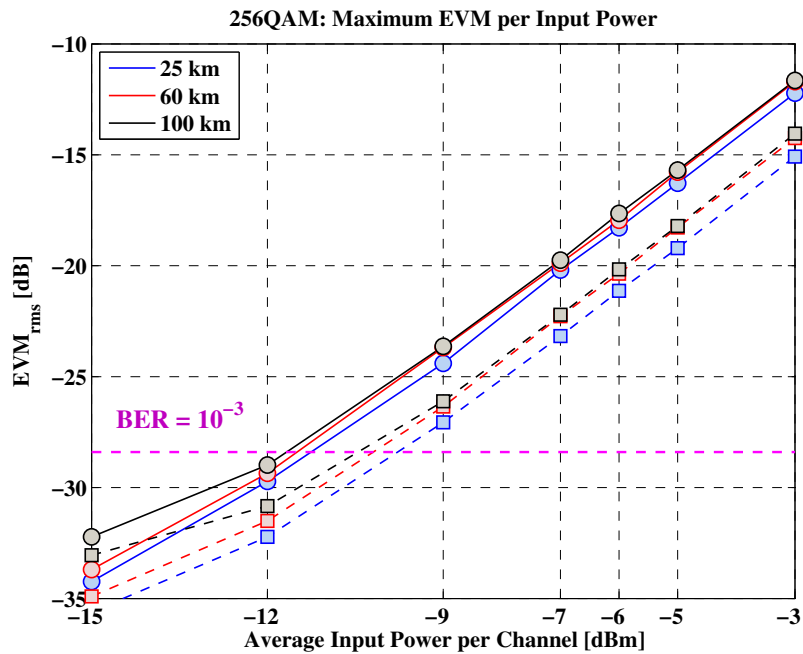
Figure 5.8: EVM of the received center channel versus input power/channel for 32×5 Gb/s– 256QAM. Solid lines plus circles: non-optimized; Dash lines plus squares: optimized.
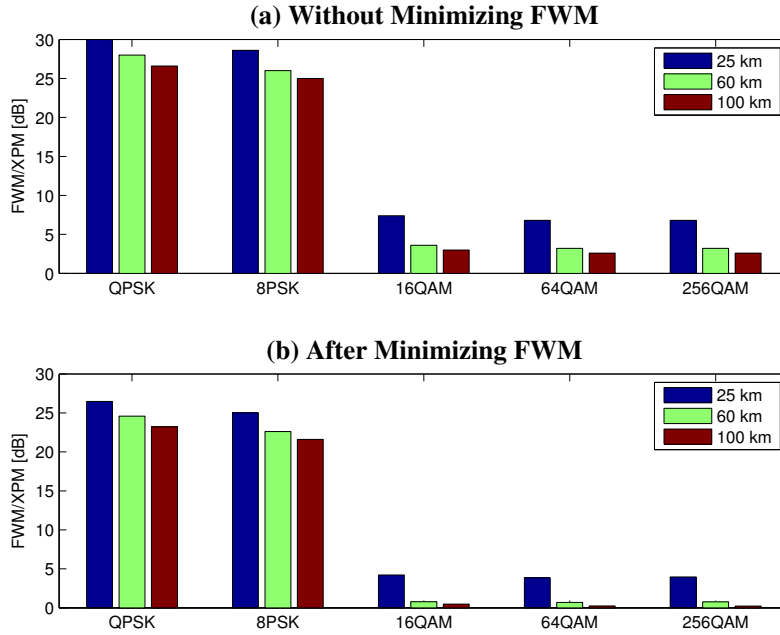
Figure 5.9: Comparison of FWM and XPM for different modulation formats before (a) and after (b) minimizing FWM.

5.2   Minimization of SPM/XPM

The discussion in previous sections indicated the directions toward nonlinear compensation for coherent UDWDM-PON. Most of the results pointed out solutions for the minimization of the most relevant transmission impairment in such a network scenario, i.e. FWM. On the other hand, XPM effect can not be neglected specially for high-order QAM modulation formats over extended reach (100 km links). Since XPM manifests in the same manner as SPM via accumulated nonlinear phase noise during transmission, the compensation strategy may follow similar directions. SPM is mostly mitigated in the digital domain via nonlinear backward-propagation (or simply back-propagation) in current coherent optical systems. XPM induced in WDM transport networks can also be mitigated using such a digital signal processing technique. On the other hand, data information from neighboring co-propagated channels have to be known (or detected) at receiver side. In order to mitigate XPM, data information from neighboring channels have to be fed to all coherent receivers in a cooperative way or all receivers should have a very broad bandwidth to detected signal from other channels.

SPM compensation are mainly based on the digital solution of NLS equation of the re-

ceived signal in the backward direction. The most used solution is based on the Split-Step Fourier (SSF) back-propagation [66, 64]. Recently, great attention has been given to Volterra series nonlinear equalizers [26], [J8]. In [J8], both linear (1st order Volterra kernel) and non-linear (3rd order Volterra kernel) transfer functions (see Chapter 3, section 3.1) are evaluated digitally after coherent detection. The main advantage of Volterra Series Nonlinear Equalizer (VSNE) relies on its superior performance compared to SSF back-propagation when the coherent receiver operates at 2 samples per symbol, i.e. the received signal is sampled at twice the symbol rate [J8]. As for the SSF back-propagation, VSNE can also be applied for Polarization-Division Multiplexing (PDM) systems. One example is shown in Fig. 5.10 where BER results versus input power are measured for a single channel 120 Gb/s–Polarization Multiplexing Quadrature Phase-Shift Keying (PM-QPSK) (R_s=30 Gbaud) transmitted over 16 spans of 100 km–NZDSF.

Multi-span propagation is achieved using a recirculating loop composed of a single fiber span. Analog-to-digital conversion is performed at 50 GSa/s using a Tektronix DPO71604 oscilloscope, whose measured -3 dB analog bandwidth is $\sim$ 13 GHz. The most relevant experimental parameters are: $R_s = 30$ Gbaud, $\alpha = 0.22$ dB/km, $\beta_2 = $ -3.29 ps^2/km, $\gamma = 2.01$ (W·km)$^{-1}$, $L_{span} = 100$ km, $SP = 1.6$ where SP denotes the number of samples per symbol at the receiver. Further details about the experimental setup employing NZDSF can be found in [67].

In this case, we compare digital compensation of chromatic dispersion (CD represented by "$\times$") in the frequency domain and SPM using back-propagation SSF (squares) and VSNE (circles). The best SSF back-propagation was obtained with only one step per span using its single-polarization or scalar back-propagation and dual-polarization using Manakov equations. VSNE was applied in a span-by-span basis. Note that both scalar versions of SSF and VSNE equalizers do not take into account nonlinear cross effect between different polarization states. The cross effect on dual-polarization systems are compensated by using the Manakov equations (see [66]) which improves the overall performance at a price of doubled complexity added to the DSP in the coherent receiver. Refer to [C17] for detailed description of the Manakov equations in the VSNE equalizer and all the DSP blocks in the coherent receiver.

The best performance of SSF back-propagation at 1 step per span shown in Fig. 5.10 comes from the fact that low temporal resolution (1.6 physical samples per symbol) associated with

narrow electrical filtering at the oscilloscope, impose severe limitations on the performance of nonlinear equalization. The same limitation is setting the performance of VSNE. On the other hand, the dual-polarization versions of SSF and VSNE (solid lines) enable to increase the optimum input power by about 0.7 dB with respect to their scalar versions (dash lines). Compared to CD compensation only (dash-dot line), dual-polarization versions improve the optimum input power by 1.7 dB. As far as BER is concerned, dual-polarization back propagation equalizers reduce BER for the 16 spans of NZDSF transmission by a factor of $2.5\times$ and $5\times$ with respect to their scalar versions and CD compensation, respectively.

Although the previous results pointed out digital equalization of SPM in a single-channel transmission systems, Volterra series nonlinear equalizer can also be very suitable for XPM compensation in coherent UDWDM-PON. The minimization of FWM with randomly set frequency coefficients improves the overall performance by 3 dB. Extra SNR improvement can be achieved by using digital equalization of XPM in the ONU. In UDWDM-PON, the ONU only requires 625 MHz of electrical bandwidth to operate at 1 Gb/s (500 Mbaud–QPSK) or more depending on the modulation format at hand. On the other hand, it is reasonable to assume that the broader bandwidth and faster ADC sampling rate allow "hearing" some data
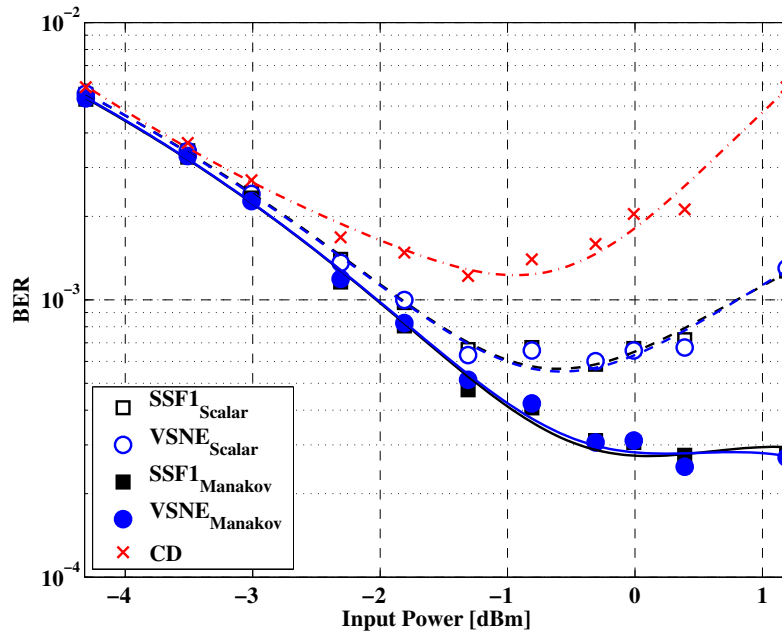
Figure 5.10: Measured BER of 30 Gbaud–PM-QPSK after transmission over 16×100 km–NZDSF. Dash-dot line: CD compensation; Dash lines: Scalar; Solid lines: Manakov.

information from other channels. Regardless of security issues, this extra information is useful for XPM compensation using digital back-propagation. This topic of research is not covered in this work and shall be investigated in future studies.

5.3   Conclusions

This chapter addressed solutions suitable for the minimization of inter-channel fiber non-linearities on coherent UDWDM-PON for various bit rates (different high-order constellations) and transmission distances.

As discussed in previous chapters, FWM is relevant for Standard Single-Mode Fibers when several channels are closely multiplexed by only 3 GHz apart. FWM frequency components cause strong crosstalk when WDM channels are equally spaced. When WDM channels are unequally spaced, FWM frequency components are spread over the entire bandwidth where some of them can be easily filtered in the receiver.

We showed that performing small frequency tuning (with respect to the channel spacing) schemes are very effective to obtain unequally spaced channels. Multi-objective Genetic Algorithm is efficient for for reduced number of channels due to the several computations of the objective function. Randomly set frequency coefficients can be applied for for very high channel count systems, e.g. 1000 channels. The main advantage of the aforementioned methods is that good FWM reduction is achieved without penalizing the overall bandwidth.

The overall system's performance can be improved even further for systems transporting QAM signaling if XPM compensation is employed in the coherent receiver. SPM is easily mitigated using advanced digital signal processing (digital back-propagation). The concept can be extended to XPM compensation in broadband receivers or in cooperative receivers.

Chapter 6

Conclusion

6.1 Summary and Concluding Remarks

It is challenging to minimize the optical network costs when ONU transceivers require a laser light source as in coherent systems. At the same time, it is more challenging to provide dedicated 10 Gb/s connections for several users in the same PON using IMDD technologies. Coherent optical communication systems have demonstrated what is the real potential of the optical fiber to convey data information. In order to better exploit the full potential of already deployed PONs infrastructure, the paradigm of intensity modulation direct detection communication has to be changed. Wide wavelength-tuning range, simple bandwidth upgrade and receiver sensitivity are just a few examples of how coherent Wavelength-Division Multiplexing Passive Optical Networks (WDM-PON) improve the network performance and management.

This Ph.D. thesis investigated coherent optical solutions for NG-OAN. The general scientific contributions within the thesis framework are listed below:

- design of network elements and subsystems required for high aggregate data rates Passive Optical Networks;

- numerical modeling of the most relevant sources of transmission impairments such as fiber nonlinearities and their dependence on feeder power, transmission distance, modulation formats and network scenarios;

- novel schemes for transmission impairment compensation based on all-optical solutions and digital signal processing techniques to boost network capabilities.

Regarding the first objective, this work addressed some of the most relevant technical as-

pects of the OLT, ODN and ONU for Next-Generation all-Optical Access Networks. Coherent transceivers employing high-order modulation formats and digital signal processing are key network elements for solving the needs for broadband in Optical Access Networks (OAN). The network design relied on UDWDM technologies in the OLT, which routes data information to tunable ONUs (without optical filter) via transparent power splitter. This solution has the advantage of providing wide-range tunable ONUs (tunable local oscillator), extended reach and/or high splitting ratios (receiver sensitivity) and data rate upgradeability (high-order constellations). In addition, digital signal processing techniques can be employed to alleviate the transceivers' requirements as well as transmission related impairments.

One of the challenges related to the network scenarios investigated in this work encompasses the impact of fiber related transmission impairments. The combination of high channel count and reduced channel spacing may invalidate the network operation if transmitter and receiver parameters are not properly optimized. As such, the second objective of this work addressed methodologies to estimate the overall performance and the most relevant sources of transmission impairments.

These studies relied on Volterra theory for modeling the total field propagation (or overall performance) over the optical fiber in coherent ultra-dense WDM based passive optical networks. By using transfer functions to represent linear and nonlinear fiber effects, VSTF is a powerful mathematical tool that provides both phase and amplitude of optical fiber channel. We presented a very efficient method for evaluating the double integral in the frequency domain of the 3rd order VSTF. This algorithm avoids zero amplitude frequency components outside the bandwidth of the optical signal to improve the numerical complexity of the method.

As far as the overall system's performance is concerned, the modified version of the 3rd order VSTF was validated against SSF simulation in UDWDM-PON. In that case for 32 channels spaced by 3.125 GHz, accurate EVM results were found for input powers limited to -3 dBm per channel over a single SSMF link with 100 km. Furthermore, estimates for the maximum input power per channel, when the bit rate scales using high-order modulation formats (MPSK and MQAM), were determined so that the performance was within the limit of current 7 % overhead FEC employed in current optical communication systems. It is important to emphasize that the simulation model (transmitters, receivers and optical fiber channel based on SSF and VSTF) developed in this Ph.D. work has been experimentally

validated in heterogeneous UDWDM network scenarios.

Most importantly, the range of dominance of the most relevant fiber nonlinearities (SPM, XPM and FWM) was determined for various network reach and capacities (obtained with high-order constellations with fixed symbol rate). For the specific case of 32 channels, UDWDM-PON network is mostly limited by FWM (25<F/X<30 dB, F/X) when transmitting only M-ary PSK channels. On the other hand, the network is impaired by both FWM and XPM (2.5<F/X<7.5 dB) when transmitting M-ary QAM channels. The main advantage of transmitting PSK is the flexibility to scale the number of users in the same optical distribution network as high as 1024 keeping similar nonlinear performance as the 32 users case. In terms of user's data rate upgradeability, the modulation format is limited to provide 8 Gb/s per channel if the 3 GHz frequency grid is employed. On the contrary, QAM signaling offers great possibilities to upgrade the user's data rate up to 24 Gb/s per user, i.e. 3 Gbaud–256QAM using the 3.125 GHz optical bandwidth. Nevertheless, the performance degradation keeps increasing as the number of QAM channels increases since QAM signaling enhances induced–XPM nonlinear phase noise. In summary, if the ODN in coherent UDWDM-PON is deigned to provide the highest number of users (e.g. 1000) at 1 Gb/s, QPSK signaling provides the best robustness against fiber impairments. If the ODN is designed to provide data rate per users as high as 10 Gb/s, QAM is the best format if the number of users does not exceed 64.

The last topic of this work discussed novel solutions suitable for the minimization of inter-channel and intra-channel fiber nonlinearities on coherent UDWDM-PON for various bit rates and distances. The main target of this research topic was the minimization of FWM since it is most relevant nonlinear effect in UDWDM-PON scenarios using channel spacing as lows as 3 GHz.

We showed that performing small frequency tuning (with respect to the channel spacing) schemes are very effective to obtain unequally spaced channels. *Multi-objective Genetic Algorithm* is efficient for reduced number of channels due to the several computations of the objective function. *Randomly set frequency coefficients* can be applied for very high channel count systems, e.g. 1000 channels. The main advantage of the aforementioned methods is that about 3 dB FWM reduction is attained without penalizing the overall bandwidth. The overall system's performance can be improved even further for systems transporting QAM signaling if XPM compensation is employed in the coherent receiver. SPM is easily mitigated using ad-

vanced digital signal processing (*digital back-propagation*). The concept can be extended to XPM compensation in broadband receivers or in cooperative receivers.

6.2   Directions for Future Works

This Ph.D. work has addressed several research topics on next-generation information and communication technologies. Around the world, several companies and universities have been collaborating towards improving network performance and flexibility at minimal cost. Related to this work, below is listed some topics to be considered in future studies.

- High-order nonlinearities such as SRS and SBS induced by high-power PON technologies in heterogeneous NG-OAN. Future PON technologies should cope with the existence of analog Video broadcasting and XG-PON for instance, whose powers can be as high as 21 dBm.

- Digital compensation of inter-channel XPM in Terabit aggregate PONs transporting high-order QAM constellations. As pointed out throughout this work, coherent ONUs can take advantage of the extra information available at receiver due to the closely packed channels. This extra information can be fed to the nonlinear compensation algorithm.

- Analysis of the network energy consumption and its relation to both economical and environmental aspects. The main challenge of this study is to investigate new algorithms and protocols to reduce the consumption of energy in the transceivers within the OLT and ONUs.

- Demonstration of high-capacity PON using special pulse shaping for improving spectral efficiency at 3 GHz frequency grid. In this work, we focused on using about one third of the available optical bandwidth per channel, i.e. 625 Mbaud at 3.125 GHz channel spacing. Therefore, there is margin to go up to higher bit rates per channel using Nyquist filtering (pulse shape), e.g. 20 Gb/s per channel.

- Experimental demonstration of Terabit PON network scenarios and Volterra nonlinear models. In this work we showed via numerical simulations that coherent WDM-PON network scenarios are promising solutions for NG-OAN. One interesting topic of research

is to demonstrate experimentally all the network transmission capabilities. The main challenge is how to generate several multiplexed optical carriers at 3.125 GHz for instance. One possible solution relies on the use of frequency recirculating loops to avoid costly ultra-dense filter technologies. The same experimental setup would be useful for the validation of the nonlinear models based on Volterra series developed in this work.

References

[1] J. Prat. *Next-Generation FTTH Passive Optical Networks: Research Towards Unlimited Bandwidth Access.* Springer, 2008.

[2] F. J. Effenberger, D. Cleary, O. Haran, G. Kramer, R. D. Li, M. Oron, and T. Pfeiffer. An introduction to PON technologies [Topics in Optical Communications]. *IEEE Communications Magazine*, 45(3):S17–S25, March 2007.

[3] ITU-T. ITU-T Recommendation G.984.1 (2008), Gigabit-capable Passive Optical Networks (GPON): General characteristics. Technical report, ITU, 2008.

[4] IEEE. 802.3-2002 IEEE Standard for Information Technology-Telecommunications and Information Exchange Between Systems- Local and Metropolitan Area Networks- Specific Requirements Part 3: Carrier Sense Multiple Access With Collision Detection (CSMA/CD) Access Me. Technical report, IEEE, 2002.

[5] ZTE. A Comparisson between GPON and EPON. *ZTE Technologies*, May 2007.

[6] ITU-T. ITU-T Recommendation G.987.1 (2010), 10-Gigabit-capable passive optical networks (XG-PON): General requirements. Technical report, ITU, 2010.

[7] IEEE. 802.3av-2009 IEEE Standard for Information technology - Telecommunications and information exchange between systems - Local and metropolitan area networks - Specific requirements Part 3: Carrier Sense Multiple Access with Collision Detection (CSMA/CD) Acc. Technical report, IEEE, 2009.

[8] J. A. Lázaro, J. Prat, P. Chanclou, G. M. T. Beleffi, A. L. Teixeira, I. Tomkos, R. Soila, and V. Koratzinos. Scalable extended reach PON. In *Optical Fiber Communication Conference (OFC)*, page OThL2, San Diego, CA, USA, 2008. Optical Society of America.

[9] E. Wong. Next-Generation Broadband Access Networks and Technologies. *Journal of Lightwave Technology*, 30(4):597–608, February 2012.

[10] E. Gottwald, H. Rohde, and S. Smolorz. Machbarkeit kohärenter Einfaser-UDWM PONs mit 1000 Teilneh- mern und 100 km Reichweite. In *2010 ITG Symposium on Photonic Networks*, pages 1–4, Leipzig, Germany, 2010. IEEE.

[11] P. Poggiolini, G. Bosco, A. Carena, V. Curri, V. Miot, and F. Forghieri. Performance Dependence on Channel Baud-Rate of PM-QPSK Systems Over Uncompensated Links. *IEEE Photonics Technology Letters*, 23(1):15–17, January 2011.

[12] A. H. Gnauck, P. J. Winzer, S. Chandrasekhar, X. Liu, B. Zhu, and D. W. Peckham. Spectrally Efficient Long-Haul WDM Transmission Using 224-Gb/s Polarization-Multiplexed 16-QAM. *Journal of Lightwave Technology*, 29(4):373–377, February 2011.

[13] N. Cvijetic. OFDM for Next Generation Optical Access Networks. *Journal of Lightwave Technology*, 30(4):384–398, 2012.

[14] R.-J. Essiambre, G. Kramer, P. J. Winzer, G. J. Foschini, and B. Goebel. Capacity Limits of Optical Fiber Networks. *Journal of Lightwave Technology*, 28(4):662–701, February 2010.

[15] F. J. Effenberger. The XG-PON System: Cost Effective 10 Gb/s Access. *Journal of Lightwave Technology*, 29(4):403–409, February 2011.

[16] N. Cvijetic, M.-F. Huang, E. Ip, Y. Shao, Y.-k. Huang, M. Cvijetic, and T. Wang. 1.92Tb/s coherent DWDM-OFDMA-PON with no high-speed ONU-side electronics over 100km SSMF and 1:64 passive split. *Optics Express*, 19(24):24540–24545, November 2011.

[17] S. Straullu, S. Abrate, F. Forghieri, V. Ferrero, and R. Gaudino. Optimization of self-coherent reflective PON to achieve a new record 42 dB ODN power budget after 100 km at 1 . 25 Gbps. In *European Conference and Exposition on Optical Communications (ECOC)*, page Th.3.D.6, Amsterdam, Netherlands, 2012. IEEE, OSA.

[18] A. Carena, V. Curri, P. Poggiolini, and F. Forghieri. Guard-Band for 111 Gbit/s coherent PM-QPSK channels on legacy fiber links carrying 10 Gbit/s IMDD channels. In *Optical Fiber Communication Conference (OFC)*, page OThR7, San Diego, CA, USA, 2009. Optical Society of America.

[19] M. G. Taylor. Coherent Detection Method Using DSP for Demodulation of Signal and Subsequent Equalization of Propagation Impairments. *IEEE Photonics Technology Letters*, 16(2):674–676, February 2004.

[20] S. J. Savory. Digital Coherent Optical Receivers: Algorithms and Subsystems. *IEEE Journal of Selected Topics in Quantum Electronics*, 16(5):1164–1179, September 2010.

[21] I. Fatadin, D. Ives, and S. J. Savory. Laser Linewidth Tolerance for 16-QAM Coherent Optical Systems Using QPSK Partitioning. *IEEE Photonics Technology Letters*, 22(9):631–633, May 2010.

[22] S. J. Savory. Digital filters for coherent optical receivers. *Optics Express*, 16(2):804–817, January 2008.

[23] A. D. Ellis, J. Zhao, and D. Cotter. Approaching the Non-Linear Shannon Limit. *Journal of Lightwave Technology*, 28(4):423–433, February 2010.

[24] M. R. Phillips and D. M. Ott. Crosstalk due to optical fiber nonlinearities in WDM CATV lightwave systems. *Journal of Lightwave Technology*, 17(10):1782–1792, 1999.

[25] K. V. Peddanarappagari and M. Brandt-Pearce. Volterra series transfer function of single-mode fibers. *Journal of Lightwave Technology*, 15(12):2232–2241, 1997.

[26] R. Weidenfeld, M. Nazarathy, R. Noe, and I. Shpantzer. Volterra Nonlinear Compensation of 112 Gb / s Ultra-long-haul Coherent Optical OFDM based on Frequency-Shaped Decision Feedback. In *European Conference and Exposition on Optical Communications (ECOC)*, number 1, page 2.3.3, Vienna, Austria, 2009. IEEE.

[27] B. Xu and M. Brandt-Pearce. Comparison of FWM- and XPM-induced crosstalk using the volterra series transfer function method. *Journal of Lightwave Technology*, 21(1):40–53, January 2003.

[28] S. Smolorz, H. Rohde, E. Gottwald, D.W. Smith, and A. Poustie. Demonstration of a coherent UDWDM-PON with real-time processing. In *Optical Fiber Communication Conference (OFC)*, page PDPD4, Los Angeles, CA, USA, 2011. Optical Society of America.

[29] H. Rohde, S. Smolorz, J. S. Wey, and E. Gottwald. Coherent Optical Access Networks. In *Optical Fiber Communication Conference (OFC)*, page OTuB1, Los Angeles, CA, USA, 2011. OSA.

[30] M. Seimetz. *High-Order Modulation for Optical Fiber Transmission*, volume 143 of *Springer Series in Optical Sciences*. Springer Berlin Heidelberg, Berlin, Heidelberg, 2009.

[31] G. P. Agrawal. *Nonlinear Fiber Optics*. Academic Press, San Diego, CA, 3 edition, 2001.

[32] J.-H. Lee. *Analysis and Characterization of Fiber Nonlinearities with Deterministic and Stochastic Signal Sources*. PhD, University of Virginia, 2000.

[33] R. A. Shafik, M. S. Rahman, and A. R. Islam. On the Extended Relationships Among EVM, BER and SNR as Performance Metrics. In *2006 International Conference on Electrical and Computer Engineering (ICECE)*, number December, pages 408–411, Dhaka, Bangladesh, December 2006. IEEE.

[34] 3GPP. 3GPP TS 45.005 - Radio Access Network; Radio transmission and reception. Technical report, 3GPP, 2009.

[35] ITU-T. ITU-T Recommendation G.984.2 (2003), Gigabit-capable Passive Optical Networks (GPON): Physical Media Dependent (PMD) layer specification. Technical report, ITU, 2003.

[36] ITU-T. ITU-T Recommendation G.987 (2010), 10-Gigabit-capable Passive Optical Network (XG-GPON) systems: Definitions, abbreviations and acronyms. Technical report, ITU, 2010.

[37] ITU-T. ITU-T Recommendation G.987.2 (2010), 10-Gigabit-capable passive optical networks (XG-PON): Physical media dependent (PMD) layer specification. Technical report, ITU, 2010.

[38] K.-P. Ho. *Phase-Modulated Optical Communication Systems*. Springer, New York, NY, 1 edition, 2005.

[39] T. Pfau, S. Hoffmann, and R. Noe. Hardware-Efficient Coherent Digital Receiver Concept With Feedforward Carrier Recovery for M-QAM Constellations. *Journal of Lightwave Technology*, 27(8):989–999, April 2009.

[40] M. Seimetz. Laser Linewidth Limitations for Optical Systems with High-Order Modulation Employing Feed Forward Digital Carrier Phase Estimation. In *Optical Fiber Communication Conference (OFC)*, page OTuM2, San Diego, CA, USA, 2008. Optical Society of America.

[41] A. Bononi, M. Bertolini, P. Serena, and G. Bellotti. Cross-Phase Modulation Induced by OOK Channels on Higher-Rate DQPSK and Coherent QPSK Channels. *Journal of Lightwave Technology*, 27(18):3974–3983, September 2009.

[42] F. Rice, B. Cowley, B. Moran, and M. Rice. Cramer-Rao lower bounds for QAM phase and frequency estimation. *IEEE Transactions on Communications*, 49(9):1582–1591, 2001.

[43] A. Mecozzi, C. B. Clausen, and M. Shtaif. System impact of intra-channel nonlinear effects in highly dispersed optical pulse transmission. *IEEE Photonics Technology Letters*, 12(12):1633–1635, 2000.

[44] S. Kumar and D. Yang. Second-order theory for self-phase modulation and cross-phase modulation in optical fibers. *Journal of Lightwave Technology*, 23(6):2073–2080, June 2005.

[45] M. Nazarathy, J. Khurgin, R. Weidenfeld, Y. Meiman, P. Cho, R. Noe, I. Shpantzer, and V. Karagodsky. Phased-array cancellation of nonlinear FWM in coherent OFDM dispersive multi-span links. *Optics Express*, 16(20):15777–15810, September 2008.

[46] X. Chen and W. Shieh. Closed-form expressions for nonlinear transmission performance of densely spaced coherent optical OFDM systems. *Optics Express*, 18(18):19039–19054, August 2010.

[47] P. Poggiolini, A. Carena, V. Curri, G. Bosco, and F. Forghieri. Analytical Modeling of Nonlinear Propagation in Uncompensated Optical Transmission Links. *IEEE Photonics Technology Letters*, 23(11):742–744, June 2011.

[48] G. Bosco, P. Poggiolini, A. Carena, V. Curri, and F. Forghieri. Analytical results on channel capacity in uncompensated optical links with coherent detection. *Optics Express*, 19(26):B440–B449, November 2011.

[49] H. M. Salgado and J. J. O'Reilly. Volterra series analysis of distortion in semiconductor laser diodes. *IEE Proceedings J Optoelectronics*, 138(6):379–382, 1991.

[50] Q. Zhang. *Performance Analysis and Design of WDM Based Optical Communication Systems Using a Volterra Series Method*. PhD, University of Virginia, 2001.

[51] B. Xu and M. Brandt-Pearce. Modified Volterra series transfer function method. *IEEE Photonics Technology Letters*, 14(1):47–49, 2002.

[52] N. Shibata, R. P. Braun, and R. G. Waarts. Phase-mismatch dependence of efficiency of wave generation through four-wave mixing in a single-mode optical fiber. *IEEE Journal of Quantum Electronics*, 23(7):1205–1210, July 1987.

[53] P. J. Winzer, A. H. Gnauck, C. R. Doerr, M. Magarini, and L. L. Buhl. Spectrally Efficient Long-Haul Optical Networking Using 112-Gb/s Polarization-Multiplexed 16-QAM. *Journal of Lightwave Technology*, 28(4):547–556, February 2010.

[54] P. J. Winzer. Beyond 100G Ethernet. *IEEE Communications Magazine*, 48(7):26–30, July 2010.

[55] W. Shieh. OFDM for Flexible High-Speed Optical Networks. *Journal of Lightwave Technology*, 29(10):1560–1577, May 2011.

[56] S. Chandrasekhar, D. W. Peckham, and R. Lingle. Ultra-Long-Haul Transmission of 1.2-Tb/s Multicarrier No-Guard-Interval CO-OFDM Superchannel Using Ultra-Large-Area Fiber. *IEEE Photonics Technology Letters*, 22(11):826–828, June 2010.

[57] A. Bononi, N. Rossi, and P. Serena. Transmission limitations due to fiber nonlinearity. In *Optical Fiber Communication Conference (OFC)*, page OWO7, Los Angeles, CA, USA, 2011. Optical Society of America.

[58] A. Bononi, P. Serena, and N. Rossi. Nonlinear signal–noise interactions in dispersion-managed links with various modulation formats. *Optical Fiber Technology*, 16(2):73–85, March 2010.

[59] F. Vacondio, O. Rival, C. Simonneau, E. Grellier, A. Bononi, L. Lorcy, J.-C. Antona, and S. Bigo. On nonlinear distortions of highly dispersive optical coherent systems. *Optics Express*, 20(2):1022–1032, January 2012.

[60] R. W. Tkach, A. R. Chraplyvy, F. Forghieri, A. H. Gnauck, and R. M. Derosier. Four-photon mixing and high-speed WDM systems. *Journal of Lightwave Technology*, 13(5):841–849, May 1995.

[61] K. O. Hill, D. C. Johnson, B. S. Kawasaki, and R. I. MacDonald. cw three-wave mixing in single-mode optical fibers. *Journal of Applied Physics*, 49(10):5098–5106, 1978.

[62] F. Forghieri, R. W. Tkach, and A. R. Chraplyvy. WDM systems with unequally spaced channels. *Journal of Lightwave Technology*, 13(5):889–897, May 1995.

[63] F. Forghieri, R. W. Tkach, A. R. Chraplyvy, and D. Marcuse. Reduction of four-wave mixing crosstalk in WDM systems using unequally spaced channels. *IEEE Photonics Technology Letters*, 6(6):754–756, June 1994.

[64] E. Ip. Nonlinear Compensation Using Backpropagation for Polarization-Multiplexed Transmission. *Journal of Lightwave Technology*, 28(6):939–951, March 2010.

[65] E. F. Mateo, F. Yaman, and G. Li. Efficient compensation of inter-channel nonlinear effects via digital backward propagation in WDM optical transmission. *Optics Express*, 18(14):15144–15154, June 2010.

[66] F. Yaman and G. Li. Nonlinear Impairment Compensation for Polarization-Division Multiplexed WDM Transmission Using Digital Backward Propagation. *IEEE Photonics Journal*, 2(5):816–832, October 2010.

[67] G. Gavioli, E. Torrengo, G. Bosco, A. Carena, S. J Savory, F. Forghieri, and P. Poggiolini. Ultra-Narrow-Spacing 10-Channel 1.12 Tb/s D-WDM Long-Haul Transmission Over Uncompensated SMF and NZDSF. *IEEE Photonics Technology Letters*, 22(19):1419–1421, October 2010.

[68] J. G. Proakis. *Digital Communications*. McGraw-Hill, 4 edition, 2002.

[69] R. Hassun, M. Flaherty, R. Matreci, and M. Taylor. Effective evaluation of link quality using error vector magnitude techniques. In *Proceedings of 1997 Wireless Communications Conference*, pages 89–94, Boulder, CO, USA, 1997. IEEE.

[70] M. D. McKinley, K. A. Remley, M. Myslinski, J. S. Kenney, D. Schreurs, and B. Nauwelaers. EVM calculation for broadband modulated signals. In *64th ARFTG Conf. Dig*, pages 45–52, Orlando, FL, USA, 2004.

Appendix A

Error Vector Magnitude, Signal to Noise Ratio and Bit Error Ratio

The most used performance metric is BER, which is the probability of error given by the erroneous bit divided by the transmitted bit. Usually, is calculated as a function of SNR. In coherent communication systems with perfect phase and carrier recovered and assuming Gaussian noise, BER is expressed for MQAM formats as [33]

$$BER_{MQAM} = \frac{2\left(1 - \frac{1}{L}\right)}{\log_2 L} Q\left(\sqrt{\left[\frac{3\log_2 L}{L^2 - 1}\right]\left[\frac{2E_s}{N_0\log_2 L}\right]}\right) \tag{A.1}$$

where $Q(\cdot)$ is the Q function, M is the order of the constellation, $L = \sqrt{M}$ is the number of encoded bits per symbol, E_s/N_0 is the SNR, E_s is the energy of the complex symbol, $N_0/2$ is the noise power spectral density. Since $Q(x) = 1/2 \cdot erfc(x/\sqrt{2})$ and replacing $SNR = E_s/N_0$ and $L = \sqrt{M}$, equation A.1 can be rewritten as [38, 30, 68],

$$BER_{MQAM} = \frac{2}{\log_2 M} \cdot \left(1 - \frac{1}{\sqrt{M}}\right) erfc\left(\sqrt{\frac{3 \cdot SNR}{2 \cdot (M - 1)}}\right) \tag{A.2}$$

where $erfc$ is the complementary error function. For MPSK, and assuming $M \geq 8$, the BER can be given by [38, 68]

$$BER_{MPSK} = \frac{2}{\log_2 M} \cdot erfc\left(\sqrt{SNR} \cdot \sin\frac{\pi}{M}\right) \tag{A.3}$$

A.1 Signal to Noise Ratio and Error Vector Magnitude

The root mean squared EVM is a performance metric which can be measured as the error vector of the received symbol information $s_i' = a_i' + j * b_i'$ with respect to the ideal or transmitted symbol information $s_i = a_i + j * b_i$, where a_i and b_i are the real and imaginary component of the signal respectively. Mathematically, EVM can be defined as [69, 70]

$$EVM_{rms} = \sqrt{\frac{\sum_{i=1}^{N} |s_i - s_i'|^2}{\sum_{i=1}^{N} |s_i|^2}} \tag{A.4}$$

EVM can be expressed in either in percentage as $EVM(\%) = EVM_{rms} \cdot 100$ or in dB as $EVM(dB) = 10 \cdot \log_{10}(EVM_{rms}^2)$. For synchronous (perfect phase and frequency recovery) coherent systems limited by Gaussian noise, EVM can be related to the SNR as [33]

$$EVM_{rms} \approx \sqrt{\frac{1}{SNR}} \tag{A.5}$$

A.2 Error Vector Magnitude and Bit Error Ratio

From equations A.2 and A.5, BER can be expressed as a function of EVM for square QAM formats as follows

$$BER_{MQAM} \approx \frac{2}{\log_2 M} \cdot \left(1 - \frac{1}{\sqrt{M}}\right) erfc\left(\sqrt{\frac{3}{2 \cdot (M-1) \, EVM_{rms}^2}}\right) \tag{A.6}$$

In the same manner, equation A.3 can extrapolated to equation A.7 for PSK as

$$BER_{MPSK} \approx \frac{2}{\log_2 M} \cdot erfc\left(\frac{1}{EVM_{rms}} \cdot \sin \frac{\pi}{M}\right) \tag{A.7}$$

Using equations A.6 and A.7, one can calculate EVM values, shown in Tables A.1, A.2, A.3 and A.4 for typical BER values in current optical communication systems.

Table A.1: EVM results for BER $= 10^{-3}$.

Modulation	EVM$_{rms}$ in (%)	EVM$_{rms}$ in (dB)
QPSK	32.40 %	-9.79 dB
8PSK	17.05 %	-15.37 dB
16QAM	14.90 %	-16.53 dB
64QAM	7.46 %	-22.54 dB
256QAM	3.80 %	-28.40 dB

Table A.2: EVM results for BER $= 10^{-6}$.

Modulation	EVM$_{rms}$ in (%)	EVM$_{rms}$ in (dB)
QPSK	21.05 %	-13.53 dB
8PSK	11.25 %	-18.98 dB
16QAM	9.53 %	-20.42 dB
64QAM	4.70 %	-26.56 dB
256QAM	2.36 %	-32.54 dB

Table A.3: EVM results for BER $= 10^{-9}$.

Modulation	EVM$_{rms}$ in (%)	EVM$_{rms}$ in (dB)
QPSK	16.68 %	-15.56 dB
8PSK	8.96 %	-20.95 dB
16QAM	7.52 %	-22.48 dB
64QAM	3.69 %	-28.66 dB
256QAM	1.85 %	-34.66 dB

Table A.4: EVM results for BER $= 10^{-12}$.

Modulation	EVM$_{rms}$ in (%)	EVM$_{rms}$ in (dB)
QPSK	14.22 %	-16.94 dB
8PSK	7.65 %	-22.33 dB
16QAM	6.40 %	-23.88 dB
64QAM	3.14 %	-30.06 dB
256QAM	1.56 %	-36.14 dB

Appendix B

Matlab Codes

B.1 Implementation of the VSTF method in Matlab

It is presented below an implementation in Matlab® of the 3rd order VSTF to emulate the total field propagation over single-mode fibers. The name of the function is `VSTF-Method`. In addition, functions `VSTF-Method-SPM`, `VSTF-Method-XPM` and `VSTF-Method-FWM` are also presented for calculating independently the contributions of SPM, XPM and FWM, respectively.

```matlab
% This function emulates the 3rd order Volterra Series Transfer Function
% Method for fiber propagation considering, SPM, XPM, FWM, Self-Steepening
% and Raman Scattering.
% INPUT: A_F_In--> input WDM signal in frequency domain, K index of the
% channel to be solved;
% OUTPUT: A_To_F, A_To_T--> output signals in the frequency and time
% domains; A_NL_F, A_NL_T: output nonlinear signals only in the frequency
% and time domains.
% Last Update: 13/01/2011
% Author: Jacklyn D. Reis, Antonio L. Teixeira.

function [A_To_F,A_To_T,A_NL_F,A_NL_T] = VSTF_Method(A_F_In,K)

global Fiber Frequency WDM

MVSTF = 'yes';
% Sampling Paramaters
Omega = 2*pi*Frequency;
NFFT = length(Frequency);
Wc = 2*pi*WDM.Fin;
Ts = 1/(2*max(Frequency));
% Fiber Parameters
Gama = Fiber.Gama;
Alfa = Fiber.Alfa;
L = Fiber.L;
Beta2 = Fiber.Beta2; % Last modification
Beta3 = Fiber.Beta3;
% Number of Frequency Samples per Channel
SPc = ceil(WDM.Spacing*(Ts*NFFT));

if WDM.Nch > floor((NFFT+2)/(3*SPc)),
    fprintf('VSTF Solution not Valid.\nIncreace the sampling frequency (Fs):
%d\nOr decrease the number of channel (Nch): %d\n',[1/Ts WDM.Nch]);
    return;
end
% Create Index Grid
i = (-round(WDM.Nch*SPc/2):round(WDM.Nch*SPc/2)-1)+NFFT/2;
j = (-round(WDM.Nch*SPc/2):round(WDM.Nch*SPc/2)-1)+NFFT/2;
if nargin < 2,
    NF = length(i);
    k = (-round(NF/2):round(NF/2)-1)+NFFT/2;
else
    k = i(1+SPc*(K-1):(K+0)*SPc); % simulated channels
end
[ii,jj] = meshgrid(i,j);
Indx = -ii+jj;
% Create Frequency Grid
w1 = Omega(i);
w2 = Omega(j);
[w11,w22] = meshgrid(w1,w2);
w1w2 = w11-w22;
% Evaluate the Signal in the Grid
A_w1w2 = A_F_In(ii).*conj(A_F_In(jj));
%------------------------------------------------------------------------
% VSTF Complete Solution: SPM, XPM, FWM, SRS and Self-Steepening
%------------------------------------------------------------------------
A_NL_F = zeros(NFFT,1);
A_Li_F = zeros(NFFT,1);
A_To_T = zeros(NFFT,1);

% G1_w1 = -Alfa/2-1i*Beta2.*w11.^2/2-1i*Beta3.*w11.^3/6;
% G1_w2 = -Alfa/2-1i*Beta2.*w22.^2/2-1i*Beta3.*w22.^3/6;
TR = 5e-15;                                  % Raman coefficient
R = Gama*TR*(w11-w22);                        % Self-Steepening coefficient
% Nonlinear Part
```

```matlab
for n=k(1):k(end),
% Implemented as in J.D. Reis et al, JLT 30(2),234-241(2012)
    w = Omega(n);
    H = (-1i*Gama).*exp(-Alfa*L/2-1i*L*Beta2*w.^2/2-1i*L*Beta3*w.^3/6)*...
        (1-exp(-Alfa*L-1i*L*Beta2*(w11-w).*(w1w2)-1i*L*Beta3/2*(w+w22).*(w11-
w).*(w1w2))).*/...
        (Alfa+1i*Beta2*(w11-w).*(w1w2)+1i*Beta3/2*(w+w22).*(w11-w).*(w1w2));
% Original Implementation: includes Self-Steeping and Raman
%       w33 = Omega(n)+w1w2;
%       G1_w3 = -Alfa/2-1i*Beta2.*w33.^2/2-1i*Beta3.*w33.^3/6;
%       G1_w = -Alfa/2-1i*Beta2.*Omega(n).^2/2-1i*Beta3.*Omega(n).^3/6;
%       H = (-1i*Gama-1i*Gama*Omega(n)/Wc-R).* ...
%     (exp(L*(G1_w1+conj(G1_w2)+G1_w3))-exp(L*G1_w))./...
%        (G1_w1+conj(G1_w2)+G1_w3-G1_w);
    Aux = H.*A_w1w2.*A_F_In(n+Indx);
    A_NL_F(n) = sum(sum(Aux));
end
% Linear Part
A_Li_F(k,1) = exp(-Alfa*L/2-1i*L*Beta2.*Omega(k).^2/2-
1i*L*Beta3.*Omega(k).^3/6).*A_F_In(k);

if strcmpi(MVSTF,'yes');
    A_NL_T = ifft(ifftshift(A_NL_F),NFFT)*NFFT;
    A_Li_T = ifft(ifftshift(A_Li_F),NFFT)*NFFT;
%-----------------------------------------------------------------------
% Modified VSTF
%-----------------------------------------------------------------------
    for n=1:NFFT,
        if abs(A_NL_T(n))<=abs(A_Li_T(n)),
            A_To_T(n) = A_Li_T(n)*exp(A_NL_T(n)/A_Li_T(n));
        elseif abs(A_NL_T(n))>abs(A_Li_T(n)),
            A_To_T(n) = A_Li_T(n)+A_NL_T(n);
        end
    end
    A_To_F = fftshift(fft(A_To_T,NFFT))/NFFT;
elseif strcmpi(MVSTF,'no');
%-----------------------------------------------------------------------
% Conventional VSTF
%-----------------------------------------------------------------------
    A_To_F = A_Li_F + A_NL_F;
    A_To_T = ifft(ifftshift(A_To_F),NFFT)*NFFT;
end
```

```matlab
% This function emulates the 3rd order Volterra Series Transfer Function
% Method for fiber propagation considering, SPM only.
% INPUT: A_F_In--> input WDM signal in frequency domain, K index of the
% channel to be solved;
% OUTPUT: A_To_F, A_To_T--> output signals in the frequency and time
% domains; A_NL_F, A_NL_T: output nonlinear signals only in the frequency
% and time domains.
% Last Update: 17/12/2010.
% Author: Jacklyn D. Reis, Antonio L.J. Teixeira.

function [A_NL_F,A_To_F,A_NL_T,A_To_T] = VSTF_Method_SPM(A_F_In,K)

global Fiber Frequency WDM

MVSTF = 'yes';
% Sampling Paramaters
Omega = 2*pi*Frequency;
NFFT = length(Frequency);
Ts = 1/(2*max(Frequency));
% Fiber Parameters
Gama = Fiber.Gama;
Alfa = Fiber.Alfa;
L = Fiber.L;
Beta2 = Fiber.Beta2;
Beta3 = Fiber.Beta3;
% Number of Frequency Samples per Channel
SPc = ceil(WDM.Spacing*(Ts*NFFT));

if WDM.Nch > floor((NFFT+2)/(3*SPc)),
    fprintf('VSTF Solution not Valid.\nIncreace the sampling frequency (Fs):
%d\nOr decrease the number of channel (Nch): %d\n',[1/Ts WDM.Nch]);
    return
end
% Create Index Grid

i = (-round(WDM.Nch*SPc/2):round(WDM.Nch*SPc/2)-1)+NFFT/2;
j = (-round(WDM.Nch*SPc/2):round(WDM.Nch*SPc/2)-1)+NFFT/2;
i = i(1+SPc*(K-1):K*SPc);
j = j(1+SPc*(K-1):K*SPc);
% i = (-SPc/2:SPc/2-1)+(NFFT*(K-1)/2);%(-SPc/2:SPc/2-1)+NFFT/2;
% j = (1+SPc*(K-1):K*SPc)+NFFT/2;%(-SPc/2:SPc/2-1)+NFFT/2;

[ii,jj] = meshgrid(i,j);
Indx = -ii+jj;
% Create Frequency Grid
w1 = Omega(i);
w2 = Omega(j);
[w11,w22] = meshgrid(w1,w2);
w1w2 = w11-w22;
% Evaluate the Signal in the Grid
A_w1w2 = A_F_In(ii).*conj(A_F_In(jj));
%-------------------------------------------------------------------------
% VSTF SPM Solution
%-------------------------------------------------------------------------
A_NL_F = zeros(NFFT,1);
A_Li_F = zeros(NFFT,1);
A_To_T = zeros(NFFT,1);

% G1_w1 = -Alfa/2-1i*Beta2.*w11.^2/2-1i*Beta3.*w11.^3/6;
% G1_w2 = -Alfa/2-1i*Beta2.*w22.^2/2-1i*Beta3.*w22.^3/6;
% Nonlinear Part
for n=i(1):i(end),
    w = Omega(n);
    H = -1i*Gama*exp(-Alfa*L/2-1i*L*Beta2*w.^2/2-1i*L*Beta3*w.^3/6).*...
        (1-exp(-Alfa*L-1i*L*Beta2*(w11-w).*(w1w2)-1i*L*Beta3/2*(w+w22).*(w11-
```

```matlab
    w).*(w1w2)))./...
        (Alfa+1i*Beta2*(w11-w).*(w1w2)+1i*Beta3/2*(w+w22).*(w11-w).*(w1w2));
%        w33 = Omega(n)+w1w2;
%        G1_w3 = -Alfa/2-1i*Beta2.*w33.^2/2-1i*Beta3.*w33.^3/6;
%        G1_w = -Alfa/2-1i*Beta2.*Omega(n).^2/2-1i*Beta3.*Omega(n).^3/6;
%        H = -1i*Gama.*(exp(L*(G1_w1+conj(G1_w2)+G1_w3))-exp(L*G1_w))./...
%            (G1_w1+conj(G1_w2)+G1_w3-G1_w);
    Aux = H.*A_w1w2.*A_F_In(n+Indx);
    A_NL_F(n) = sum(sum(Aux));
end
% Linear Part
A_Li_F(i,1) = exp(-Alfa*L/2-1i*L*Beta2.*Omega(i).^2/2-...
1i*L*Beta3.*Omega(i).^3/6).*A_F_In(i,1);

if strcmpi(MVSTF,'yes');
    A_NL_T = ifft(ifftshift(A_NL_F),NFFT)*NFFT;
    A_Li_T = ifft(ifftshift(A_Li_F),NFFT)*NFFT;
    %--------------------------------------------------------------------
    % Modified VSTF
    %--------------------------------------------------------------------
    for n=1:NFFT,
        if abs(A_NL_T(n))<=abs(A_Li_T(n)),
            A_To_T(n) = A_Li_T(n)*exp(A_NL_T(n)/A_Li_T(n));
        elseif abs(A_NL_T(n))>abs(A_Li_T(n)),
            A_To_T(n) = A_Li_T(n)+A_NL_T(n);
        end
    end
    A_To_F = fftshift(fft(A_To_T,NFFT))/NFFT;
elseif strcmpi(MVSTF,'no');
    %--------------------------------------------------------------------
    % Conventional VSTF
    %--------------------------------------------------------------------
    A_To_F = A_Li_F + A_NL_F;
    A_To_T = ifft(ifftshift(A_To_F),NFFT)*NFFT;
end


% This function emulates the 3rd order Volterra Series Transfer Function
% Method for fiber propagation considering, SPM and XPM only.
% INPUT: A_F_In--> input signal in frequency domain representing the test
% signal; WDM_F_In--> is the remaining channels; K is the index of the test
% signal.
% OUTPUT: A_To_F, A_To_T--> output signals in the frequency and time
% domains; A_NL_F, A_NL_T: output nonlinear signals only in the frequency
% and time domains.
% Last Update: 17/12/2010
% Author: Jacklyn D. Reis, Antonio L.J. Teixeira.

function [A_NL_F,A_To_F,A_NL_T,A_To_T] = VSTF_Method_XPM(A_F_In,WDM_F_In,K)

global Fiber Frequency WDM

MVSTF = 'yes';
% Sampling Paramaters
Omega = 2*pi*Frequency;
NFFT = length(Frequency);
Ts = 1/(2*max(Frequency));
% Fiber Parameters
Gama = Fiber.Gama;
Alfa = Fiber.Alfa;
L = Fiber.L;
Beta2 = Fiber.Beta2;
Beta3 = Fiber.Beta3;
% Number of Frequency Samples per Channel
SPc = ceil(WDM.Spacing*(Ts*NFFT));
```

```matlab
if WDM.Nch > floor((NFFT+2)/(3*SPc)),
    fprintf('VSTF Solution not Valid.\nIncreace the sampling frequency (Fs): %d\nOr decrease the number of channel (Nch): %d\n',[1/Ts WDM.Nch]);
    return
end
% Create Index Grid
i = (-round(WDM.Nch*SPc/2):round(WDM.Nch*SPc/2)-1)+NFFT/2;
j = (-round(WDM.Nch*SPc/2):round(WDM.Nch*SPc/2)-1)+NFFT/2;
k = i(1+SPc*(K-1):K*SPc);

[ii,jj] = meshgrid(i,j);
Indx = -ii+jj;
% Create Frequency Grid
w1 = Omega(i);
w2 = Omega(j);
[w11,w22] = meshgrid(w1,w2);
w1w2 = w11-w22;
% Evaluate the Signal in the Grid
A_oj = A_F_In;
A_om = WDM_F_In;
A_m1 = A_oj(ii).*conj(A_om(jj));
A_m2 = A_om(ii).*conj(A_om(jj));
%--------------------------------------------------------------------
% VSTF XPM Solution
%--------------------------------------------------------------------
A_NL_F = zeros(NFFT,1);
A_Li_F = zeros(NFFT,1);
A_To_T = zeros(NFFT,1);

% G1_w1 = -Alfa/2-1i*Beta2.*w11.^2/2-1i*Beta3.*w11.^3/6;
% G1_w2 = -Alfa/2-1i*Beta2.*w22.^2/2-1i*Beta3.*w22.^3/6;
% Nonlinear Part
for n=k(1):k(end),
    w = Omega(n);
    H = -1i*Gama*exp(-Alfa*L/2-1i*L*Beta2*w.^2/2-1i*L*Beta3*w.^3/6)*...
        (1-exp(-Alfa*L-1i*L*Beta2*(w11-w).*(w1w2)-1i*L*Beta3/2*(w+w22).*(w11-w).*(w1w2)))./...
        (Alfa+1i*Beta2*(w11-w).*(w1w2)+1i*Beta3/2*(w+w22).*(w11-w).*(w1w2));
%       w33 = Omega(n)+w1w2;
%       G1_w3 = -Alfa/2-1i*Beta2.*w33.^2/2-1i*Beta3.*w33.^3/6;
%       G1_w = -Alfa/2-1i*Beta2.*Omega(n).^2/2-1i*Beta3.*Omega(n).^3/6;
%
%       H = -1i*Gama.*(exp(L*(G1_w1+conj(G1_w2)+G1_w3))-exp(L*G1_w))./...
%           (G1_w1+conj(G1_w2)+G1_w3-G1_w);
    Aux = H.*(A_m1.*A_om(n+Indx)+A_m2.*A_oj(n+Indx));
    A_NL_F(n,1) = sum(sum(Aux,1));
end
% Linear Part
A_Li_F(k,1) = exp(-Alfa*L/2-1i*L*Beta2.*Omega(k).^2/2-1i*L*Beta3.*Omega(k).^3/6).*A_F_In(k,1);

if strcmpi(MVSTF,'yes');
    A_NL_T = ifft(ifftshift(A_NL_F),NFFT)*NFFT;
    A_Li_T = ifft(ifftshift(A_Li_F),NFFT)*NFFT;
%--------------------------------------------------------------------
% Modified VSTF
%--------------------------------------------------------------------
    for n=1:NFFT,
        if abs(A_NL_T(n))<=abs(A_Li_T(n)),
            A_To_T(n) = A_Li_T(n)*exp(A_NL_T(n)/A_Li_T(n));
        elseif abs(A_NL_T(n))>abs(A_Li_T(n)),
            A_To_T(n) = A_Li_T(n)+A_NL_T(n);
        end
    end
```

```matlab
    A_To_F = fftshift(fft(A_To_T,NFFT))/NFFT;
elseif strcmpi(MVSTF,'no');
%--------------------------------------------------------------------------
% Conventional VSTF
%--------------------------------------------------------------------------
    A_To_F = A_Li_F + A_NL_F;
    A_To_T = ifft(ifftshift(A_To_F),NFFT)*NFFT;
end


% This function emulates the 3rd order Volterra Series Transfer Function
% Method for fiber propagation considering, FWM only.
% INPUT: A_F_In--> input signal in frequency domain representing the test
% signal; WDM_F_In--> is the remaining channels; K is the index of the test
% signal.
% OUTPUT: A_To_F, A_To_T--> output signals in the frequency and time
% domains; A_NL_F, A_NL_T: output nonlinear signals only in the frequency
% and time domains.
% Last Update: 17/12/2010
% Author: Jacklyn D. Reis, Antonio L.J. Teixeira.

function [A_NL_F,A_To_F,A_NL_T,A_To_T] = VSTF_Method_FWM(WDM_F_In,K)

global Fiber Frequency WDM FWM

MVSTF = 'yes';
% Sampling Paramaters
Omega = 2*pi*Frequency;
NFFT = length(Frequency);
Ts = 1/(2*max(Frequency));
% Fiber Parameters
Gama = Fiber.Gama;
Alfa = Fiber.Alfa;
L = Fiber.L;
Beta2 = Fiber.Beta2;
Beta3 = Fiber.Beta3;
% Number of Frequency Samples per Channel
SPc = ceil(WDM.Spacing*(Ts*NFFT));

if WDM.Nch > floor((NFFT+2)/(3*SPc)),
    fprintf('VSTF Solution not Valid.\nIncreace the sampling frequency (Fs):
%d\nOr decrease the number of channel (Nch): %d\n',[1/Ts WDM.Nch]);
    return
end
% Create Index Grid
i = (-round(WDM.Nch*SPc/2):round(WDM.Nch*SPc/2)-1)+NFFT/2;
j = (-round(WDM.Nch*SPc/2):round(WDM.Nch*SPc/2)-1)+NFFT/2;
k = i(1+SPc*(K-1):K*SPc);

[ii,jj] = meshgrid(i,j);
Indx = -ii+jj;
% Create Frequency Grid
w1 = Omega(i);
w2 = Omega(j);
[w11,w22] = meshgrid(w1,w2);
w1w2 = w11-w22;

FWM_Prod_CW = FWM.Prod(FWM.Prod(:,1) + FWM.Prod(:,2) - FWM.Prod(:,3) == K,:);


%--------------------------------------------------------------------------
% VSTF FWM Solution
%--------------------------------------------------------------------------
A_Flmn_f  = zeros(NFFT,size(FWM_Prod_CW,1));

A_NL_F = zeros(NFFT,1);
```

```matlab
A_Li_F = zeros(NFFT,1);
A_To_T = zeros(NFFT,1);

% G1_w1 = -Alfa/2-1i*Beta2.*w11.^2/2-1i*Beta3.*w11.^3/6;
% G1_w2 = -Alfa/2-1i*Beta2.*w22.^2/2-1i*Beta3.*w22.^3/6;
for n=k(1):k(end),
    w = Omega(n);
    H = -1i*Gama*exp(-Alfa*L/2-1i*L*Beta2*w.^2/2-1i*L*Beta3*w.^3/6)*...
        (1-exp(-Alfa*L-1i*L*Beta2*(w11-w).*(w1w2)-1i*L*Beta3/2*(w+w22).*(w11-
w).*(w1w2)))./...
        (Alfa+1i*Beta2*(w11-w).*(w1w2)+1i*Beta3/2*(w+w22).*(w11-w).*(w1w2));
%       w33 = Omega(n)+w1w2;
%       G1_w3 = -Alfa/2-1i*Beta2.*w33.^2/2-1i*Beta3.*w33.^3/6;
%       G1_w = -Alfa/2-1i*Beta2.*Omega(n).^2/2-1i*Beta3.*Omega(n).^3/6;
%       H = (-1i*Gama).*(exp(L*(G1_w1+conj(G1_w2)+G1_w3))-exp(L*G1_w))./...
%           (G1_w1+conj(G1_w2)+G1_w3-G1_w);
    for nn=1:size(FWM_Prod_CW,1),
        A1 = WDM_F_In(:,FWM_Prod_CW(nn,1));
        A2 = WDM_F_In(:,FWM_Prod_CW(nn,3));
        A3 = WDM_F_In(:,FWM_Prod_CW(nn,2));
        Aux = H.*A1(ii).*conj(A2(jj)).*A3(n+Indx);
        if FWM_Prod_CW(nn,1)~=FWM_Prod_CW(nn,2),
            Aux = 2*Aux;
        end
        A_Flmn_f(n,nn) = sum(sum(Aux));
    end
    A_NL_F(n) = sum(A_Flmn_f(n,:));
end

% Linear Part
A_Li_F(k,1) = exp(-Alfa*L/2-1i*L*Beta2.*Omega(k).^2/2-
1i*L*Beta3.*Omega(k).^3/6).*WDM_F_In(k,K);

if strcmpi(MVSTF,'yes');
    A_NL_T = ifft(ifftshift(A_NL_F),NFFT)*NFFT;
    A_Li_T = ifft(ifftshift(A_Li_F),NFFT)*NFFT;
%-------------------------------------------------------------------------
% Modified VSTF
%-------------------------------------------------------------------------
    for n=1:NFFT,
        if abs(A_NL_T(n))<=abs(A_Li_T(n)),
            A_To_T(n) = A_Li_T(n)*exp(A_NL_T(n)/A_Li_T(n));
        elseif abs(A_NL_T(n))>abs(A_Li_T(n)),
            A_To_T(n) = A_Li_T(n)+A_NL_T(n);
        end
    end
    A_To_F = fftshift(fft(A_To_T,NFFT))/NFFT;
elseif strcmpi(MVSTF,'no');
%-------------------------------------------------------------------------
% Conventional VSTF
%-------------------------------------------------------------------------
    A_To_F = A_Li_F + A_NL_F;
    A_To_T = ifft(ifftshift(A_To_F),NFFT)*NFFT;
end
```

B.2   GPU acceleration of the SSF method

It is presented below an implementation in Matlab$^{\circledR}$ of the SSF method for emulating the total field propagation over single-mode fibers. We point out that this implementation is based on a previous implementation presented by the authors in [32].

This implementation calls the function `gpuArray` withing the Parallel Computing Toolbox$^{\text{TM}}$, which makes use of `NVIDIA`$^{\circledR}$ `CUDA`$^{\text{TM}}$ architecture to enable the communication between Graphics Processing Unit (GPU) cards and Central Processing Unit (CPU). As such, `CUDA`$^{\text{TM}}$ drivers and Matlab$^{\circledR}$ R2010b or later versions including the Parallel Computing Toolbox$^{\text{TM}}$ are required. More information about the system requirements and documentation can be found in http: // www.mathworks.com / discovery / matlab-gpu.html. The required `CUDA`$^{\text{TM}}$ drivers for supported `NVIDIA`$^{\circledR}$ GPU can be found in http: // developer.nvidia.com / cuda / cuda-downloads.

```matlab
%%%%%%%%%%%%%%%%%%%%%%%%%%%%%%%%%--------------%%%%%%%%%%%%%%%%%%%%%%%%%%%%%%%%%
% Subject: GPU-accelerated Split-Step Method for Fiber Propagation
% Target: ultra-dense WDM with very short step sizes
% Version: v3.0
% Date: 30/06/2011
% Last Update: 30/06/2011
% PS: Include second and third order dispersion coefficients and kerr
% effect in the fiber propagation model
%%%%%%%%%%%%%%%%%%%%%%%%---------Main Function------------%%%%%%%%%%%%%%%%%%%

function [A_Lf,A_Lt] = Split_Step_Fourier_Method_GPU(Signal_Input_F)

global Fiber Frequency WDM

% Fiber Parameters
L = Fiber.L;
Alfa = Fiber.Alfa;
Gama = Fiber.Gama;
Beta2 = Fiber.Beta2;
Beta3 = Fiber.Beta3;
% Sampling Parameters
Omega = 2*pi*Frequency;
NFFT = length(Frequency);
% Spatial Resolution Parameters
h = fix(0.0000500/(Gama*WDM.P(WDM.Probe)));      % Step Size
M = round(L/h);                                  % Number of Fiber Sections
Dh = exp((h/2)*(-Alfa/2 - 1i*Beta2.*Omega.^2/2 - 1i*Beta3.*Omega.^3/6));   %
Linear Operator in the Frequency Domain
uf0 = Signal_Input_F*NFFT;            % Initial Field in the Frequency Domain

% Create GPU Arrays to be processed
uf0 = gpuArray(uf0);
Dh = gpuArray(Dh);
Gama = gpuArray(Gama);
h = gpuArray(h);

% Main Loop
for i = 1:M,
%================================================================
% Propagation in the first half dispersion region, z to z+h/2
%================================================================
    Hf = uf0.*Dh;
    ht = ifft((Hf));
    pq = ht.*conj(ht);
    u2e = ht.*exp(-1i*Gama*pq*h);
%================================================================
% Propagation in the second Dispersion Region, z+(h/2) to z+h
%================================================================
    u2ef = (fft(u2e));
    u3ef = u2ef.*Dh;
    u3e = ifft((u3ef));
    u3ei = u3e.*conj(u3e);
%================================================================
% Iteration for the nonlinear phase shift(two iterations)
%================================================================
    u2 = ht.*exp(-(h/2)*1i*Gama*(pq+u3ei));
    u2f = (fft(u2));
    u3f = u2f.*Dh;
    u4 = ifft((u3f));
    u4i = u4.*conj(u4);
    u5 = ht.*exp(-(h/2)*1i*Gama*(pq+u4i));
    u5f = (fft(u5));
    uf0 = u5f.*Dh;
end
```

```matlab
A_Lf = gather(uf0)/NFFT; % Collect the processed data from the GPU
A_Lt = ifft(ifftshift(A_Lf))*NFFT; % Time domain representation

%%%%%%%%%%%%%%%%%%%%%%%%%%========END OF CODE========%%%%%%%%%%%%%%%%%%%%%%%%%
```